THE PHOTOLUMINESCENCE TRANSITIONS AND SITE SYMMETRY OF THE EL2 DEFECT IN GALLIUM ARSENIDE

by

Mark K. Nissen
B.Sc., Simon Fraser University, 1986

THESIS SUBMITTED IN PARTIAL FULFILLMENT OF
THE REQUIREMENTS FOR THE DEGREE OF
DOCTOR OF PHILOSOPHY
in the Department
of
PHYSICS

SIMON FRASER UNIVERSITY
January 1992

APPROVAL

Name: Mark K. Nissen

Degree: Ph.D. (Physics)

Title of Thesis: The Photoluminescence Transitions and Site Symmetry of the EL2 Defect in Gallium Arsenide

Examining Committee: Chairman: Dr. E.D. Crozier

Dr. M.L.W. Thewalt
Senior Supervisor

Dr. R.F. Frindt

Dr. D.J. Huntley

Dr. J.C. Irwin

Dr. E.E. Haller
External Examiner
University of California at Berkeley
Berkeley, California

Date Approved: Jan 16, 1992

PARTIAL COPYRIGHT LICENSE

I hereby grant to Simon Fraser University the right to lend my thesis, project or extended essay (the title of which is shown below) to users of the Simon Fraser University Library, and to make partial or single copies only for such users or in response to a request from the library of any other university, or other educational institution, on its own behalf or for one of its users. I further agree that permission for multiple copying of this work for scholarly purposes may be granted by me or the Dean of Graduate Studies. It is understood that copying or publication of this work for financial gain shall not be allowed without my written permission.

Title of Thesis/Project/Extended Essay

The Photoluminescence Transitions and Site Symmetry of the EL2 Defect in Gallium Arsenide.

Author:

(signature)

Mark Missen

(name)

Feb 7, 1992

(date)

ABSTRACT

The EL2 defect in gallium arsenide is among the most active topics in semiconductor physics today. It is responsible for the technologically important semi-insulating property of liquid encapsulated Czochralski grown material and its pronounced metastability is a prototypical example of behaviour which is currently an area of intense interest in condensed matter physics. As is the case for much of the work done on this system, the previous EL2-related photoluminescence studies have been full of controversial and contradictory results. The work presented here takes advantage of the power of Fourier transform interferometry to settle these questions with unambiguous results that clearly identify and define the photoluminescence associated with the EL2 defect, and the transitions responsible for it. A key result is the observation of an EL2 photoluminescence band that is distinguished for the first time from a competing process that arises from another common defect. This band, which has never been previously reported, is weak but very significant because it features fine structure that is the sharpest spectroscopic signature yet of EL2. This allows sensitive studies of the site symmetry of EL2 by observing the behaviour of the fine structure under the perturbations of applied uniaxial stress and magnetic field. The results are a strong indication that the defect has full tetrahedral symmetry and supports the identification of EL2 as an arsenic atom on a gallium site. This is commonly referred to as the isolated arsenic antisite model of EL2 as opposed to the stongest competing model which has the arsenic antisite paired with an arsenic interstitial.

AKNOWLEDGEMENTS

I would first like to express my gratitude and respect for my senior supervisor, Dr. Mike Thewalt, who has not only built a world class research lab but also fosters an atmosphere that is conducive to productive work with a healthy dose of cooperation and friendship. All my other fellow workers in the lab, past and present, have also been of help but in particular, Dr. Tom Steiner has devoted much time and expertise to this work and it has greatly benefitted from his participation. The wide variety of samples provided by Dr. Maria Maciaszek of Johnson-Matthey Electronics was also invaluable.

Financial support from the Natural Sciences and Engineering Research Council, the B.C. Advanced Systems Foundation, Simon Fraser University and Dr. M.L.W. Thewalt is gratefully acknowledged.

A special thank you goes to my parents who have always supported me in every way with all my endeavours. Thanks also to Tessa, who gave lots of support and encouragement.

TABLE OF CONTENTS

TABLE OF CONTENTS (CONTINUED)

TABLE OF CONTENTS (CONTINUED)

LIST OF TABLES

LIST OF FIGURES

LIST OF FIGURES (CONTINUED)

LIST OF ABBREVIATIONS

BE	Bound Exciton
BN	Boron Nitride
DAP	Donor-Acceptor Pair
DLTS	Deep Level Transient Spectroscopy
EMT	Effective Mass Theory
EPR	Electron Paramagnetic Resonance
ESR	Electron Spin Resonance
FE	Free Exciton
FT	Fourier Transform
FTS	Fourier Transform Spectroscopy
IC	Integrated Circuit
LEC	Liquid Encapsulated Czochralski
LO_{Γ}	Zone Centre Longitudinal Optical (Phonon)
LVM	Local Vibrational Mode
MCDA	Magnetic Circular Dichroism Absorption
N_A	Shallow Acceptor Concentration
N_D	Shallow Donor Concentration
N_{EL2}	Concentration of the EL2 Defect
NP	No-phonon
ODENDOR	Optically Detected Electron Nuclear Double Resonance
ODMR	Optically Detected Magnetic Resonance
OPO	Optical Parametric Oscillator
PL	Photoluminescence
PLE	Photoluminescence Excitation
ppm	Parts per million
ODENDOR	Optically Detected Electron Nuclear Double Resonance
SI	Semi-Insulating
SNR	Signal to Noise Ratio
(D^0, A^0)	Donor-Acceptor Pair Transition
$(D^0, EL2^+)$	Donor Bound Electron to EL2 Bound Electron Transition
(e, D^+)	Free Electron to Shallow Donor Bound Electron Transition
$(e, EL2^+)$	Free Electron to EL2 Bound Electron Transition
(h, D^0)	Bound Electron to Valence Electron Transition
$(h, EL2^0)$	EL2 Bound Electron to Valence Electron Transition

CHAPTER 1. INTRODUCTION

1.1 Rationale

The EL2 defect in gallium arsenide is a topic that has attracted the attention of researchers in semiconductor physics for many years. The motivation for this interest lies both in its technological importance in the production of GaAs integrated circuits and its intriguing metastable excited state. The exact identity of EL2 and the nature of the metastability, however, remain controversial subjects. There is much debate as to whether it is a point defect consisting of one atom alone which, barring a symmetry breaking lattice relaxation, has the full symmetry of the GaAs lattice or whether it is a complex with reduced symmetry. The models of the metastability depend on the structure of the defect and therefore hinge on this question.

Photoluminescence is a powerful experimental technique that has contributed greatly to our understanding of semiconductors. This has not been the case, however, for the EL2 defect. The photoluminescence studies of EL2 have been fraught with confusion and contradictions and little, if any, useful information has been obtained. The work presented here identifies for the first time the electronic transitions responsible for the photoluminescence from EL2 [90N1]. In doing so, a new photoluminescence band with sharp structure is reported. This structure is the narrowest feature yet observed in the optical spectroscopy of EL2. This in turn allows detailed studies where the symmetry of the host GaAs crystal lattice is lowered by perturbing the crystal with applied uniaxial stress and magnetic field so that the site symmetry of the defect itself can be studied [91N1].

The balance of this chapter will introduce some of the relevant basic concepts and experimental techniques of semiconductor physics. In particular, the importance of defects in semiconductors will be discussed. The EL2 defect introduces an electronic energy level that is deep within the bandgap, and since deep levels are not as well understood as shallow levels, the difference between deep and shallow levels will be stressed.

1.2 Semiconductors Compared to Insulators and Conductors

The electrical properties of materials are often classified into only two categories, insulators and conductors. This black and white picture is, however, very incomplete; between these two extremes is a rich spectrum of shades of grey. At the very heart of modern electronics are materials whose electrical properties can be controlled to an astounding extent [81S1]. These materials are semiconductors.

Although it is not central to the work presented in this thesis, an understanding of why a given material falls into a certain category is a useful way of introducing some key concepts to the uninitiated reader. A thorough treatment requires some knowledge of the quantum theory of solids but it is hoped that a few simple concepts will allow a qualitative understanding of these three basic classifications and in particular, some of the basic properties of semiconductors. The details can be found in any introductory solid state physics textbook such as Kittel [81K1] or, for a more complete treatment, a textbook on semiconductor physics such as Seeger [89S1].

When atoms are joined together to form a crystalline solid, the discrete allowed energy levels of the electrons bound to the atoms merge together to form continuous bands of allowed states. These bands can be overlapping in energy or can be separated by a bandgap, E_g, which is a range of energies forbidden to the electrons. The Fermi level, E_f, is the highest occupied electronic energy level when the crystal is in its lowest energy configuration, the crystal ground state.

Conductors characteristically have the Fermi level falling either within a band so that the band is only partially filled or at the top a band with zero bandgap between it and the next highest band. The availability of states immediately above the electrons near the Fermi level in either of these two cases allow them to be moved by an applied electric field and hence conduct electricity. In the case of insulators, however, the Fermi level lies at the top of a band above which there is a large bandgap and hence there are no accessible states and electrical conduction is not readily achieved. The bandgap of an insulator is typically on the order of 10 electron volts (eV).

Semiconductors are similar to insulators, except that the bandgap is sufficiently small so that some electrons can be thermally excited at room temperature from the highest filled band, called the valence band, to the first empty band, called the conduction band. The bandgap of a semiconductor is typically around 1 eV, for instance, the GaAs bandgap at room temperature is 1.42 eV and at liquid helium temperatures (the boiling point of helium is 4.2 K) the bandgap is 1.519 eV [82B1]. When an electron is excited to the conduction band, the resulting absence of an electron in the valence band behaves like a positively charged particle and is called a hole. Both the positively charged hole and the negatively charged electron contribute to the conductivity.

Electrons can also be optically excited from the valence band to the conduction band. When light of photon energy greater than the bandgap is incident on the crystal, it can be absorbed with the photon energy transferred directly to exciting an electron into the conduction band. The conduction of electrical current that can result is called photoconductivity and is a simple illustration of how semiconductors can be used as optical detectors. The reverse process also occurs. The recombination of an electron and a hole can result in the emission of a photon and this is the most fundamental form of luminescence. This is the principle behind devices such as light emitting diodes and semiconductor lasers. Photoluminescence is the luminescence that results from photo-excitation and as will be discussed, photoluminescence spectroscopy is a powerful method for the study of the electronic energy levels of semiconductors.

The detailed band structure of a crystalline solid determines the electrical and optical properties. The band structure is given as a function of the electron crystal momentum. This is because the allowed energies in a perfect crystal depend not on the position but on the momentum of the electron which is described by its wavevector or **k**-vector. As a result of the periodicity of the lattice, electron momentum can be expressed in terms of the reciprocal space or **k**-space of the lattice and the complete band structure can be given in the **k**-space equivalent of the crystal unit cell which is known as the first Brillouin zone.

Many differences between distinct semiconductors can be characterized by the nature of their bands. Clearly, the size of the bandgap is important with obvious implications on the conductivity and the photoluminescence. It will also be seen that another very important parameter is the curvature of the band edges. Finally, semiconductors can be classified into two distinct groups on the basis of another band structure feature. Materials in which the extrema of the valence band and the conduction band are both found at the same point in the Brillouin zone are called direct-gap, whereas those in which the conduction band minima are displaced by non-zero **k**-vector from the valence band maximum are called indirect-gap. This characteristic has important ramifications on the optical properties of the material.

Analagous to momentum for particles in free space, **k**-vector must in general be conserved in the electronic transitions in the crystal. Since photons carry essentially zero wavevector, it is only in direct-gap material that radiative recombination of electron-hole pairs can occur directly without the participation of another entity to mediate the conservation of **k**-vector. This allows these transitions to proceed with much higher probability than is the case for indirect-gap materials where conservation of **k**-vector is typically mediated by the participation of an appropriate phonon, the quantum of lattice vibrations. This is the fundamental difference between the optical properties of direct and indirect-gap semiconductors.

1.3 The Role of Defects and Impurities in Semiconductors

The electrical and optical properties of semiconductors are profoundly affected by the presence of defects and impurities within the crystal lattice. This is discussed in the introductory texts that were referred to earlier [81K1, 89S1] and a more complete treatment of the physics of defects and impurities can be found in the two volume series by Lannoo [81L1] and Bourgoin [83B1].

Although the class including defects also includes the class of impurities, it is useful to make a distinction between the two. An impurity is the presence of a foreign atom in the crystal lattice. It can be a substitutional impurity, where the impurity atom replaces a host atom in the lattice or it can be an interstitial where the impurity resides between lattice sites. A defect, on the other hand, can be any kind of local imperfection in the crystal lattice and does not necessarily involve an impurity. Except in cases where the context clearly indicates the presence of an impurity, the term defect will be restricted here to refer to intrinsic or native lattice defects which do not include an impurity. Some simple examples of defects are for instance, a vacancy, which is the absence of an atom from a lattice site, or a self-interstitial, which is the presence of a native atom between lattice sites. In a compound semiconductor such as GaAs, another type of simple defect is possible, the anti-site [81L1]. The GaAs lattice can be thought of as consisting of two separate but interlocking sublattices, the Ga sublattice and the As sublattice. An arsenic atom substituting on a gallium site is called an arsenic anti-site, As_{Ga}. Similarly there is also a gallium anti-site, Ga_{As}. It should also be mentioned that two or more defects together may constitute a species that is said to be a complex defect rather than a point defect. These are to be distinguished from defects such as dislocations, stacking faults, *etc.* which are of a macroscopic extent [86P1].

A simple feeling for the consequences of the presence of impurities and defects can be obtained by considering that the atomic bonding is altered in their vicinity. In this way, defects and impurities can introduce electronic energy levels in the bandgap and even in very pure materials these energy levels have a dominant effect on the conductivity. Two types of impurities have had an especially important role in the development of semiconductor physics and technology. These are shallow donors and shallow acceptors [81R1].

A shallow donor is typically a substitutional impurity with one more valence electron than the host atom that it replaces. This extra electron will not be involved in the forming of bonds in the crystal but will be loosely bound to the impurity atom by a Coulomb potential that is screened by the dielectric constant, ε, of the host material and at low temperature will occupy a level just below the conduction band. This electron is easily "donated" to the conduction band and hence the name donor.

Similarly, a shallow acceptor is typically a substitutional impurity with a valency of one less than the atom it replaces and it requires an extra electron to form the required bonds. This kind of impurity forms a level near the valence band and because it readily "accepts" electrons from the valence band, it is called a shallow acceptor. When the acceptor is occupied by an electron from the valence band there is a resulting hole in the valence band. An equivalent way of looking at this is to say that the acceptor binds a hole in the same way that the donor binds an electron.

In GaAs, the shallow donor ground state lies approximately 5.7 meV below the conduction band and the shallow acceptors are in the vicinity of 30 meV above the valence band [89L1]. It is in this sense that these energies are small compared to the bandgap energy, and hence the levels are near one of the two band edges, that these levels are called shallow.

The controlled addition of such impurities is called doping. Through this process it is possible to change the conductivity by many orders of magnitude [81S1]. It is primarily this property that has made semiconductors so useful in the field of electronics. In a pure intrinsic (undoped) semiconductor, the Fermi level is located very near the middle of the bandgap and the material is highly resistive. By adding impurities (dopants) and thereby introducing levels in the bandgap, the Fermi level can be moved anywhere between the valence band and the conduction band. Such a semiconductor is said to be extrinsic because its electrical characteristics are controlled by electronic levels that are not inherent to the pure crystal. When the concentration of acceptors, N_A, is greater than that of the donors, N_D, the majority charge carriers are the positively charged holes in the valence band with concentration $N_A - N_D$ and the material is said to be p-type. Conversely when donors outnumber acceptors, the majority charge carriers are conduction band electrons with concentration $N_D - N_A$ and the material is said to be n-type. Hence by controlling the relative concentrations of the donors and acceptors, the type of charge carrier and its concentration can be chosen. This is called compensation [81K1,89S1].

It is unlikely that the current status of semiconductor technology would have been achieved without an understanding of the underlying physics, and likewise, future progress will certainly be governed by a greater understanding of the relevant physical processes. Hence the study of defects and impurities is a dominant part of semiconductor physics. This is particularly true of shallow donors and acceptors which are now relatively well understood and are described by effective mass theory (EMT), which is summarized in the following section. The physics of levels that are deeper in the bandgap are, however, less well understood. The EL2 defect forms such a deep level. Before discussing deep levels in more detail, it is useful to first present some of the basic ideas of EMT and its limitations [81L1,82J1].

1.4 Effective mass theory

The energy of a free electron in terms of its wave vector **k** is

$$E = \frac{\hbar^2 \mathbf{k}^2}{2m_o} \qquad 1.1$$

where $\hbar$ is the reduced Planck's constant and m_o is the mass of the electron. Similarly, if the shape of the conduction band in a semiconductor is roughly parabolic at its minimum, then it can be described by the relation [81K1]

$$E = \frac{\hbar^2 \mathbf{k}^2}{2m^*} \qquad 1.2$$

where m^* is now an effective mass which is determined by the curvature of the band. Thus an electron moving in the conduction band of a semiconductor with parabolic bands can be approximated as a free electron with an effective mass m^*. The effective mass theory of impurity states extends this approximation to electrons and holes occupying shallow levels.

A great deal of the experimental knowledge of the electronic states of shallow levels has been obtained by exploiting their impact on the optical properties of the crystal and a thorough review of these results and EMT theory is given by Ramdas and Rodriguez [81R1]. In the far infra-red (FIR) region of the spectrum where a pure crystal would be completely transparent, well defined and spectrally narrow absorption lines are observed that correspond to transitions of the bound electron or hole from a ground state to a series of excited states similar to the Rydberg excited states of the hydrogen atom. The photoluminescence is also greatly affected by the presence of impurities, essentially because the recombination can take place in the vicinity of the impurity or can even be due to the relaxation of either an electron or hole at the impurity level. This will be further discussed in a later section. The essential point to make here is that for shallow levels, the binding energy of the electron or hole is small compared to the bandgap, and the wavefunction of the bound particles are highly delocalized in real space. The Heisenberg uncertainty principle tells us that they must then be highly localized in momentum space or **k**-space.

This was recognized by Kohn and Luttinger [55K1, 55L1] who showed that the problem of shallow levels in semiconductors could be reduced to an analogue of the hydrogen atom. The ultimate success of this theory lies in transforming a very complicated many body problem into a relatively simple two body problem. Kohn and Luttinger found that they could include the effect of the anisotropy and many body nature of the crystal lattice by approximating its influence with an effective mass of the shallow bound electron or hole moving in the screened Coulomb potential. If the level is shallow enough, the effective mass of the electron or hole is well approximated by the respective curvature of the bottom of the conduction band or the top of the valence band. Formally, the wavefunction of the bound particle, given that it is sufficiently shallow is composed only from the perfect crystal eigenfunctions of the nearest band extrema [82J1].

Although very successful, it is instructive to realize the limitations of EMT. In the near vicinity of the impurity atom, it is no longer valid to consider the bound particle as moving in a hydrogenic potential with dielectric constant of the host material [82J1]. In this region the Coulomb potential from the impurity atom is not completely screened and the potential takes on a stronger, short range form that depends on the chemical identity of the impurity atom. This deviation from the EMT approximation of a long range Coulomb potential is most significant for the ground state of shallow levels and causes a species-dependent variation in the binding energies [81R1]. This is known as the central cell correction or chemical shift. The excited states, on the other hand, remain largely unaffected [82J1]. Even for a relatively deep level such as the triple acceptor copper in germanium, the excited states are still extremely hydrogenic despite the fact that the ground state energy is approximately four times that of an EMT acceptor [90N2].

The key to understanding the successes and failures of EMT lies in considering the localization in real space of the states [82J1]. The theory is very successful at describing the excited states but much less so with the more localized ground states. This is due in part to the perturbation of the purely hydrogenic potential near the impurity atom but, more seriously, the approximation of deriving an effective mass from the band edge states becomes less valid as the localization of the bound particle increases and the wavefunction becomes more diffuse in momentum space. If the level is near neither the conduction band nor valence band, the bound particle can no longer be approximated by the properties of the nearby band edge; all the bands in their entirety must be taken into account. In this deep level case, the effective mass approximation breaks down completely and very different effects are encountered that require new techniques to understand [81J1].

1.5 Deep Levels

The essential characteristic of deep levels in comparison to shallow levels is the presence of strong, short range potentials [82J1,86P2]. Beyond this, the simplest description of a deep level is to say that it does not behave like a shallow level. This is not terribly informative, but it is useful in making the point that there is no "magic" energy that demarcates these two types of levels and it also emphasizes that there are very fundamental differences between them. For a moderately deep level, there may still be properties, especially excited states, that are said to be effective mass like, but there will be other features which are completely foreign to shallow levels. Although it is possible to have a shallow level that is not well described by EMT, a good rule of thumb is that the farther a level is from the band edge the more its behaviour will deviate from that of effective mass like levels. The topic of this thesis is the EL2 defect in GaAs, which has as its ground state a midgap level that must certainly be classified as a deep level.

1.5.1 Electrical Properties of Deep Levels

In terms of their manifestation on the electrical properties of the host material, deep levels typically act as charge traps that control the lifetime of carriers and have a rather complex effect on the conductivity [86P2]. This is in contrast to shallow levels which are fully ionized at room temperature and contribute excess charge carriers that modify the conductivity in a relatively straight forward manner. This charge trapping behaviour can be useful in the case where high resistivity material is desired, but as will be seen, this has proven difficult to control and understand.

1.5.2 Lattice Relaxation

On a more fundamental level, the major physical difference between shallow levels and deep levels is that shallow impurities constitute a very minor local perturbation to the crystal whereas deep levels, while still local, present more of a severe perturbation [86P2]. The binding potentials are deeper and more short range in nature resulting in both higher binding energies and higher localization for the bound particles. A direct consequence of this is a stronger interaction and coupling with the lattice. The binding potential, if sufficiently strong, can significantly perturb the valence electrons in the surrounding crystal which alters the stability of the lattice in the vicinity of the defect. This can result in a rearrangement of the lattice which is known as lattice relaxation. This fundamental property of deep levels has many important consequences and is treated thoroughly in many references [81L1, 82J1, 83B1, 86L1, 86P2]. The treatment presented here is a synthesis of these references.

The lattice relaxation contributes an elastic energy component to the total binding energy which is dependent on the charge state of the defect. It is typically approximated by a harmonic potential acting on a generalized coordinate, Q, which can represent the motion of one or more atoms in the vicinity of the defect. The effects of lattice relaxation are often presented in a configuration coordinate diagram, such as the one shown in Figure 1.1, which shows the effect of the lattice relaxation between the ground state of an occupied donor level, D^o, and an excited state which for concreteness will be taken to be the unoccupied donor level, $D^+ + e$. The parabolas represent the total energy, elastic plus electronic, of the crystal as a function of the defect coordinate, Q. The horizontal straight lines within the parabolas represent the energy levels of the local vibrational modes (LVM) of the harmonic potential with eigenvalues

$$E_n = (n + \frac{1}{2})\hbar\omega. \qquad n = 0,1,2... \qquad 1.3$$

The LVMs are localized phonons with energy $\hbar\omega$ and are a characteristic of the defect and not the lattice as a whole. The lattice relaxation is evident in the shift of the centre of the parabola from Q_o to Q_R and the lattice relaxation energy, E_R is the increase in the binding energy due to lattice relaxation [86L1].

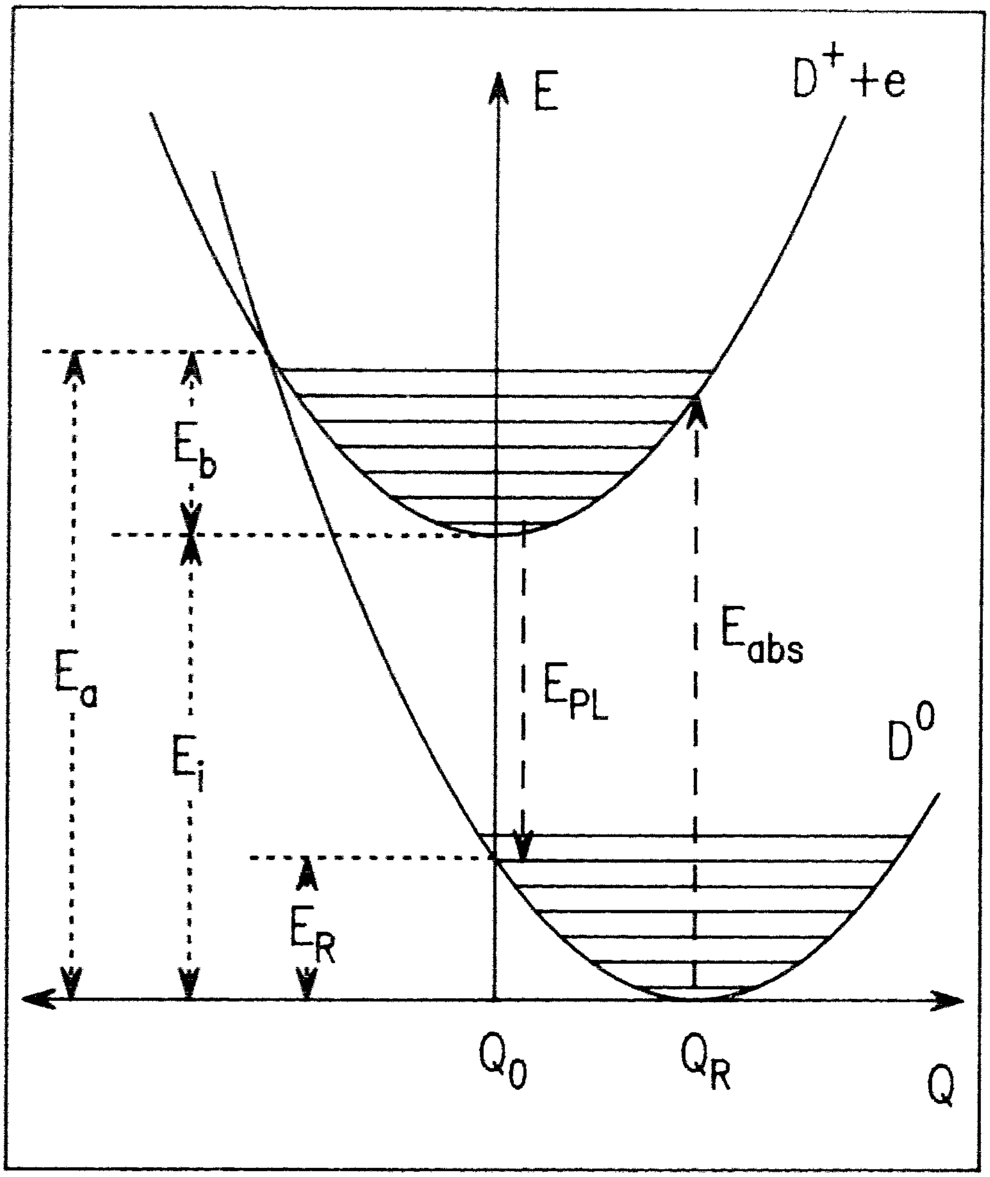

Figure 1.1
Configuration coordinate diagram showing the lattice relaxation, E_R, for a neutral donor, D^0, at energy E_i below the ionized donor, $D^+ + e$. The most probable optical transitions for a strongly phonon coupled system are shown with energy E_{PL} and E_{abs}. E_b is the barrier for electron recapture and E_a is the thermal activation energy measured in deep level transient spectroscopy.

The configuration coordinate diagram is also very useful to illustrate how lattice relaxation is closely tied to the observed phonon coupling of the level. In the case of shallow levels, where the bound electron or hole is essentially decoupled from the motion of the nuclei, most electronic transitions occur without the participation of phonons except when they are needed to conserve momentum. This is not the case for deep levels which by their very nature are much more sensitive to the lattice. The coupling of electrons to the lattice is mediated by the electron-phonon interaction and the electronic transitions of deep levels are greatly affected by the electron-phonon interaction in that the transition is most often accompanied by the absorption or emission of multiple phonons.

The most probable absorption and photoluminescence transitions for a strongly phonon coupled system are indicated on Figure 1.1 with energies E_{abs} and E_{PL}, where the transition is followed by the relaxation of the lattice and the relaxation energy is taken up by multiple phonon emission. Other transitions, where either more or less of the lattice relaxation energy is taken up by the photon, are also allowed and in the theory of Huang and Rhys [50H1] the transition probabilities depend only on the overlap of the harmonic oscillator wavefunctions. In a simplified model that is commonly used, the same harmonic potential is used for both levels and for transitions from the lowest harmonic state of one level to the n^{th} harmonic state of the other level followed by the emission of n phonons, the relative intensities are given by [82J1]

$$\sigma_{0,n} \propto e^{-S}\frac{S^n}{n!} \qquad 1.4$$

where S is a measure of the strength of the electron phonon coupling given by

$$S = \frac{E_R}{\hbar\omega}. \qquad 1.5$$

and is known as the Huang-Rhys factor [82J1]

In the limit of strong coupling, $S > 10$, the locus of points given by equation 1.4 approaches a Gaussian distribution and the dominant transitions will be those indicated in Figure 1.1. They both differ from the true ionization energy, E_i, by the lattice relaxation energy which is also known as the Franck-Condon shift [82J1, 83B1]. In such a case, the no-phonon transition at energy E_i is extremely weak and may not even be observable. The observed lineshape is a broad gaussian shaped band of unresolved phonon assisted transitions [82J1].

1.5.3 Metastability

Lattice relaxation is also associated with the peculiar phenomenon of metastability that is observed with some deep levels. The overlap of the parabolas in Figure 1.1 is found at an energy, E_b, above the bottom of the upper parabola. If the transition from the higher state to the ground state cannot proceed radiatively, this represents a thermal barrier which must be overcome before the electron can relax back to the ground state. This is thought to be the case for extremely large lattice relaxations [86L1] where the intersection of the parabolas occurs between Q_0 and Q_R and there is negligible overlap of the harmonic oscillator wavefunctions between the two levels. If a sufficiently high barrier is formed, an electron or hole can be trapped in an excited state for hours or even days. If a significant proportion of the population of a given deep level are put into this metastable state, the normal properties of the deep level can be quenched or extinguished as if it were no longer present. This gives rise to the phenomenon of persistent photo-quenching which is a characteristic of the EL2 defect in GaAs [77B1].

1.5.4 Electronic Structure Calculations

It has already been argued that EMT-type calculations are inappropriate for deep levels [82J1] and a theoretical formalism describing deep levels remains a major challenge [86P2]. The research presented in this thesis is of an experimental nature and does not include any calculations of energies of deep levels, but some results of such calculations will be quoted. This section is intended only to give the reader a flavour of the nature of the calculations. The interested reader can see Pantelides [86P2] for a historical perspective or Jaros [82J1] and Lannoo and Bourgoin [81L1] for a more complete treatment.

In contrast to the EMT formalism where the effect of the lattice is almost seen to be added as an afterthought, calculations of the electronic properties of deep levels must proceed in a much more detailed fashion and carefully consider the lattice coupling in the total energy. The calculations must first include choosing a detailed potential that reflects the difference between the atomic orbitals of the defect and the host atom that it replaces. A decision must be made on how to incorporate the effect of the lattice. This can be done by doing detailed calculations on a cluster or cell of atoms that is repeated in a periodic manner to simulate the effect of an infinite lattice [86P2, 82J1, 89D1]. Another way of incorporating the effect of the lattice is through the use of the mathematical construct of Green's functions using an appropriate choice of basis functions associated with the crystal eigenfunctions to construct the Green's function. Both of these methods require numerical methods to obtain solutions and the advent of faster computers has improved matters dramatically, so that the agreement between theory and experiment has improved. No one complete formalism has yet emerged, and the results are very much dependent on the choice of Hamiltonian and numerical method. The crucial point is that the choice of the technique must be consistent with the properties to be calculated.

A useful qualitative understanding of the electronic nature of states introduced by deep levels can be obtained by considering simple arguments regarding first a vacancy in a crystal and then introducing a potential related to a substitutional atom [81L1, 86P2]. The covalent bonds in a diamond structure crystal lattice are formed by tetrahedral sp^3 hybrid orbitals. The removal of an atom to create a vacancy leaves four dangling bonds from the surrounding atoms with the strong positive lobe pointing towards the vacancy. In the absence of any interactions between them, the positive lobes form a four-fold degenerate bonding state (neglecting spin) and the negative lobes form a four-fold degenerate anti-bonding state. By simply allowing the orbitals to interact amongst themselves, the four-fold degeneracy is replaced by two states. One of these is s-like and nondegenerate and the other is p-like and three-fold degenerate. These states can be classified by their symmetry within the tetrahedral point group T_d which describes the symmetry of the lattice. The former is fully symmetric under the operations of the tetrahedral group T_d and hence is labelled A_1, while the latter transform as T_2. In this very simple picture there are then two types of levels introduced, A_1 and T_2.

If the removed host atom is now reinserted, the interaction of its orbitals with the A_1 and T_2 states form bonding states that merge exactly with the valence band and anti-bonding states that merge with the conduction band. If, however, the inserted atom has orbitals with considerably different energies than those of the host crystal, the exact merging with the valence bands and conduction bands does not occur and a pair of vacancy-like A_1 and T_2 states remain. The bandgap states of donors derive from anti-bonding states and and those of acceptors, from bonding states.

1.6 Experimental Methods of Studying Deep Levels

The experimental study of deep levels also differs in many ways from the established techniques used for shallow levels [86P2]. Although many of the techniques used in the study of shallow levels, such as absorption and photoluminescence spectroscopy, can still be applied, the physical processes can be quite different. This often necessitates a new approach both in performing the experiments and interpreting the results. The influence of strong electron-phonon coupling in broadening and shifting the absorption and photoluminescence transitions has already been introduced. It should be stressed, however, that this effect can be so strong as to make it difficult to determine the nature of the transition or even which defect is responsible for the process if the material is not well characterized. The strong electron-phonon coupling can also result in very low radiative efficiencies because the recombination process at a deep level can be dominated by multi-phonon emission rather than photon emission, making the photoluminescence a very weak process. While optical techniques are often misinterpreted in their application to deep levels, they can nevertheless provide precise and sensitive measurements of the electronic levels, especially if a no phonon transition can be observed. In addition to these all-optical techniques, many other techniques are also used. Photoluminescence and the other techniques that have been useful in the study of deep levels, particularly EL2, will now be briefly discussed.

1.6.1 Photoluminescence

Photoluminescence spectroscopy is a technique that is fundamental to semiconductor physics because it relies on the radiative recombination of electrons and holes that is an intrinsic property of any semiconductor. Most of the electron-hole recombination paths give rise to luminescence with photon energies near the bandgap energy, and for many of the important semiconductors, such as GaAs and Si, this allows the use of sensitive photon counting detectors such as photomultiplier tubes. The near-gap luminescence, as it is called, is thus a central part of PL spectroscopy and is a natural starting point for a discussion of some of the basic photoluminescence transitions

[72B1].

It was stated earlier that an electron in the conduction band can recombine with a hole in the valence band resulting in the emission of a photon. This band to band recombination, however, is not the process most commonly studied in photoluminescence. At the low temperatures at which PL spectroscopy is typically performed, the free electron and hole, before recombining, form a bound pair called an exciton which can remain as a free exciton (FE) or can itself be bound to an impurity in which case it is called a bound exciton (BE). The radiative recombination of these systems gives rise to the excitonic luminescence which typically dominates the PL spectrum in the energy region nearest the bandgap.

The initial state of the FE transition will, since it is free, have kinetic energy and for an ensemble of FE the distribution of kinetic energies is given by the Boltzmann statistics. The final state of the transition is the crystal ground state, the same as for simple band to band electron-hole recombination. The difference in energy between the FE luminescence and the bandgap is then just the binding energy of the electron-hole pair and the lineshape is characterized on the high energy side by a Boltzmann-tail which reflects the kinetic energy distribution of the FE.

The BE can be considered as a localized excitation of the neutral impurity state which, in the case of a simple donor or acceptor, consists of three particles. The final state of the transition is again the crystal ground state but differs from the FE case in that one of the particles of the BE state remains bound to the neutral impurity. Hence both the initial and final states are bound states of the same centre and each has a set of distinct, discrete energy levels. The principal BE luminescence is the transition from the BE ground state to the crystal ground state, which in the simplest case is a sharp line that is lowered in energy from the FE line by the binding energy of the exciton to the impurity. This binding energy is typically on the order of a couple of meV and is usually referred to as the localization energy. The linewidths of the BE transitions can be extremely narrow; for instance the phosphorus donor BE transition in Si has been measured to have a linewidth of 5 μeV [90T1].

While exciton physics is an important aspect of PL spectroscopy and its omission would have left this discussion incomplete, it will be shown that excitons do not play a role in the PL transitions of EL2. More relevant, however, are some of the other processes seen in the near-gap of direct-gap semiconductors [72B1]. Donor-acceptor-pair (DAP) luminescence is denoted (D^0, A^0) and is the radiative recombination between a neutral donor-bound electron and a neutral acceptor-bound hole or, equivalently, the relaxation of an electron from a neutral donor, D^0, to a neutral acceptor, A^0, leaving the both the donor and the acceptor ionized. Such a transition involving a deep donor is depicted in Figure 1.2. The photon energy of DAP transitions is dependent not only on the donor and acceptor energies but also on the final state Coulomb interaction between the ionized donor and acceptor. For large donor-acceptor separation, R, the photon energy is given by

$$h\nu = E_g - E_D - E_A + e^2/\varepsilon R \qquad 1.6$$

where h is Planck's constant, E_g is the bandgap, E_D is the donor binding

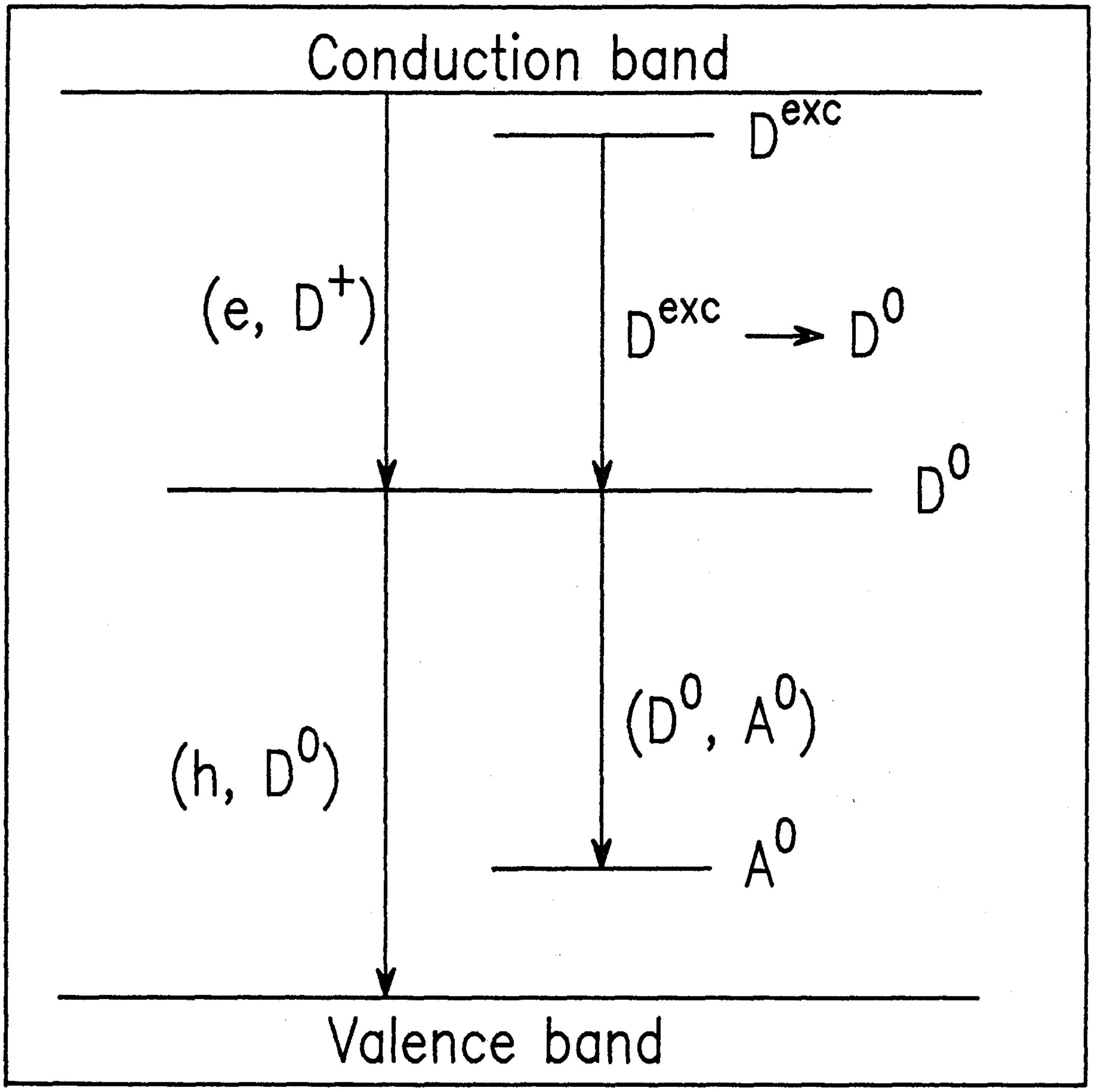

Figure 1.2

Energy level diagram showing some of the transitions which will be important. The most unusual of these is the transition from a shallow excited state to the ground state of a deep donor, $D^{exc} \rightarrow D^0$. Also shown are the free to bound transitions associated with the deep donor, (e,D^+) and (h,D^0), as well as DAP transitions, (D^0,A^0).

energy relative to the conduction band edge, E_A is the acceptor binding energy relative to the valence band edge, e is the electron charge and ε is the dielectric constant of the host semiconductor [81L1]. The low energy onset of the luminescence is thus the energy separation between the donor and acceptor levels, and the transition is broadened to higher energy by the final state Coulomb interaction.

If, however, the acceptor is much shallower than the donor, then at temperatures at which the acceptors are ionized, this process is no longer favourable and the donor bound electron recombines instead at an empty valence band state and is then denoted as an (h, D^0) free-to-bound transition. A complementary free-to-bound transition is the (e, D^+) transition where a free electron is captured by the ionized donor. This type of transition has not been observed for shallow donors because the transition energy falls in the far-infrared region where emission spectroscopy is hampered by the room temperature blackbody radiation of the instruments themselves.

The EL2 defect in GaAs, however, is a deep midgap donor and the (e, $EL2^+$) transition will therefore occur at an energy of approximately 750 meV which is well above the region where room temperature blackbody radiation is a problem. From the preceding discussion of effective mass theory, it is clear that even a very deep donor can have shallow hydrogenic excited states just below the conduction band. A transition from such an excited state to the ground state is depicted in Figure 1.2 and will occur at an energy just below the ground state binding energy. Like a BE transition, both the initial and final states are bound states localized at the same centre and these transitions can give rise to narrow lines in PL spectra. The onset of the free to bound (e, D^+)

transition, also depicted in Figure 1.2, corresponds to the binding energy of the ground state or in other words, the level itself. The lineshape of free to bound transitions is determined by the Boltzmann distribution of the kinetic energy of the free electron in the initial state.

These transitions involving a deep donor, however, are typically well below the energy for which photon counting detectors are available and, unless the luminescence is very strong, can be difficult to study. In Chapter 2, some of the previous work done on the PL of deep levels in GaAs will be reviewed and the confusion apparent in these results will show that there have indeed been many difficulties. As will be discussed in Chapter 3, the advantages of Fourier transform interferometry, when applied to PL spectroscopy [90T1], can go a long way to overcome these obstacles.

1.6.2 Capacitance Techniques

Deep level transient spectroscopy (DLTS), as the name suggests, is a technique designed specifically for the study of deep levels [82J1]. The method is based on measuring the capacitance transients caused by carrier emission and trapping in the depletion region of a reverse biased Schottky barrier. The following discussion describes the technique as applied to a deep donor.

If the bias is rapidly reduced, the width of the depletion region decreases as the deep levels or traps are quickly filled and the capacitance initially increases rapidly as well. When the reduced bias is removed, the traps slowly empty via thermal emission at a rate represented by g_e and the capacitance will slowly decrease as the depletion region grows. This capacitance transient in response to a pulse in the bias voltage is the DLTS signal.

The change in capacitance as a function of time is given by [83B1]

$$\Delta C(t) = \Delta C_0 \exp(-g_e t) \qquad 1.7$$

where ΔC_0 is the initial increase in capacitance and g_e is the thermal emission rate of electrons from the level. Thus g_e is readily measured and it can be easily shown by differentiating once by the time, t, and once by the temperature, T, that if the capacitance transient is measured at $t = t_0 = g_e^{-1}$ that it will reach a maximum or minimum at a given temperature T. In this way a DLTS spectrum is the capacitance transient given as a function of temperature. The energy of the level is not, however, read directly from the spectrum. Detailed balance arguments can be used to show that [83B1]

$$g_e = \sigma_a v_{th} N_C \exp(-E_a/kT) \qquad 1.8$$

where σ_a is the apparent capture cross section, [88B1] v_{th} is average thermal velocity of the electrons, N_C is the effective density of states in the the conduction band and E_a is the the thermal activation energy of the defect as shown in Figure 1.1. Both v_{th} and N_C are known quantities whose product, as a function of temperature, goes as T^2. Hence by plotting the logarithm of g_e/T^2 versus T^{-1} a slope of E_a/k is obtained and the logarithm of the intercept gives the apparent capture cross section, σ_a. The concentration of the level can be obtained from ΔC_0 [88B1].

Clearly DLTS is a very powerful technique for the characterization and measurement of deep levels. In contrast to PL, which can be performed on any sample, it is limited to specially prepared n-type samples which allow the fabrication of Schottky barriers. It also suffers from somewhat poor energy resolution and the need to subtract the energy barrier for recapture, E_B, (see Figure 1.1) from E_a to obtain the energy of the level below the bandgap. A variation of DLTS is deep level optical spectroscopy (DLOS) where optical pulses replace the electrical pulses and the optical cross sections for exciting a hole to the level, σ_p, or ionization of an electron, σ_n can be measured.

1.6.3 **Magnetic Resonance Techniques**

Magnetic resonance measurements can provide a very different kind of information on the nature of levels in the bandgap. If a defect binds a single electron, the resulting electronic state is said to be paramagnetic and is at least two-fold degenerate because of the spin of the electron. The degeneracy can be lifted by the application of a magnetic field; this is the well known Zeeman effect. The electronic Zeeman splitting of two states, one with $m_s = 1/2$ and the other with $m_s = -1/2$ is

$$\Delta E = g \mu_B B \qquad 1.9$$

where g is the g factor of the bound electron, μ_B is the electron Bohr magneton and H is the applied magnetic field. For a free electron, the g factor is approximately equal to two. The g factor for an electron bound to a defect in a semiconductor can vary considerably from this value due to its effective mass and spin-orbit interactions with the atoms in the neighbourhood of the defect and will in general be a tensor [83B1]. The electronic Zeeman splitting can in principle be observed in optical spectroscopy as a splitting of a transition energy but a more sensitive technique is electron spin resonance (ESR) which is also called EPR, where the P stands for paramagnetic [82J1, 83B1]. This technique measures the splitting by monitoring the microwave power of a given energy absorbed by a sample as the applied magnetic field is slowly varied. Resonant absorption of the microwave energy occurs when the applied field is such that the electronic splitting is equal to the microwave energy.

The real utility of EPR is achieved when the hyperfine interaction between the electron spin and nuclear spins can be resolved [83B1]. The nuclear spin is a characteristic of the atoms involved in the defect. For instance, arsenic has nuclear spin, $I = 3/2$, and the hyperfine interaction with an arsenic nucleus will split each electronic spin state into four sub-states with $m_I = 3/2, 1/2, -1/2, -3/2$ [82W1]. From the hyperfine spectrum, the symmetry of a group of nucleii interacting with the spin of the electron can sometimes be extracted. Hence, EPR can provide information on the identity and structure of a defect [83B1]. This technique as described does not, however, give any information on where in the bandgap the given defect lies. The information gained from EPR must somehow be related to the energy levels obtained from PL, absorption or DLTS. One way of doing this is to measure the photo-response of the EPR signal. By monitoring which optical energies put the defect into or out of its paramagnetic EPR-active state, information can be obtained which allows correspondence of the EPR signature to the levels measured in these other techniques [84M1, 85T1].

A closely related technique is electron nuclear double resonance (ENDOR) where in addition to the microwave frequency, a radiofrequency signal is also applied to induce transitions between adjacent m_I states. Since this is a double resonance experiment, it will be more sensitive than EPR and may be able to resolve transitions not seen in the EPR spectrum and also allows observation of the nuclear Zeeman splitting. This technique is often used by measuring a related optical signal and is then called optically detected ENDOR or ODENDOR [83B1]. Optically detected EPR is usually referred to as optically detected magnetic resonance (ODMR).

1.6.4 Uniaxial Stress

Another powerful probe of the defect symmetry is the application of uniaxial stress, where the crystal is compressed along a given direction to reduce the symmetry of the crystal lattice. The reduction in symmetry can lift degeneracies in two distinct ways [81L1].

Consider for instance a substitutional point defect in a diamond structure crystal. The electronic states of such a defect are classified in terms of the T_d group which describes the full symmetry of the crystal. The s-like states which have no orbital degeneracy are labelled A_1 and the three-fold orbitally degenerate p-like states are labelled T_2. The application of a uniaxial stress reduces the symmetry of the crystal from T_d to one of its sub-groups and the methods of group theory can be used to predict the reclassification of the defect states within this sub-group and it can be shown that the effect of the uniaxial stress is to lift the degeneracy of the orbitally degenerate states. By comparing the observed splitting of electronic transitions under uniaxial stress with the splittings allowed by group theory, information on the symmetry of the defect can obtained.

The application of uniaxial stress can also be used to probe for orientational degeneracy. For example, a defect with two constituent atoms may be aligned with axial symmetry along the [111] directions and equivalent directions. The electronic states of such a defect are described by the C_{3v} sub-group of T_d, which reflects the fact that some of the orbital degeneracy of these states will have been lifted by the reduced symmetry of the defect itself. A further reduction in symmetry by applied uniaxial stress along, for instance, the [111] direction will perturb the one quarter of the defects aligned along the [111] axis in a different way than the other three quarters that are aligned along the other three equivalent $[1\bar{1}\bar{1}]$, $[\bar{1}\bar{1}1]$ and $[\bar{1}1\bar{1}]$ directions. Assuming that the defect does not realign under the influence of the stress and ignoring the possibility of remaining orbital degeneracies, the above situation should result in a two-fold splitting with a three to one intensity ratio. Similarly, stress along [110] would also result in a two-fold splitting but with equal intensities and [100] stress would induce no splitting for a defect with C_{3v} symmetry. Uniaxial stress will be further discussed in greater detail in Chapter 5 in the context of the results presented there.

CHAPTER 2.

SEMI-INSULATING GALLIUM ARSENIDE AND THE EL2 DEFECT

2.1 Introduction

The EL2 defect and undoped semi-insulating (SI) GaAs are topics that go hand in hand. Under the appropriate growth conditions, GaAs can be produced with very high resistivities, typically between 10^7 and 10^8 Ω-cm [88H1]. This is several orders of magnitude higher than that found in silicon even though the concentrations of shallow impurities in silicon can be made much less than in GaAs [88S2]. This high resistivity leads to the name semi-insulating GaAs and is caused by the presence in high concentrations of the deep EL2 defect level.

This chapter will first describe some of the basic properties of GaAs and why the semi-insulating form of this material is technologically significant. Aspects of the most common commercial growth method will also be introduced, and will be seen in a later chapter to have a strong effect on the deep PL. The importance of EL2 will then be motivated, first by outlining the role it plays in the production of semi-insulating GaAs and then by introducing the intriguing metastable behaviour that it displays under optical excitation. This will be followed by a literature review which will introduce the properties of the EL2 defect in greater detail, including a discussion of the two prevalent models of its identity and concluding with a review of the previous work done on the photoluminescence spectroscopy of EL2.

2.2 Semi-insulating Gallium Arsenide

Gallium arsenide, GaAs, is a III-V compound semiconductor, the III and V representing the group from the periodic table to which gallium and arsenic belong, respectively. It crystallizes in the zinc-blende structure which is identical to the diamond structure or face centred cubic lattice of silicon and has full tetrahedral symmetry, except that in zinc-blende crystals, the adjacent atoms alternate between the two chemical constituents. The binary nature of GaAs complicates the production of high quality crystals [88Y1] and it will be seen that anti-site defects play an important role.

There are several intrinsic properties of GaAs which make it an alluring alternative to silicon as a material for integrated circuit (IC) fabrication. The GaAs electron effective mass of GaAs of $0.066m_0$ is considerably less than that of Si, resulting in higher electron mobilities and hence ideally to faster device performance, which is obviously a crucial parameter. In practice, however, the realized gains in speed are less than the factor of five that is naively predicted by a simple comparison of the effective masses. The higher lying conduction bands in GaAs have a higher effective mass and for high electric fields where the electrons are excited into these higher sub-bands, the electron mobility actually decreases and eventually becomes less than that of silicon [81S1]. This fundamental process combined with the sophistication of silicon device fabrication techniques over that for GaAs currently reduce the GaAs to Si speed advantage to approximately 1.4:1. [88S2] It is thought that when the relative immaturity of the

GaAs device technology is overcome, the speed could increase to two or three times that of silicon.

A more striking advantage and less easily overcome is the direct bandgap of GaAs compared to the indirect bandgap of Si which results in much higher radiative efficiencies in the former [89S1]. This admits the possibility of fully integrated optoelectronic ICs which will include optical emitters and detectors with other electronic components on a single substrate [88H1, 89P1]. It is recognized that achieving very high speed individual devices based on Si or GaAs is less of a problem than electrically connecting them in a complex circuit and operating them at high speeds and hence the importance of increasing integration. Realization of a mass producible integrated optical-electrical interconnect is of vital interest, especially to the telecommunication industry where fibre optics are already in use and will undoubtedly be a big part of the future.

Beyond the promise of higher speed devices and integrated optoelectronic circuitry, there exists another much more practical advantage for GaAs over Si. This advantage arises from an extrinsic property of bulk as-grown GaAs that is not found in Si; this is the existence in high concentrations of deep mid-gap levels that give semi-insulating behaviour [88H1]. This can be understood by considering, for instance, a deep donor situated near the middle of the band-gap. If the major residual impurities in the material are shallow acceptors and the deep donor is present in considerably higher concentrations than the acceptors, then the acceptors will be completely compensated by the deep donor and the Fermi level will be pinned just below the deep donor level [88H1, 80M1]. Thus the material behaves very much like an intrinsic semiconductor with very high resistivity and is said to be semi-insulating.

The importance of the semi-insulating property of GaAs is that it provides high resistivity substrates for IC fabrication [88Y1]. The high resistivity ensures electrical isolation of individual devices and the resulting reduction of parasitic capacitance between the devices themselves. Thus even for sophisticated devices which require elaborate epitaxial growth techniques, bulk semi-insulating GaAs is used as the substrate. The greatest impact of semi-insulating substrates came, however, once they could be produced with sufficient perfection and uniformity to allow their direct use in IC fabrication with the technique of ion-implantation [88H1]. By selectively implanting impurities to make conductive regions, devices can be made directly into the substrate. The majority of GaAs devices are made with this technique, particularly monolithic microwave integrated circuits in which the semi-insulating property is further exploited by integrating low loss inductors with the other circuit elements, a process that is not possible with current Si technology [89S2].

The semi-insulating behaviour of GaAs was first noted in 1962 [62A1]. It was originally attributed to the presence of oxygen, and later on, semi-insulating behaviour was obtained by doping with chromium, which forms a deep acceptor, [80M1] but there were problems with the uniformity and thermal stability of the material . The breakthrough came when the liquid encapsulated Czochralski (LEC) growth method was developed and it was discovered that undoped, as-grown LEC

GaAs was semi-insulating under As-rich growth conditions [88H1].

The LEC growth method is an adaptation of the Czochralski method which is extensively used for Si growth. The basic idea is to insert a seed crystal into molten material inside a crucible and then slowly pull the seed out at a rate such that the interface between the solid and liquid phases remains stationary. In this way a large boule or ingot of single crystal material can be pulled from the melt.

This technique could not be immediately used with GaAs because the arsenic would quickly boil off leaving a pool of molten gallium in the crucible. A simple and elegant solution to the problem was obtained when it was found that arsenic dissociation could be prevented by capping the melt with a floating layer of molten boric oxide, B_2O_3, hence the name liquid encapsulated Czochralski growth [65M1]. Initially, silicon contamination was a problem when the melt was enclosed in a quartz crucible as used in Si growth, but this was overcome with the use of pyrolitic boron nitride, BN, crucibles [77S1]. Further refinements were achieved by noting that the water content of the B_2O_3 encapsulant is also an important parameter in controlling the incorporation of residual impurities. Wet B_2O_3 serves to reduce both the carbon and silicon concentrations [85E1, 88H1].

The dominant residual shallow impurity in the LEC GaAs of today is the carbon acceptor with concentrations on the order of 10^{15} cm^{-3}. These acceptors are compensated by a deep midgap donor that is typically present in concentrations on the order of 10^{16} cm^{-3} and the material is hence semi-insulating. This deep donor is called EL2 and after many years of study is still far from fully understood.

2.3 The Significance of EL2

The two most often cited properties of EL2 are that it is the dominant midgap level in as-grown bulk LEC GaAs and that it has an optically accessible metastable excited state which when occupied leaves the level both optically and electrically inactive. These two properties establish its importance and allow it to be identified, at least conceptually, apart from other deep levels in GaAs.

2.3.1 EL2 and Semi-insulating GaAs

The EL2 story begins some thirty years ago with the first report of semi-insulating GaAs [62A1]. Since that time it has become apparent that although many levels can be present in GaAs, one particular level is almost always present and in concentrations much higher than the others and hence it is the dominant trap responsible for the semi-insulating behaviour of as-grown bulk GaAs. In a general classification of the deep levels observed in GaAs using DLTS, Martin *et al* gave the name EL2 to this ubiquitous level [77M1].

As mentioned in the previous section, semi-insulating GaAs came of age with the advent of LEC growth methods in pyrolitic BN crucibles. Before this, high concentrations of the Si_{Ga} shallow donor were the majority residual impurities. Semi-insulating crystals were obtained then by doping with chromium which forms a deep acceptor level. The Si contamination was, however, so severe that the levels of chromium needed to compensate it frequently led to precipitation of chromium. Other problems with chromium doping included the diffusion rate of chromium in

GaAs which complicated the activation-anneal of ion-implanted impurities [88H1].

In contrast to the early days, undoped semi-insulating GaAs with resistivities upwards of 10^7 Ω-cm can now be reliably produced by LEC growth under near stoichiometric or slightly As-rich conditions. The EL2 concentration can be made very uniform by annealing the whole ingot and also by growing the material in a magnetic field to damp out turbulent convection currents. This results in greater uniformity in the resistivity, which is crucial for ion-implantation. The thermal stability of EL2 is also sufficiently high that implant activation-annealing is readily done [88H1]. These properties have been vital in the progress of GaAs IC technology, but even without this technological importance, EL2 would still attract a lot of attention because of its unusual metastable behaviour.

2.3.2 The Metastability of EL2

In 1977, Bois and Vincent observed peculiar transient behaviour in a photocapacitance study of EL2 [77B1, 86M1]. When subjected to photo-excitation in the infrared region of $1.0 < h\nu < 1.4$ meV, the capacitance was found to initially undergo a rapid increase as the width of the depletion region decreases as is expected from the photo-ionization of EL2, but then was observed to decay slowly back down to a value close to what it was before excitation. Subsequent excitation resulted only in the capacitance increasing to the value to which it decayed after the initial excitation. This was the first quantitative observation of the photo-quenching property of EL2, and

Bois and Vincent attributed this behaviour to a metastable excited state of EL2 that is often referred to as $EL2^{*}$. Although it has been a subject of intense research, until very recently there had been no observations of any optical or electrical manifestations of $EL2^{*}$. The defect appears to become inactive and its observable optical and electrical properties are quenched or extinguished. It is interesting to note that in the recent work of Baj and Dreszer [91B1], an absorption feature attributed to $EL2^{*}$ was observed but only under the perturbation of hydrostatic pressure.

Subsequent to the initial discovery of the metastability, studies have shown that recovery from the metastable state can take place thermally through a barrier of about 0.3 eV which can be reduced by the presence of free electrons in the conduction band. Annealing at $T \geq 140$ K is the standard method to affect full recovery but a partial optical recovery can also be achieved by exciting electrons into the conduction band [86M1].

2.4 The Identification Problem

Despite its importance and the intriguing metastability, fundamental questions regarding EL2 remain unanswered. Foremost among these is the detailed identification of the structure of the EL2 defect. An understanding of the mechanisms involved in the transition to the metastable state is also an important issue, but this is likely to be contingent on the identification question. Before summarizing the progress to date on the identification of EL2, it is useful to establish some of the other properties of this defect and its associated electronic levels.

As stated several times already, the EL2 defect is a deep mid-gap donor level. The donor nature was firmly established by comparing the profiles of the free electron concentration to EL2 profiles under temperature conditions for which the EL2 would be ionized or neutral. The free electron concentration was found to correlate to the ionized EL2 profiles, proving that EL2 is in fact a donor [86M1].

The first ionization energy of a donor is denoted (0/+), and gives the position of the level in the gap with respect to the conduction band. Before the present work, the best estimates of the exact value of the neutral EL2 (0/+) level in the gap at T = 0 K were derived from either DLTS and photocapacitance. DLTS, however, is a thermal technique and cannot give the temperature dependence of the level. Photocapacitance suffers from problems with free carrier freeze-out and the unreliability of Schottky diodes at low temperatures and hence neither of these techniques can give a direct measurement of the level in the low temperature limit [86O1, 90O1]. With the aid of thermodynamical arguments and extrapolating down to low temperatures, the T = 0 K EL2 (0/+) level is given by DLTS to be at 749 ± 6 meV and by photocapacitance, at 735 ± 10 meV below the conduction band [86O1]. These two methods have also located a deeper level in p-type material at approximately 1.0 eV below the conduction band and this is interpreted as the singly ionized level (+/++) of EL2 and hence it is a double donor [89K1].

There has been speculation on the existence of a shallow hydrogenic excited state of EL2 just below the conduction band that contributes to the electron capture process [82M1, 86M1]. This would account for the fact that the measured electron capture cross-section is larger than that predicted by theories of multiphonon capture of electrons from the conduction band. Although there is no reason not to expect there to be shallow hydrogenic excited states in the gap, until the present work there was no strong experimental evidence of any EL2 related states in the gap other than the (0/+) and (+/++) levels.

2.4.1 EL2 and Oxygen

The first indication of the semi-insulating nature of GaAs was reported in the early sixties [62A1]. It was found that the presence of oxygen during the growth of GaAs by the horizontal Bridgman method could induce very high resistivity and sometimes even semi-insulating material. The Hall effect measurements used to characterize these samples gave an activation energy of approximately 0.75 eV and an oxygen related level near mid-gap was postulated [86M1]. This began a long association of oxygen with EL2 that, although refuted in the late seventies [79H1, 88B1], on occasion still causes confusion. Readers of early papers on deep levels in GaAs are cautioned that the "O" level or ELO level is, in most cases, likely to be the EL2 level. This persisted even after the EL2 label was suggested in the general classification scheme of Martin *et al* [77M1].

The role of oxygen in the production of semi-insulating GaAs is now better understood. Oxygen is recognized as contributing in two ways to the semi-insulating property of GaAs but the factors that govern its influence are numerous and somewhat complex. One effect of oxygen, however, is clear; its presence during growth has the advantageous effect of gettering some of the important residual impurities [82M2, 88H1]. This is particularly significant for the Si_{Ga} donors that were present in high concentrations when quartz vessels were used in early growth techniques [82M2]. The reduction of the active silicon concentrations is so effective that the carbon acceptor, C_{As}, becomes the dominant residual impurity which then in turn is compensated by the EL2 [88H1]. It was likely this effect which led to the early association of oxygen with the deep level responsible for the semi-insulating behaviour of GaAs.

The issue was further clouded by the fact that there is also an oxygen related deep level, but the conditions under which it becomes present in significant quantities were not clear. It is now understood that it is virtually impossible to incorporate oxygen during horizontal Bridgman growth [82M2], unless the oxygen doping is very high [84L1]. In LEC grown GaAs, there have been many reports that hint that the water content of the boric oxide encapsulant is a crucial factor in determining whether or not oxygen is incorporated during this growth technique [82Y1, 86K1, 87T1, 89A1]. This question is, however, explicitly addressed in a paper that deals specifically with the effect of the water content of the B_2O_3 encapsulant [85E1]. This work, which for some reason is seldom referenced, reports that the use of "super dry" B_2O_3 (100 ppm H_2O) results in low oxygen concentrations of less than 3×10^{15} cm^{-3} whereas, in the material grown with wet B_2O_3 (2000 ppm H_2O), the oxygen concentration is high, between 6×10^{15} cm^{-3} and

2×10^{16} cm^{-3}. The main conclusion was that semi-insulating GaAs could be produced with a lower initial As atomic fraction when wet B_2O_3 was used. This was attributed not to the existence of oxygen related deep levels but to diffusion of excess Ga from the melt.

The above discussion shows that oxygen is still an important consideration in semi-insulating GaAs and many of the points will be relevant to the discussion of EL2 photoluminescence later in this chapter and in a subsequent results chapter. The actual confusion between EL2 and oxygen is well summarized in a review article by Martin and Makram-Ebeid [86M1]. The association of oxygen and EL2 had long been questioned on the basis of uncertainties in correlation between the concentrations of the two and the final refutation came when it was shown that the O concentrations were in fact much lower than that of the dominant midgap level. The oxygen related deep level was subsequently distinguished from the EL2 level in an elegant DLTS study whereby the difference in the electron capture cross sections of the two levels was exploited to resolve two otherwise overlapping electron emission features [84L1]. The resulting activation energies were 815 ± 2 meV for EL2 and 825 ± 5 meV for the oxygen level.

The confusion between oxygen and EL2 surfaced again recently in a series of events that serves to illustrate the danger inherent in associating optical quenching of an observed feature directly with EL2. The feature in question here is a pair of local vibrational modes (LVM) at 715 cm^{-1} and 730 cm^{-1} reported by Song *et al* that were observed to interconvert in a way that resembled the metastability of EL2 [87S1]. It was thus claimed that one of the LVMs was due to the ground state of

EL2 and the other, the metastable state. When it became clear that these LVMs were found only in oxygen-containing material, the idea that some EL2 centres are oxygen related and are called "EL2O" was resurrected from a much earlier work [88Z1]. The idea of a family of EL2 centres is commonly evoked to explain complexities in observed behaviour [83T1, 88M1, 91D1]. This is convenient but not often productive. The issue of the origin of the two LVMs has since been clarified and they are attributed to two charge states of a deep oxygen-related donor in the upper half of the gap. The interconversion is due to charge exchange with EL2. This is a good example of how the drastic change in the Fermi level caused by EL2 photo-quenching can indirectly affect many observable properties that are not directly related to EL2. This has also led to much confusion.

2.4.2 The Arsenic Antisite and EL2

Once it became clear that oxygen was not present in sufficient quantities to account for EL2, attention turned to the idea of native defects, if for no other reason than simply because no impurities could be found in concentrations that were consistently high enough [86M1]. The breakthrough came with the observation in as grown horizontal Bridgman bulk GaAs of a four line ESR spectrum which was identified with the paramagnetic arsenic antisite, $As_{Ga}{}^{+}$, in concentrations of approximately 10^{16} cm^{-3} [80W1, 82W1]. EPR can only detect the $As_{Ga}{}^{+}$ charge state because the neutral arsenic antisite, As_{Ga}, is diamagnetic and hence is EPR inactive. The analysis of the $As_{Ga}{}^{+}$ EPR spectrum gave an electron g-factor of 2.04 and indicated that the wavefunction was strongly localized at the antisite and its four neighbours implying that the As_{Ga}^+ defect formed a deep level [89K1].

This was confirmed by photo-ESR studies which showed that the As_{Ga}^+ defect is a double donor very similar to EL2 with its (0/+) level near midgap and (+/++) level about 1.0 eV below the conduction band [82W2]. The identification of the As_{Ga}^+ ESR defect with EL2 was strengthened when more detailed spectral dependence of the photo-ESR were shown to be virtually identical to the optical cross sections for EL2 [85B1, 85T1] and also showed the same characteristic photo-quenching property found for EL2 [89K1].

These results leave little doubt that the As_{Ga}^+ EPR is from the EL2 defect and it is now widely agreed that the EL2 defect is closely associated with As_{Ga} but an active controversy still exists as to whether it is the isolated As_{Ga} or complexed with other constituents [89K1]. The ESR spectrum was found to be isotropic which would indicate that the As_{Ga}^+ is isolated, but the technique is insufficiently sensitive to conclusively determine whether the antisite is isolated or not [82W1]. The next two sections present results that are difficult to reconcile. Optical absorption studies support the isolated As_{Ga} model and ODENDOR studies show that an arsenic interstitial, As_i, is paired with the As_{Ga}.

2.4.3 Optical Absorption and the Isolated As_{Ga}

The photo-quenching of EL2 into its metastable state occurs for photon energies $1.0\ \text{eV} \leq h\nu \leq 1.3\ \text{eV}$. By noting the difference between the photocurrent and absorption spectra, Kaminska *et al* [83K1] showed that this spectral region corresponded to an intracentre transition from the EL2 ground state to an excited state that is resonant with the conduction band. Spectrally, the transition is characterized by a wide band indicative of strong phonon coupling, and at low temperature the onset of the band is marked by fine structure consisting of a distinct no-phonon (NP) transition at 1.039 eV followed by 11 ± 1 meV phonon replicas. This was the first observation of a transition between two discrete states of EL2 and was at that time, the sharpest spectroscopic signature of the defect. Kaminska *et al.* quickly followed up their initial work with a study of the behaviour of the 1.039 eV NP line under the external perturbations of uniaxial stress and magnetic field [85K1].

The application of the magnetic field was found to induce no splitting or shifting of the NP line and it could only be concluded that the initial and final state were both spin singlets. The observed splittings under uniaxial stress were far more informative and represent one of the most important experimental findings in the study of EL2. The splittings were interpreted as evidence of a transition $A_1 \rightarrow T_2$ in T_d symmetry with a Jahn-Teller relaxation of the final state. They thus concluded that the EL2 defect ground state has full tetrahedral symmetry and in light of the EPR results must therefore be the isolated As_{Ga} [85K1].

This interpretation was met with some initial opposition and is still questioned by advocates of the As_{Ga}-As_i model [90S1]. Inconsistencies in the original reported data were exploited in a reinterpretation in which it was argued that the data was evidence of an orthorhombic centre with C_{2v} symmetry [87F1]. Subsequently, the experiment was reproduced [90T2, 88B2] and the results were shown to be consistent only with the original interpretation of Kaminska *et al.*

The issue has also been clouded by uncertainty over the nature of the final state of the transition, especially concerning the lattice relaxation involved [89B1, 90B1, 90D1]. It has been noted that the degree of phonon coupling that is indicated by the separation between the NP line and the centre of the intracentre absorption band is consistent with calculations of the lattice relaxation but is so strong that the NP line should be unobservable [90B1]. This problem is compounded by observations that the NP line and the centre of the band move in opposite directions under hydrostatic pressure [88B3]. Although much of the work on these problems has not questioned the validity of the isolated As_{Ga} interpretation, it has made it clear that a full understanding of the processes has not yet been achieved. On the other hand, calculations have been made which argue that the presence of the As_i would have been observable in the stress experiments and hence support the As_{Ga} interpretation of Kaminska [89B1, 89B2]. This has been countered with suggestions that the 1.039 eV NP absorption line is not from EL2 [90S1] despite very strong evidence linking the two [83K1, 86S1].

2.4.4 ODENDOR and the As_{Ga}- As_i Pair

The As_{Ga}- As_i pair model has been proposed by several authors. Using experimental results obtained with ESR, DLTS and thermal treatments, von Bardeleben *et al* then used thermodynamical arguments to identify EL2 as an As_{Ga}- As_i pair [86B1]. These results were disputed on several grounds. It was suggested that both the samples and techniques used were abnormal and the thermodynamical arguments were naive [87G1]. Uniaxial stress has been used in conjunction with DLTS and the results were said to be consistent with an axial defect such as the As_{Ga}- As_i pair but it was also noted that there was a very strong isotropic coupling of the defect to the lattice. [87N1] The transient photocapacitance quenching of EL2 has also been studied under uniaxial stress and the results were interpreted as evidence that the site symmetry was C_{3v}, consistent with the As_{Ga}- As_i model [87L1]. This experiment, however, is bound to reflect the the distortion of the final state and hence it is difficult to make any conclusions on the symmetry of the initial ground state. The conclusions of this experiment were in fact based on the argument that the isolated As_{Ga} is not expected to undergo any symmetry-lowering distortion. The most direct and frequently cited evidence in favour of the As_{Ga}- As_i model is, however, the ODENDOR study of Meyer *et al* [87M1].

In the first report of ODENDOR studies of the As_{Ga}^+ EPR, it was suggested that in addition to the isolated As_{Ga}, there were additional As_{Ga} complexes that were obscured under the isolated As_{Ga} signal [84H1]. Improved samples and experimental conditions led them to revise this interpretation in a later study [87M1]. Here it was concluded that the all the ODENDOR lines belong to the same defect. The previously noted additional lines were studied in greater detail and were attributed to the presence of an As_i situated 1.5 bond lengths along the [111] anti-bonding direction giving a As_{Ga}- As_i pair with C_{3v} symmetry.

The optical signal used in these experiments is the magnetic circular dichroism absorption (MCDA) and it is not clear that this is, in fact, an EL2 process. The ODENDOR work was preceded by a study of the MCDA which included optically detected EPR using the MCDA [84M1]. Here it was argued that the MCDA does not arise from EL2; the inferred energy levels were attributed to $A_1 \rightarrow T_2$ transitions (ground state to an excited state resonant with the conduction band) and did not agree with the EL2 levels. Shortly thereafter, they published their first ODENDOR results [84H1]. These results were interpreted as being from the isolated As_{Ga} and since the same MCDA was used, the indication is that EL2 is not the isolated As_{Ga}. In a subsequent paper, they give evidence that the same ODENDOR lines are in fact EL2 related, but now attribute them to the As_{Ga}- As_i pair [87M1].

To confuse matters even more, Kaufmann, [84K1] questioned the first interpretation of the MCDA and argued that the integrated MCDA did closely resemble the EL2 optical cross sections reported by Chantre, Bois and Vincent [81C1]. Subsequently, calculations by Kaufmann and Windscheif showed that photoneutralization of the isolated As_{Ga}, $As_{Ga}^{+} + h\nu \rightarrow As_{Ga}$ + hole, can account for the MCDA [88K1]. This controversy has cast some doubt on the ODENDOR results [90T2].

It has also been noted that the interpretation of ODENDOR is complicated and indirect in comparison to uniaxial stress [89B2, 90T2]. There has also been speculation that the portion of the ODENDOR results that indicate the presence of the As_i may arise from an As_{Ga} complex that is present in lower concentrations than EL2 [89D2].

2.4.5 Theoretical Support for the Two Models

When it became clear that the EL2 defect involved As_{Ga}, there was initial skepticism that it could be the isolated As_{Ga}, primarily on the grounds that it was not believed that the simple antisite could give rise to metastable behaviour [86B1]. This led to speculation that the As_{Ga} is present as part of a complex defect [87B1] and this undoubtedly motivated many As_{Ga}-X models, where X can be an As_i, an arsenic vacancy (V_{As}) [87W1], or even oxygen again [83T1].

Early electronic structure calculations on the isolated As_{Ga} revealed that the separation between the (0/+) and (+/++) levels were comparable to that found for EL2, but suggested that lattice relaxation effects were unlikely [83B2]. The situation changed dramatically with the simultaneous publication of two independent calculations that showed that the isolated As_{Ga} could be distorted by optical excitation to an optically inactive neutral metastable state [88C1, 88D1].

Both proposed that the normal state consists of the As_{Ga} bonded four-fold to its nearest neighbour arsenic atoms and that the metastable state arises from a distortion of the As_{Ga}. They show that this configuration could be optically achieved by a process in which one of the four bonds is broken and the As_{Ga} is displaced in the opposite direction to the broken bond and passes through the plane formed by the three other nearest neighbour arsenic atoms, becoming three-fold bonded to them. Both papers also give values for the thermal recovery barrier encountered in the transition back to the normal state that are in close agreement with the observed value.

These papers were followed by others which further compared the

As_{Ga} calculations with observed properties of EL2 [89D1, 89D2] and have led to much acceptance of the isolated As_{Ga} model of EL2. One major remaining problem is in understanding the nature of the final state of the intracentre transition. As mentioned previously, the separation between the 1.039 eV NP line of the infrared absorption and the peak of the band at 1.18 eV indicates that if the lattice relaxation phonon is the observed 11 meV local mode, then the phonon coupling as given by the Huang-Rhys factor would be so strong as to render the NP line completely unobservable. This problem is compounded by observations that under hydrostatic pressure, the NP line and the band are observed to move in opposite directions with the NP line in fact moving over the band [88B3]. Progress has been made towards understanding these problems [90B1, 90D1] but they have not been fully resolved.

Similarly, calculations have been performed on the As_{Ga}- As_i pair in a variety of configurations [87D1, 87B1, 88B4]. Of these, only one [88B4] is compatible with the ODENDOR results in that the As_i is separated from the As_{Ga} by 1.5 bond lengths along the [111] anti-bonding direction. Although this model does account for the metastability of EL2 and is useful in explaining other observed behaviour by including two distinct electronic transitions to the metastable state, it also raises two serious questions about the viability of the As_{Ga}- As_i model.

These calculations, and subsequent ones [88D2], show that the As_{Ga}- As_i has a shallow donor level in the gap. There have been some experimental suggestion that such a level exists [83S1, 83W1], but this has never been generally accepted. The work presented in this thesis will show that there is in fact a hydrogenic excited shallow donor-like state of EL2, but it is quite different from that predicted or previously reported. A second problem with the As_{Ga}- As_i model is that there is no apparent mechanism for the binding of the As_i with the As_{Ga} making the formation of such a defect in the required concentrations very implausible [88B4].

Both of these models of EL2 have hence been shown to be consistent with the observed deep levels in the gap and can produce the necessary metastable state. Yet minor incongruities are seen to exist for both. It is clear that more work needs to be done to resolve these questions and that new experimental avenues must be pursued to resolve the conflict between the absorption under uniaxial stress and the ODENDOR results.

2.5 Photoluminescence of EL2

The literature on the photoluminescence (PL) of EL2 is much like a microcosm of the larger EL2 story itself. It is full of the same confusion, controversy and contradiction. The themes of oxygen in GaAs, identifying features as EL2 related on the basis of observed quenching behaviour, and uncertainty on the nature of the transitions involved are all present.

The long wavelength or deep PL of semi-insulating GaAs is dominated by broad bands, the centres of which are found anywhere between 0.63 eV and 0.68 eV [86M1, 88B1, 89K1]. The study of these bands has been beset with problems largely because their broad and typically featureless nature has made them difficult to identify and characterize.

Nonetheless, they have often been associated with EL2 because of their peak energies, photo-quenching behaviour and usual presence in semi-insulating material.

The bands can roughly be separated into two classes, one with peaks in the range of 0.67 eV and 0.68 eV and the other with peaks between 0.63 eV and 0.65 eV.

When it was becoming clear that EL2 was not oxygen-related the origin of commonly observed deep PL bands began to be re-evaluated. On the basis of its peak energy and width, a band at 0.645 eV, which was previously thought to be oxygen related [79Y1], was instead attributed to recombination of a free hole at neutral EL2, (h, $EL2^0$) by Mircea-Roussel and Makram-Ebeid [81M1]. Subsequent work showed that a broad band, this time reported at 0.65 eV, could be quenched under 1.06 μm (1.17 eV) excitation, the characteristic optical quenching wavelength of EL2 [82L1]. This reinforced the identification of this band with EL2 and the authors agreed that the process was (h, $EL2^0$) recombination.

Shortly thereafter, Shanabrook *et al.* [83S1] reported work on bands at 0.635 eV and 0.68 eV. The 0.635 eV band was assumed to be the same band as in the two above mentioned works and they attributed this luminescence to recombination between the deep donor and shallow acceptors and the 0.68 eV band was instead the (h, $EL2^0$) recombination. The latter conclusion was in agreement with an earlier suggestion of Yu [82Y2]. The identification of the deeper band with EL2, however, was challenged by Yu and Walter [82Y1].

They showed in a systematic study that oxygen doping consistently gave rise to a band at 0.63 eV that is dominant at liquid helium temperatures. The evidence that the 0.63 eV band was not EL2-related was strengthened when it was found that the quenching of the 0.635 eV band was not observed when exciting with above gap excitation after the exposure to 1.06 μm light. The previously observed quenching for below bandgap excitation was explained as due to the fact that neutral EL2 provided an excitation path for longer wavelength photons that is lost when the EL2 is quenched [84S1].

Despite the evidence that the deeper, ≃ 0.65 eV, band was oxygen related many more EL2-related processes were suggested for it and the 0.68 eV band. This is perhaps because of the uncertainty of the role of oxygen in semi-insulating GaAs and the vague character of the bands. Nonetheless, many contradictory theories abounded. Martin and Makram-Ebeid proposed transitions from a relatively deep EL2 excited state to the ground state for the deeper band and recombination of a conduction band electron at ionized EL2, (e, $EL2^+$) for the 0.68 eV band [86M1]. A similar view of the 0.68 eV band was taken by Von Bardeleben *et al.* but they proposed that the ≃ 0.65 eV band was due to recombination between neutral EL2 and the double acceptor Ga_{As} [88B1].

Progress was made when a weak NP line and 11 meV phonon replicas were resolved on the 0.68 eV band [86T1]. Tajima followed up his discovery of this structure by comparing the PLE spectra of the two bands with the optical cross sections of EL2. He concluded that the 0.68 eV band was (h, $EL2^0$) recombination and the 0.63 eV band was due to oxygen when present and to (e, $EL2^+$) otherwise [87T1, 87T2]. Although this was at the time the clearest account yet of the deep PL processes in semi-insulating GaAs, it too was not without its detractors. Kaminska noted that the PLE spectrum of the 0.68 eV band was similar to the integrated MCDA spectrum and she argued that the transition responsible was from an excited state of $EL2^+$ to the $EL2^+$ ground state [88K2].

2.6 The Relevance of this Work

The results presented in this thesis clarify without question the origin of these deep PL bands in semi-insulating GaAs and the transitions involved in the EL2-related bands will be unequivocally identified. A band centred at 0.61 eV is clearly distinguished from the oxygen band at 0.65 eV. Fine structure in the 0.61 eV band reveals that at liquid helium temperatures this band results from an electron in a shallow, hydrogenic bound state dropping into the EL2 ground state ($EL2^0_{n=2} \rightarrow EL2^0_{n=1}$), whereas at higher temperatures ($T > 30$ K) the free-to-bound (e, $EL2^+$) transitions begin to dominate the spectrum. The results on the structured 0.68 eV band reported by Tajima reveal that at low temperature it is not (h, $EL2^0$) but rather a donor-acceptor pair transition ($EL2^0$, A^0) typically involving carbon. At $T > 35$ K, this switches over to (h, $EL2^0$) [90N1].

The fine structure on the 0.61 eV band has a much narrower line width than the 1.039 eV NP absorption line and also arises from a much simpler transition. This has been exploited in the studies of its behaviour under uniaxial stress and magnetic field which are described here. The results strongly favour the isolated As_{Ga} model for EL2 [91N1].

CHAPTER 3. EXPERIMENTAL

3.1 Introduction

High performance photoluminescence spectroscopy requires a multitude of complex and sophisticated equipment. On a basic level, however, the essential equipment can be separated into four categories. It is useful to keep the samples at temperatures near absolute zero so that in the absence of any excitation, they are near the crystal ground state. This is accomplished by mounting the samples in an optical cryostat where the samples are cooled by liquid helium or cold helium gas. There must also be an excitation source. This is typically a laser, which provides an intense source of photons of known energy and, in the case of a tunable laser, control of the photon energy as well. The emitted luminescence is then collected into a spectrometer where it is spectrally analyzed in some fashion. The final element is the detection of the spectrally processed light that leaves the spectrometer.

The deep level photoluminescence bands in GaAs which are the focus of this work fall in the energy range between 0.5 eV and 0.7 eV or in terms of wavelengths, between 2.5 μm and 1.6 μm. Some of them are quite intense and others are very weak. This is in contrast to the near-gap PL of this material where the intensities are generally very high and the wavelengths are shorter than 1.0 μm which is within the range of very sensitive photon-counting detectors. The technique of Fourier transform spectroscopy (FTS) has many advantages over the diffraction grating spectroscopy typically used for the study of near-gap PL. This is particularly true for the wavlengths where no photon-counting detectors are available.

With the exception of some photoluminescence excitation (PLE) spectroscopy, all the results reported here were obtained by using a Fourier transform interferometer. The first part of this chapter will focus on this technique and the particular instrument used. This will be followed by a discussion of the detection system, the excitation sources, the cryostats, various specific measurements and the samples themselves.

3.2 Fourier Transform Spectroscopy

Fourier transform spectroscopy is a well established technique, especially in the mid and far-infrared regions. This is especially true in the field of semiconductor spectroscopy where FTS has been extensively used to study the absorption spectra of the shallow donors and acceptors. Very little use, however, of FTS methods have been made in photoluminescence spectroscopy and for this reason some of the basic principles of FTS will be reviewed here in the context of PL spectroscopy. A detailed treatment of FTS is certainly beyond the scope of this thesis and readers who are interested in more details are referred to the reasonably complete and current book by Griffiths and de Haseth [86G1].

It is useful, before going any further, to clarify the choice of units used throughout this thesis. In grating spectroscopy it is convenient to collect the data as a function of wavelength. This is not the case in FTS where the spectra are collected as a function of wavenumbers,

$$\bar{\nu} = 1/\lambda, \qquad 3.1$$

where λ is the wavelength of light with photon energy, $h\nu$. The standard unit of wavenumbers is the inverse centimeter or cm^{-1}. The conventional notation is perhaps confusing, but the energy in wavenumbers is related to the photon frequency, ν, by $\nu = c\,\bar{\nu}$ where c is the speed of light. Another convention is the use of the electron volt, eV, or milli-electron volt, meV, as the standard unit of energy in semiconductor spectroscopy. The energy in meV is related to wavenumbers by

$$E(\mathrm{meV}) = h\,c\,\bar{\nu}(\mathrm{cm}^{-1}) = \bar{\nu}(\mathrm{cm}^{-1}) \,/\, 8.065541. \qquad 3.2$$

To conform with this latter convention and to allow ready comparison of the results presented in subsequent chapters to those reviewed in Chapter 2, all the spectra will be presented as a function of $h\nu$ in meV.

The simplest optical layout of an FT interferometer is just that of a Michelson interferometer as shown in Figure 3.1. Incident light is split and sent into the two arms of the interferometer by the beamsplitter, and then reflected back through the beamsplitter where the two beams recombine. One of the two mirrors is fixed at some distance L from the centre of the beamsplitter and the other moves at a constant velocity about a point also at the same distance L from the beamsplitter. If at time t = 0, the moving mirror is at L and moving away from the beamsplitter with velocity, v, the path difference for the

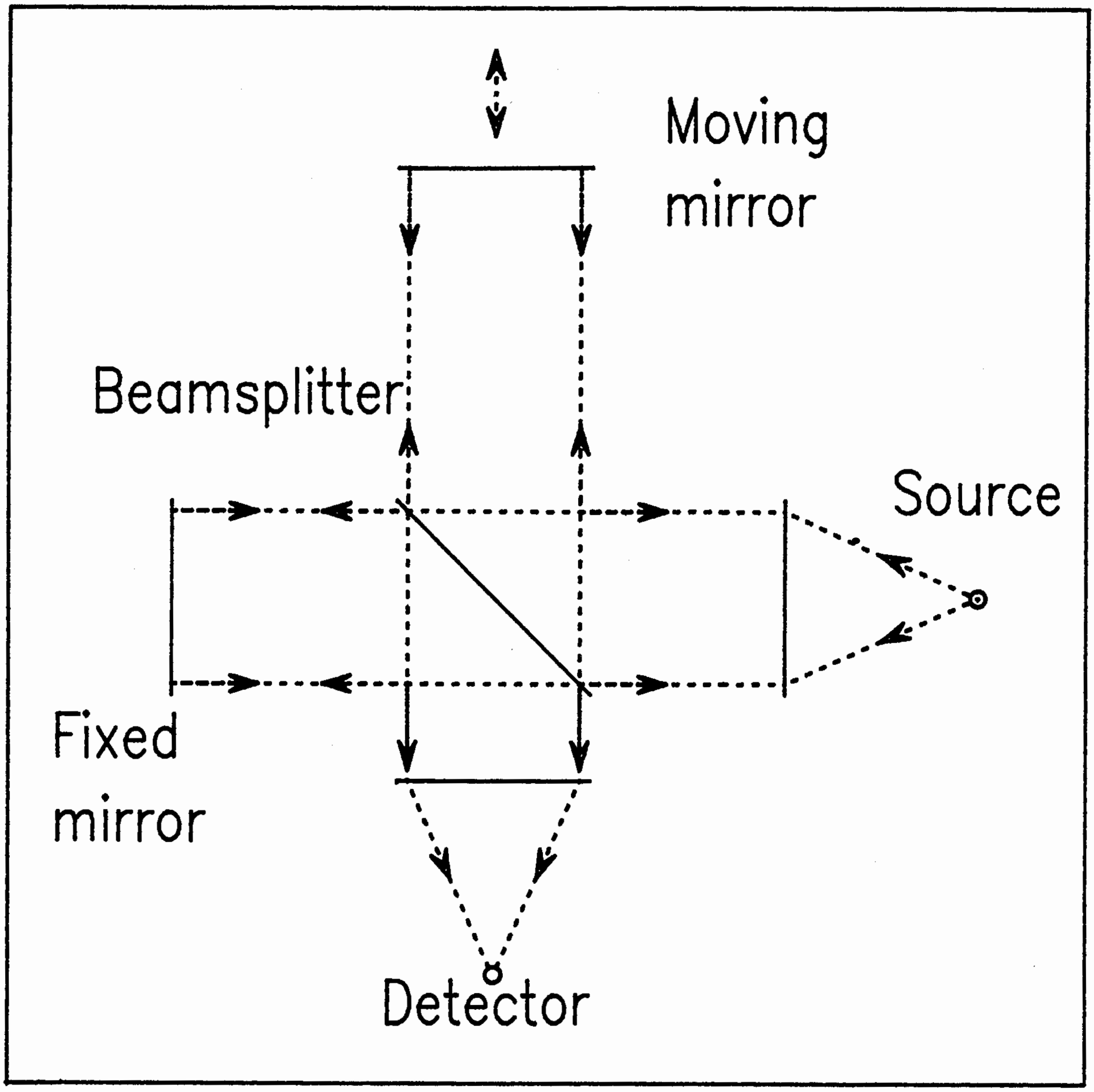

Figure 3.1

The optical layout of a simple Michelson interferometer. The arrows indicate the direction of the light traversing the interferometer. Note that for an ideal beamsplitter, half of the light returns to the source and is lost.

two beams when they recombine is $\delta = 2\upsilon t$.

With this simple picture of an interferometer the basic ideas of FTS can be outlined. The ac signal from the interference of the recombined beams at the detector is measured as a function of the path difference δ and is called the interferogram, $I(\delta)$. For monochromatic light of wavenumber $\bar{\nu}_0$ passing through an ideal interferometer, the signal is modulated sinusoidally as the conditions for constructive and destructive interference are successively met. The interferogram is

$$I(\delta) = 0.5\, I(\bar{\nu}_0) \cos 2\pi\bar{\nu}_0\delta = 0.5\, I(\bar{\nu}_0) \cos 2\pi f_e t \tag{3.3}$$

where $f_e = 2\upsilon\bar{\nu}_0$ is the electronic frequency that corresponds to the measured interference from light of wavenumber $\bar{\nu}_0$ at a given mirror velocity υ. The crucial point here is that the spectrum, $I(\bar{\nu}_0)$, can be recovered by performing a cosine Fourier transform on the measured interferogram $I(\delta)$. Any spectrum, however, can be thought of as a superposition of discrete wavelengths, each of which will have a distinct cosine interference pattern with an amplitude proportional to the intensity at the given wavelength. The interferogram for such a spectrum will just be the continuous sum of these cosine terms and the spectrum can still be recovered by performing the cosine Fourier transform on the interferogram.

For a given velocity of the moving mirror, the time taken for an individual scan is determined by the maximum displacement of the mirror. For a perfectly monochromatic source, however, the true spectrum could only be obtained if the mirror travelled infinitely far from the point of zero path difference (ZPD) between the two mirrors. In reality of course the mirror moves only a finite distance, ℓ, giving a maximum path difference, $\delta_{max} = 2\ell$. The resulting lineshape obtained from a monochromatic source described by $I(\bar{\nu}_0)$, is then given by

$$S(\bar{\nu}) = 2\delta_{max} I(\bar{\nu}_0) \text{ sinc } [2\pi(\bar{\nu}_0-\bar{\nu})\delta_{max}] \qquad 3.4$$

where sinc(x) = sin(x)/x is the sinc function. The measured spectrum will then consist of a central peak at $\bar{\nu}_0$ with side lobes that oscillate about S = 0 and successively decay with increasing distance from $\bar{\nu} = \bar{\nu}_0$. The first zero crossings on either side of the central peak are separated by $\Delta\bar{\nu} = 1/\delta_{max}$ which gives a measure of the line broadening that results from the finite path difference of the interferometer. This simple argument shows that the quantity that fundamentally determines the maximum spectral resolution is the maximum path difference, δ_{max}. The resolution is simply proportional to the maximum path difference δ_{max}. The above discussion, however, gives only the upper limit on the maximum resolution obtainable, since two other factors are also important in determining the actual resolution.

The unavoidable truncation of the interferogram at δ_{max} is equivalent to multiplying the interferogram by a function which is equal to one for $\delta \leq \delta_{max}$ and is equal to 0 for $\delta > \delta_{max}$. This is called boxcar truncation and although it gives the highest resolution for a given δ_{max}, it has some undesirable consequences. These can be understood by considering the strong oscillatory nature of the sinc function which would give spurious side lobes and negative undershoots to a spectrally narrow feature in the spectrum if δ_{max} does not extend far enough.

To circumvent this problem, the interferogram is typically multiplied by another function. This is called apodization and serves to reduce or remove the strong oscillatory side lobes of the sinc function. The standard apodizing functions are chosen so as to taper the interferogram down to zero at δ_{max} more gradually than the boxcar truncation. The simplest apodizing function is known as triangular apodization and is the line that passes through one at $\delta = 0$ and zero at $\delta = \delta_{max}$. The resulting lineshape from a monochromatic source is then

$$S(\bar{\nu}) = \delta_{max} I(\bar{\nu}_0) \operatorname{sinc}^2 [\pi(\bar{\nu}_0-\bar{\nu})\delta_{max}]. \qquad 3.5$$

The side lobes are much reduced with no negative undershoot but the linewidth has been increased as can be recognized by noting that the zero-points are now separated by $\Delta\bar{\nu} = 2/\delta_{max}$. This reflects the fact that the linewidth invariably increases from apodization and illustrates the trade-off between lineshape and resolution that must be made when choosing an apodizing function. The side lobes are reduced at the cost of reduced resolution. The cost in the resolution is not as severe as it first seems from the increase noted in the separation of the zero-crossings. The full width of the line at the half maximum points (FWHM) is a better measure of the resolution and triangular apodization results in an increase in the FWHM of just below fifty percent [86G1].

The above discussion implicitly assumes that the light traversing the interferometer is perfectly collimated. This too is not possible and is a further limitation to the attainable resolution. Assuming perfect optical surfaces, the collimation of the light beam is determined by the f-number of the optics and the entrance or exit aperture. Qualitatively, the effect can be understood by considering the path difference between a purely axial ray and a ray from an extreme edge of the aperture to the centre of the collimating mirror. If this path difference is greater than half a wavelength, the interference will be lost. It can easily be shown [86G1] that the maximum allowed beam divergence, α_{max}, for a given resolution is approximately

$$\alpha_{max} \cong (\Delta\bar{\nu} / \bar{\nu}_{max})^{1/2} \qquad 3.6$$

where $\bar{\nu}_{max}$ is the maximum wavenumber at which the chosen resolution is needed. Thus for a given wavelength of light an increase in resolution can only be obtained if the aperture is suffiently small. This restriction is obviously more severe for shorter wavelengths. These three factors, the distance from zero path difference that the mirror travels, the apodization and the aperture size, are the major constraints on the resolution.

It was convenient to introduce the relation between the interferogram and the spectrum for the simple case of monochromatic light and then extend the argument to the polychromatic case. Although the extension seems like a very unspectacular result that follows simply from the principle of superposition, it is responsible for one of the main advantages of Fourier transform interferometry. The significance is that all the spectral information is obtained simultaneously in contrast to most dispersive techniques where each spectral element is obtained separately. This is known as the multiplex or Fellget advantage.

If the major source of noise is detector noise, then the multiplex advantage will give an increase in the signal-to-noise ratio (SNR) by a factor approaching $\sqrt{N}$ where N is the number of resolution elements in the spectrum [86G1]. Since there are no photon-counting detectors available for the wavelengths of light typical of the deep level PL studied here, ≅ 1.5 μm to 3.0 μm, detector noise is unavoidable. Typical spectra contained ≅ 3000 resolution elements so the multiplex advantage would ideally give rise to an increase of ≅ 55 in the SNR.

The real multiplex advantage will certainly be less than this because noises other than detector noise are present. The most problematic source of noise in Fourier transform spectroscopy is flicker noise or fluctuation noise in the source intensity. If severe enough, this can cause a disadvantage which can completely negate the multiplex advantage. For this reason, great care is taken to minimize flicker noise. This will be discussed in greater detail in a following section.

The other often mentioned advantage of FTS is the throughput or Jacquinot advantage. Although the desired resolution does place an upper limit on the size of the entrance or exit aperture, this restriction does not affect the optical throughput as severely as is the case for a grating spectrometer where the apertures are typically two or three orders of magnitude smaller for the same resolution. An exact value for the throughput advantage depends on the spectral region and the details of the two instruments being compared, but Griffiths and de Haseth give a throughput advantage of well over 200 near 0.5 eV [86G1].

The multiplex and throughput advantages describe the increased sensitivity available with interferometry. Another advantage is the inherent high accuracy and precision of FT interferometers. Modern interferometers are equipped with a stabilized single mode He-Ne laser that is collinear with the IR optical path through the beamsplitter and the fixed and moving mirrors. The sampling of the interferogram is triggered by the He-Ne interference fringes so the path difference is very precisely measured and this precision is carried through to the spectrum. The accuracy of the energy scale is most dependent on the alignment of the IR beam with the He-Ne laser. A recent test on the calibration of the FT spectrometer used for this work gave an accuracy of 0.002 cm^{-1}.

Like any spectrometer, a FT spectrometer has an instrumental response function that depends on the nature of the components in the optical path. The most important of these include windows, beamsplitter, filters and detector. The instrumental response can vary quite dramatically over a large energy range and when displaying spectra which cover such a large energy range it is necessary to correct for this. For emission spectroscopy like PL, the spectra can be corrected by dividing by a white light spectrum which has been obtained through the same optical path.

While FTS has many advantages, there are clearly aspects of it that have made it less desirable to the PL spectroscopist than the much more common grating spectrometers. By its very nature, FTS does not provide a direct measurement of the spectrum and caution must be exercised to distinguish possible artifacts arising in the transformation of the interferogram into a spectrum. A common example of these are known as phase errors.

In a perfect interferometer the interferogram is always an even function and it is the cosine Fourier transform of the spectrum. In a real interferometer, however, factors other than the displacement of the moving mirror contribute to the phase difference of the light traversing the two arms. For instance, optical dispersion due to the finite thickness of the beamsplitter can introduce a wavenumber dependent phase difference that will be unequal in the two arms of the interferometer.

This is especially true for the shorter wavelength regions from the mid-infrared through the visible where the beamsplitters consist of a dielectric coating on a transparent substrate. In order to minimize the phase difference caused by the substrate, a compensating thickness of the substrate material is placed in the other arm of the interferometer, but perfect compensation is never achieved. Other factors that introduce phase differences that are independent of the position of the moving mirror are sampling errors and the frequency dependence of the detector and the electronic amplifiers and filters used in the data acquisition.

The result of these phase variations is to introduce sine components into the interferogram that can have severe effects if not properly corrected for. Errors in the phase correction can cause a sharp emission line to have a derivative shape or even invert it into a negative feature. The phase could be rigorously accounted for by collecting an interferogram with an equal number of data points on each side of the zero path difference point and then calculating the full complex Fourier transform. This gives a complex function of which the real and imaginary parts correspond to the cosine and sine Fourier components, respectively. The phase angle as a function of the wavenumber, $\theta(\bar{\nu})$, can then be calculated by taking the arctangent of the ratio of the sine and cosine components at each data point which can then be used to obtain the real spectrum.

In practice this kind of detailed phase correction is never done; the interferometer would have to be much larger than is the case for single sided interferograms and the number of calculations would be prohibitively large. Instead, the fact that the phase is generally a slowly varying function of wavenumber is used to advantage and only a small, low resolution double sided interferogram is collected and the phase information is interpolated to higher resolution.

Once the variation of the phase with respect to wavenumber is known, two distinct methods of correcting the spectra are available. The most common and straightforward is the Mertz method whereby the cosine and sine components of the spectrum are corrected and added to give the true spectrum after the Fourier transformation. In the Forman method, the phase, $\theta(\bar{\nu})$, is Fourier transformed to give $\theta(\delta)$ which is then convolved with the full interferogram to give a phase corrected, symmetric interferogram from which the spectrum can be obtained with only a cosine Fourier transform. The difficulty in Forman phase correction is in efficiently calculating the convolutions, but it offers the advantage of numerical filtering since the Fourier transformation of $\theta(\bar{\nu})$ into $\theta(\delta)$ can be done over a selected range of wavenumbers which allows for much smaller data files and faster transforms once the interferogram is phase corrected.

Beyond the indirectness, the most obvious disadvantage of interferometry for PL is the lack of any inherent ability to reject the intense laser light that is used for excitation. This is in stark contrast to the nature of dispersive techniques where only one resolution element is allowed to pass to the detector at any given time.

This disadvantage can be largely overcome by the use of appropriate filters that block the laser but still pass the luminescence. The flexibility that is offered by a grating spectrometer would, however, require a prohibitively large selection of filters.

One of the great conveniences offered by a grating spectrometer is the ability to choose a wavelength or range of wavelengths and vary other parameters to monitor the effects on the selected luminescence. A good example of this is photoluminescence excitation (PLE) spectroscopy. In this technique, the spectrometer can be set to any PL feature of interest and the excitation wavelength can be varied over any region with the exclusion of the wavelengths open to the spectrometer. In this way an excitation spectrum for any PL feature may be obtained, depending of course on the strength of the feature. Dispersive techniques also lend themselves much more naturally to the measurement of the luminescence lifetimes and to time resolved spectroscopy.

In addition to their relative simplicity, dispersive spectrometers are also less expensive. They are certainly adequate for many PL applications, but when broad spectra and/or high resolution is required, especially for wavelengths for which no photon-counting detectors are available, FTS has a very significant advantage.

3.3 The BOMEM DA3.01 FT Interferometer

The interferometer used for this work is a BOMEM DA3.01 [BM] which has been modified to perform photoluminescence spectroscopy. The optical layout is depicted in Figure 3.2. The modifications allow the interferometer to be run with the luminescence traversing the IR path in the opposite direction from the normal use of the instrument in absorption spectroscopy.

As shown in Figure 3.2, the DA3 has a two position mirror which selects an optical path from either the internal sources which are intended primarily for absorption spectroscopy, or alternatively, from what is called the emission port. The manufacturer's intention was that the emission port could then be chosen as an external source with all the detectors housed in a separate compartment designed for that purpose. Rather than using this configuration, it was found to be practical to place the PL detectors at the emission port and essentially run the interferometer backwards.

The luminescence is collected and collimated by a 30 cm focal length off-axis paraboloid mirror and sent into the interferometer through a quartz window on one of the side ports. Once it is modulated, the luminescence is then refocused by another 30 cm focal length off-axis paraboloid mirror and sent out through a CaF_2 window to the detector at the emission port. The focus of this second paraboloid mirror is just outside the CaF_2 window and an iris has been placed there to allow for the selection of an aperture diameter appropriate for the chosen resolution. The PL detector assembly is attached to the outside of the interferometer and consists of a small compartment for optical filters and an off-axis ellipsoid mirror to focus the luminescence onto the detector.

One very convenient result of this arrangement is that the internal sources can be selected so that the sample can be illuminated with light from a quartz halogen lamp. This allows for very rapid location and tight focus of the collection mirror. For this work, a Schott [SC] KG-5

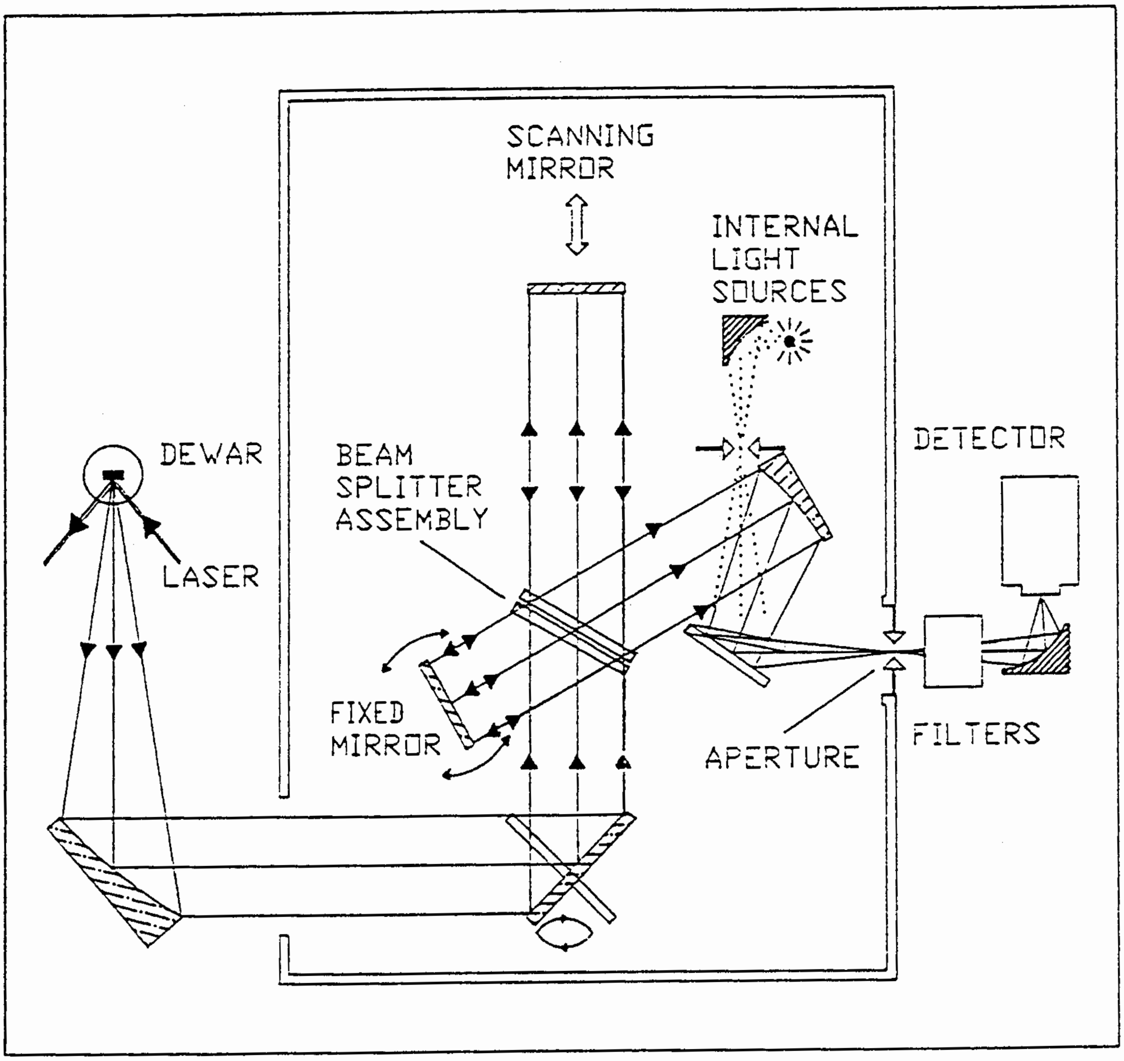

Figure 3.2
Schematic of the optical layout of the Bomem DA3.01 as operated for PL spectroscopy. The dotted lines indicate the path taken for the internal light sources when selected. The arrows near the fixed mirror are related to the dynamic alignment system.

glass filter was placed in the optical path from the internal source compartment. This filter is transparent in the visible but blocks the near infrared radiation that would optically quench the EL2.

Sending the collimated PL into the interferometer through the side port also allowed for greater distance between the sample cryostat and the instrument. This extra room gives much greater versatility and even allowed for the collection of luminescence from cryostats in different locations, such as a superconducting magnet cryostat which by necessity must be far away because of the high magnetic fields.

To study a given range of wavelengths with an interferometer, the appropriate beamsplitter must be chosen. The reflecting surface should have a reflectivity of close to fifty percent and the entire beamsplitter should be transparent over the selected spectral range. The early work presented here was done with a quartz substrate beamsplitter which is very efficient for wavelengths of 1.2 μm and shorter and is adequate out to approximately 2 μm, with the exception of an absorption band near 1.3 μm. This beamsplitter was extremely useful for collecting very broad spectra extending over the entire region starting from the deep PL at ≅ 2.5 μm, right out to the near gap PL at 815 nm. For some of the later work that concentrated only on the deep PL a CaF_2 beamsplitter was used. It is efficient between 1 and 10 μm and is considerably better than the quartz between 1.5 and 2.5 μm, but is especially useful for spectra which extend out past 2.5 μm where the quartz has a strong absorption band.

In addition to the straight-forward and minimal modifications, the BOMEM DA series of interferometers are particularly suited for PL in several ways. The most significant of these is the dynamic alignment system that keeps the moving and fixed mirrors aligned so as to maintain interference under conditions where other interferometers have practically no modulation.

The development of interferometry has been motivated largely by its usefulness in the mid to far-infrared regions where the wavelengths are of the order of 10 μm and longer. These long wavelength applications did not place great demands on the relative alignment of the fixed and moving mirrors unless very high resolution was required. The PL of most semiconductors is in the near infrared and the wavelengths are as long as ≅ 3 μm and usually much shorter, down to 815 nm for near-gap PL from GaAs. The alignment of the interferometer mirrors is therefore far more crucial if high modulation efficiency is to be attained.

The dynamic alignment system found on the BOMEM DA series of interferometers operates by continually reorienting the fixed mirror so as to maintain alignment with the moving mirror. It consists of a single mode He-Ne laser with its beam expanded and collimated into a ≅ 1 inch diameter which then passes through the interferometer. After the He-Ne beam has recombined at the beamsplitter, an array of photo-diodes monitor the intensity across the expanded beam and servos two motors which adjust the angle of the "fixed" mirror so as to maintain one interference fringe over the width of the He-Ne beam. This system allows the DA interferometers to operate into the near ultraviolet region of the electromagnetic spectrum and ensures very high modulation efficiency in the near-infrared.

The dynamic alignment system also allows for larger mirrors to be used in the interferometer. This is simply because alignment across a larger surface is more difficult to maintain. The throughput of an interferometer is directly proportional to the mirror area so this is yet another advantage that is very crucial, especially when studying a system with weak PL.

The dynamic alignment also allows the collection of extremely high resolution data since the mirror alignment is maintained even over large δ. Resolution as high as 0.01 cm^{-1} is possible on the DA3.01, but this resolution was not necessary for the work reported here. The highest resolution used was 0.5 cm^{-1}. More typically, the highest resolution necessary was 1.0 cm^{-1} at which point the detector size, rather than the aperture, limited the throughput.

The BOMEM interferometers are also the only commercially available instruments that make use of the Forman phase correction method. This is made possible by a computer board that is dedicated to performing the digital convolution of the uncorrected interferogram with the phase correction in real time. The concomitant numerical filtering capabilities greatly reduced the time taken for the Fourier transforms of near infrared PL spectra as compared to a Bruker IFS-113 which was used in our lab before the acquisition of the BOMEM.

3.4 Detectors and Filters

The advantages of FTS for the PL spectroscopy of deep levels have been pointed out in previous sections. High quality results are still, however, very much contingent on the use of a sensitive detector which covers the appropriate spectral range. It is also important to restrict the radiation reaching the detector to the spectral region of interest, especially if very intense sources are present which lie outside of this region but still within the range of the detector. Since an interferometer offers practically no inherent rejection, filters are thus a very important component in the detection system.

All the work reported here was obtained with a liquid nitrogen cooled InSb photodiode. The detector is mounted on a hybrid flat-pack which includes a cooled dual J-FET pre-amplification stage. The feed-back resistor of this stage can be set at 10^7, 10^8, or 10^9 Ω by changing soldered connections to the flat-pack. This allows some interplay between the sensitivity and time response of the detector. The high frequency cut-off is approximately 6 kHz, 2 kHz and 600 Hz for the above three feed-back resistors, respectively. The 6 kHz cut-off from the 10^7 Ω feed-back resistor was, as it turned out, sufficiently fast to measure the lifetime of the EL2 PL. For the spectroscopy, however, the increased SNR obtained with the higher resistors was exploited.

The signal from the detector is fed into another pre-amplifier that was supplied with the detector. This was usually followed by yet another stage of amplification to ensure adequate voltage at the analogue to digital converter on the BOMEM. This last stage also included some electronic filtering to reduce high and low frequency noise.

The bandgap of the InSb detector corresponds to a wavelength of approximately 5.5 μm which at first glance should allow sensitivity from the visible to just beyond 2000 cm^{-1}. The room temperature blackbody radiation, however, is still very strong at 2000 cm^{-1} and operation without a cold filter to block some of this radiation is not feasible as it would not only contribute excessive shot noise but actually cause the detector to saturate. With this in mind, a detector dewar was constructed with a compartment in front of the detector where filters could be inserted and cooled to liquid nitrogen temperature (77 K) for which the blackbody radiation is small as far into the infrared as 1000 cm^{-1}.

The highest sensitivity was achieved with a cold 2 μm short pass interference filter. This filter passed all wavelengths between 2 μm and 1 μm where it was again blocking and thus allowed operation between 5000 and 10000 cm^{-1} or 620 and 1200 meV. Although this region does not allow the observation of the full extent of the deep PL bands, it does include the important no-phonon region and also provided sufficient rejection of the laser as long as the excitation wavelength was less than 1 μm.

This 2.0 μm short pass filter was, however, too restrictive for some of the work. Besides extending the long wavelength cut to observe the full width of the band, it was also sometimes desirable to obtain one spectrum that simultaneously included the near-gap and the deep luminescence. For these applications, a Hoya Optics [HO] UV-22 glass filter was used as the cold filter in the detector dewar. Although the UV-22 is actually intended for use in the ultraviolet region, it is also an efficient short-pass filter that opens up at 3200 cm^{-1} (400 meV) and remains transparent right through the visible region. Although this filter passes more of the 300 K blackbody radiation than the 2.0 μm short pass interference filter, the increase in noise was tolerable and it allowed the full spectrum of the various PL bands to be recorded. When the UV-22 was the only cold filter, other filters were necessary to block the laser excitation. These included standard glass filters such as a Schott [SC] RG-780 or in other cases a 1.6 μm long pass interference filter which could be tilt tuned to pass slightly lower wavelengths if and when required.

The combined system of the InSb detector and the cold filters as described offers both increased spectral range and sensitivity compared to other detectors that are commonly used for PL in this spectral region such as Ge and PbS detectors.

3.5 Excitation Sources

The importance of the spectrometer and detection system has now been stressed, but this should not lead the reader to undervalue the role of the excitation source. Indeed the laser excitation is a crucial and central part of PL spectroscopy. Of particular importance is the availability of a wide range of lasers, especially tunable lasers, which allow the spectroscopist to explore the wavelength dependence of the excitation process. This not only gives valuable information but can also lead to great experimental advantage by finding the excitation conditions that favour the process under study or sometimes by finding conditions in which a competing process is absent.

Without question, the most important excitation source for this work was a Spectra-Physics [SP] Model 3900 titanium sapphire ,$Ti:Al_2O_3$, laser. This is a continuous wave (cw) laser which is tunable over the range from 700 nm to 1000 nm with powers well in excess of 1 W. One set of output mirrors is used for wavelengths between 700 nm and 850 nm and a second set covers the rest of the range. The range covered by the first set of mirrors is significant in that it includes the band-gap of

GaAs and also large regions both above it and below it.

The lasing medium of this laser is a Brewster-angled rod of titanium doped sapphire, hence the name Ti:Al_2O_3 laser. This material has a broad fluorescence band which extends from 600 nm to 1.1 μm which is efficiently pumped by an Ar^+ laser. The laser is tuned by a birefringent filter, also at Brewsters angle, which allows only one mode of the emission band to be linearly polarized, all other frequencies are elliptically polarized and the losses at the Brewster angled surfaces are sufficient to prevent lasing action. Accurate and continuous measurements of the wavelength are made with a Fizeau wavemeter manufactured by Lasertechnics [LT]. The principle of operation is based on measuring the separation of interference fringes from a wedged cavity. This gives information on the wavelength of the light and is more completely described elsewhere [84M2].

As mentioned previously, flicker noise is very detrimental in FTS and hence it is vital to stabilize the output power of the laser. This is accomplished by passing the beam through an acousto-optic power stabilization device. The acousto-optic cell is typically a glass medium which is driven by radio-frequency (RF) sound waves. The resulting standing wave pattern induces a corresponding spatial variation in the index of refraction and Bragg refraction proportional to the RF intensity occurs. Power regulation is achieved by sampling a small portion of the output beam and using this to servo the RF intensity and hence maintain constant power output.

Broad band spectra that included both the near-gap and deep luminescence were obtained with 514.5 nm excitation from an Ar^+ laser with the same power stabilization technique as described for the

$Ti:Al_2O_3$ laser. Long wavelength excitation, well below the band-gap at 1.55 μm, 1.3 μm and 1.2 μm, was provided by semiconductor diode lasers. The laser system used for the PLE will be described in the next section.

3.6 Photoluminescence Excitation Spectroscopy

Although it is possible to perform PLE on an interferometer, it is generally more efficiently done with a grating spectrometer if the range of interest can be accessed with a tunable laser. For these measurements, the excitation range was approximately between 1.6 and 1.7 μm, a region that can be covered by an optical parametric oscillator (OPO) laser system. An OPO system is based on a crystal with a susceptibility that is a non-linear function of the electric field. When pumped with laser light of a given frequency, two lower energy photons are emitted for every pump photon, subject to conservation of energy and phase matching of the three photons [82D1]. Under the appropriate conditions, lasing action is achieved in the OPO crystal with two optical branches.

The OPO system used here consisted of a Cu vapour laser which pumped a dye laser which then in turn pumped the OPO crystal. The tuning action is achieved by tuning the dye laser and the range can be varied somewhat by adjusting the temperature of the crystal. The OPO crystal used was $LiNbO_3$ held at a temperature of 400 °C and the dye laser was operated with Oxazine 720. This enabled tuning over the range of 1.57 to 1.72 μm with the average power between 30 and 50 mW. For more details, the reader is referred to a paper written specifically on this system [88T1].

The excitation was chopped at 40 Hz and focused onto the end of a 2 cm long sample with a 5 by 5 mm square cross section that was immersed in superfluid liquid helium. The long sample was used so as to maximize the absorption of the long wavelength excitation to which the sample is almost transparent. The luminescence was collected from the same end of the sample and focused onto the slits of single pass grating spectrometer set at 2.0 um. The InSb detector with the 2.0 μm long pass cold filter was mounted at the exit of the spectrometer with additional room temperature 2.0 μm band pass filter to provide more complete rejection of the laser. The signal from the detector was amplified with the electronics previously described and then fed into a phase lock amplifier that was referenced to the chopping frequency of the excitation, and spectra were collected as a function of the excitation wavelength.

3.7 Cryostats

Ordinarily, when the temperature dependence of a system is not being studied, it is most convenient to mount the samples in an immersion dewar. This is a cryostat where there is no separation of the sample chamber from the liquid He reservoir and the sample is immersed in the liquid. Temperature control is very precise but the range is limited in this case. The maximum temperature is the 4.2 K boiling point of liquid helium at atmospheric pressure, but normally the vapour pressure of the He is lowered by a mechanical vacuum pump so that the liquid helium undergoes the phase transition at 2.18 K to its superfluid state. In this state, the liquid is more transparent and flicker noise from the boiling action is eliminated. Under typical conditions, the liquid helium temperature is then in the range of 2 K.

The use of an immersion dewar for much of this work was impractical for primarily one reason, the metastability of the EL2 defect. Since accidental or intentional exposure of the samples to light in the range $0.9 < \lambda < 1.2$ μm can quickly bleach or quench the observable properties, it was necessary to be able to anneal the samples at temperatures above 140 K. This necessitated the use of a variable temperature (vari-temp) dewar for almost all the experiments.

A vari-temp dewar has a sample chamber that is separate from the He reservoir. The liquid helium is introduced into the sample chamber from the reservoir through a capillary tube and the flow is controlled by a needle valve. Once in the sample chamber, it can be allowed to collect or else be vaporized into cold gas by a heater either at the base of the sample chamber or on the sample holder itself.

The temperature was measured and controlled with a Lake Shore Cryotronics Model 805 Temperature Controller [LS] that reads the temperature dependent voltage across specially made Si diode sensors that are mounted on the sample holder or the bottom of the sample chamber. The temperature controller displays the temperature in degrees Kelvin and controls the current sent to the heaters. The Si diodes are capable of great accuracy; the limiting factor is ensuring good thermal contact between the sample and the diode sensor. This is especially crucial when the temperature dependence of the PL was being investigated as the sample is continually being heated by the laser excitation. In this case, a temperature sensor was mounted directly on the sample itself with a layer of vacuum grease between the two to ensure good thermal contact.

The vari-temp dewar used was a Janis Model 8DT Supervaritemp [JA] that was custom ordered with sapphire windows instead of the usual quartz windows since quartz has a strong absorption band at 2.2 µm which interferes with the deep PL bands. It should be noted, however, that caution must be exercised with the sapphire windows because the inner cold windows give rise to sharp photoluminescence lines themselves. This was usually overcome by directing the excitation through a side window of the cryostat so that virtually none of this extraneous luminescence was collected. A second disadvantage of the vari-temp dewar is the reduced efficiency that arises from increased thermal contact with the warm top part of the cryostat through the walls of the sample chamber. This is especially problematic when the sample is immersed in superfluid liquid helium as was often the case. The cryostat used for studying the influence of magnetic fields on the PL will be discussed in a separate section.

3.8 Samples

This work was greatly facilitated by the availability of a wide range of well characterized samples. Most of these were provided by Johnson-Matthey Electronics and were grown by the LEC method in pyrolitic boric nitride crucibles encapsulated with B_2O_3. The encapsulant is characterized by three classes, B, C and D, that describe its water content. The water content is 2000 parts per million (ppm) H_2O for B, 1000-1200 ppm for C and 500 ppm for D. The B-type encapsulant is described as wet, whereas both C and D are called dry.

For the most part, the samples were as-grown and undoped but some samples were intentionally doped. These included a carbon doped sample, a heavily oxygen doped sample and samples that were grown with Ga_2O_3 added to the melt and grown under dry B_2O_3 encapsulant. Samples from other manufacturers were also investigated but less is known about their growth characteristics.

3.9 Uniaxial Stress

A crucial aspect of part of this work is the application of well characterized and controlled uniaxial stress and magnetic field as perturbations. This is straightforward in the case of magnetic fields but can be somewhat more problematic for uniaxial stress. Conventional methods of applying uniaxial stress rely on compression of samples with flat ends. This method is hampered by imperfectly flat ends which causes inhomogeneous stress and significant broadening of lines. We have used an alternative method in which the ends of the sample are ground and polished into sharp pyramid shaped tips and the compression is performed between metal surfaces with small, shallow, cone shaped recesses into which the sharpened tips of the samples are placed [82K1]. This method has been found to give rise to very little broadening of the lines as will be discussed in a later chapter.

The samples were aligned in [100], [110] and [111] crystallographic directions using a Laue X-ray diffraction camera and cut from a one centimeter slice of a bulk-annealed boule of LEC grown GaAs. The resulting stress samples had a uniform square cross-section with an area between 1 to 2.5 mm^2. The length of these samples was always between 5 to 10 times the width. The lower limit ensures that the stress is uniaxial in the central region of the length and the upper limit is imposed to prevent premature bowing of the sample which would lead to sample failure. After cutting and then polishing with 1 μm diamond paste, the samples were exposed to a light chemical etch in a solution of one part bromine to ten parts methanol to remove surface damage.

The samples were then mounted in a stress rig which was inserted into the vari-temp dewar. Low stress was applied by placing weights on a platform that was supported by a rod which rested on the upper piston. To achieve higher stresses, it is impractical and somewhat dangerous to increase the stress by the further addition of weights. Instead, a lever system that could be tightened with a screw was used. The stress was continuously measured with a strain gauge between the samples and the compressive force. The PL was performed with the samples immersed in superfluid liquid helium and with both the excitation and collection optics tightly focused to reduce the possibility of line broadening due to inhomogeneities in the stress.

3.10 Magneto-Photoluminescence

For the magnetic field studies the samples were placed in an optical cryostat with the sample chamber in the bore of an Oxford Instruments [OI] NbTi/Nb_3Sn superconducting solenoid. This is a large bore magnet which allows the insertion of large, specialized sample holders into the centre of the solenoid. The field could be continuously varied up to 12 T without cooling the magnet below 4.2 K. Higher fields could be attained by further cooling the magnet, but this was not found to be necessary. The optical access to the sample chamber is through the bottom of the magnet cryostat and the luminescence is collimated by a lens and sent along the ≅ 3 metre path into the interferometer. This large separation is a precautionary measure to reduce the influence of the large magnetic fields on the interferometer.

The sample chamber in the magnet was originally designed only for use as an immersion dewar. Early on, it was evident that sample temperatures higher than 4.2 K were necessary to thermally populate the higher lying Zeeman split states that were involved in the transitions under study. A vari-temp cryostat was then built that could be inserted into the magnet and cooled by the surrounding liquid helium in the sample chamber reservoir.

This consisted of a long, non-magnetic stainless steel tube with a window at the bottom which could be evacuated and back-filled with helium gas. It was large enough to accept a sample holder from the vari-temp dewar which is equipped with a heater and Si diode temperature sensor. This sensor, however, is inappropriate for use in high magnetic fields and a second sensor was added. This was a temperature sensitive capacitor which was calibrated against the diode at zero field.

The samples were mounted on a large 2.5 cm diameter by 1 cm thick disk of GaAs. Thermal contact of the samples to this disk was established by a small amount of vacuum grease between them. This large disk acted as a heat sink to prevent excessive sample heating from the laser excitation. The temperature sensors were directly mounted onto the disk to provide reasonably accurate measurements of the sample temperature. With the cryostat evacuated and the surrounding liquid helium in the superfluid state, the equilibrium temperature with the excitation on the sample was ≅ 8 K and this was sufficiently high to observe the transitions up to 12 T.

CHAPTER 4. THE EL2 PHOTOLUMINESCENCE TRANSITIONS

4.1 Introduction

This chapter will present results that clearly distinguish the three bands commonly observed in the photoluminescence of semi-insulating GaAs between 0.5 eV and 0.7 eV. One of these bands will be identified with oxygen and the other two will be shown to due to transitions involving the deep EL2 level. Detailed and unequivocal information will be presented that allows the unambiguous identification of the EL2 related transitions. This includes the first observation of a shallow, hydrogenic state of neutral EL2, which leads to spectrally sharp structure in the luminescence spectrum. These new transitions locate the energy position of the neutral EL2 level within the band gap with unprecedented precision. The new fine-structure has also been studied under the perturbations of uniaxial stress and magnetic field. These results will be discussed in Chapter 5.

The first issue that will be addressed is the role of oxygen in deep PL in the region between 0.61 and 0.65 eV. It will be shown that there are in fact two distinct bands in this region; one is oxygen-related and the other is EL2-related. These results support the conclusion of Tajima [87T1] that the band that is often reported at ≈0.63 eV can either be due to O or EL2, but a clear distinction between the two spectra will be made here for the first time. The exact nature of the EL2-related PL is dependent on the concentrations of the residual impurities, but in high quality samples the band due to EL2 is centred at 0.61 eV and is distinctly different from the 0.63 eV O-band.

The initial identification of this 0.61 eV band with EL2 will be made on the basis of several observations. The band is demonstrated to be present in all of the SI samples studied, it shows the optical quenching that is characteristic of EL2, and the 11 meV LVMs seen in the 1.039 eV absorption transition are clearly present. Furthermore, this conclusion will be continually reinforced by subsequent results throughout this and the next chapter.

The nature of the transition responsible for the 0.61 eV band will then be elucidated. Fine structure on this band reveals that at liquid helium temperatures this PL results from an electron in a shallow, hydrogenic bound state dropping into the EL2 ground state ($EL2^{0}_{n=2} \longrightarrow EL2^{0}_{n=1}$), whereas at temperatures above approximately 30 K the ($e, EL2^{+}$) free to bound transitions begin to dominate the spectrum.

The other important band is the structured 0.68 eV band reported by Tajima [86T1]. The results presented here reveal that at low temperatures, it is not an ($h, EL2^{0}$) free to bound transition as initially reported but rather an $EL2^{0}$ – carbon (or other shallow acceptor) donor acceptor pair (DAP) band. Only at temperatures over 35 K does this switch over to the ($h, EL2^{0}$) free to bound transitions.

The fine structure of the new transitions allows for determination of the energetic position of EL2 in the bandgap with unprecedented precision, and it is shown that the ($h, EL2^{0}$) and ($e, EL2^{+}$) edges add up to precisely the bandgap energy as they should. New details on the phonon coupling of the two transitions will be important in improving the precision of fits to the multiphonon bands.

4.2 The Oxygen Related Deep PL

The role of oxygen in the history of the EL2 defect has been discussed at length in Chapter 2. The question of whether oxygen is a constituent of the EL2 defect is now well understood; oxygen in GaAs and EL2 are separate entities. There is, however, an ongoing controversy over the origin of the often observed deep PL band that peaks in the range ≅ 0.63 to 0.65 eV. It has often been thought to be due to EL2 but the evidence relating it to oxygen is very strong. Therefore no discussion of the photoluminescence transitions of EL2 can proceed without first clarifying and defining the influence of oxygen on the deep level PL.

This research grew out of the observation of fine structure in the deep PL of SI GaAs samples. The dominant feature was a sharp line at ≈ 703 meV, but its intensity relative to the band on which it lay varied from sample to sample. In some samples it was very sharp and distinct whereas in others it was insignificant in relation to a broad band that lay below it. It was, however, present in all the samples. This, and other properties that will be introduced later, indicated that this structured band was EL2 related. This notion was tempered though by the possibility that oxygen rather than EL2 was responsible.

It was only when a large number of well characterized samples had been studied that a pattern emerged and this question could be unraveled. These included a sample doped with oxygen by ion-implantation to a known concentration and a large number of undoped samples that were grown with the wet B grade, and dry C and D grades of

B_2O_3 encapsulant that were described in Chapter 3. The significance of the moisture content of the encapsulant was discussed in Chapter 2 where it was shown that the wet B_2O_3 promotes oxygen incorporation whereas dry B_2O_3 produces material that is oxygen-free within the limits of detection [85E1]. The typical PL from these types of samples are summarized in Figure 4.1.

These PL spectra are from samples at liquid helium temperature with above-gap excitation and span an energy range which includes the deep bands under question, right through to the near-gap region. The PL spectrum, Figure 4.1(a), of the heavily oxygen doped sample (Ga-O-Ga = 2×10^{15} cm^{-3}) [90A1] is completely dominated by a band at 0.63 eV. It is a broad, structureless band with peak intensity greater than the near gap DAP luminescence. In the undoped B-type sample, Figure 4.1(b), the peak intensity of the deep PL is approximately 200 times weaker than the near gap luminescence but is still strong. The peak has shifted down in energy somewhat, but in relation to the width of the band, the change is slight. The deep PL found in the oxygen free C-type and D-type samples is, however, dramatically different. The luminescence is much weaker and is unusually long lived, with a lifetime that can be as long as $\tau \cong 5$ ms. The spectrum, Figure 4.1(c), is also markedly different; the band now peaks at 0.61 eV and is characterized by sharp structure on the high energy side of the band.

All of the undoped C-type and D-type samples studied under these conditions had this same distinctive band and fine structure, whereas the B-type samples were normally dominated by the much stronger O-related band at 0.63 eV. Although in some cases the sharp feature

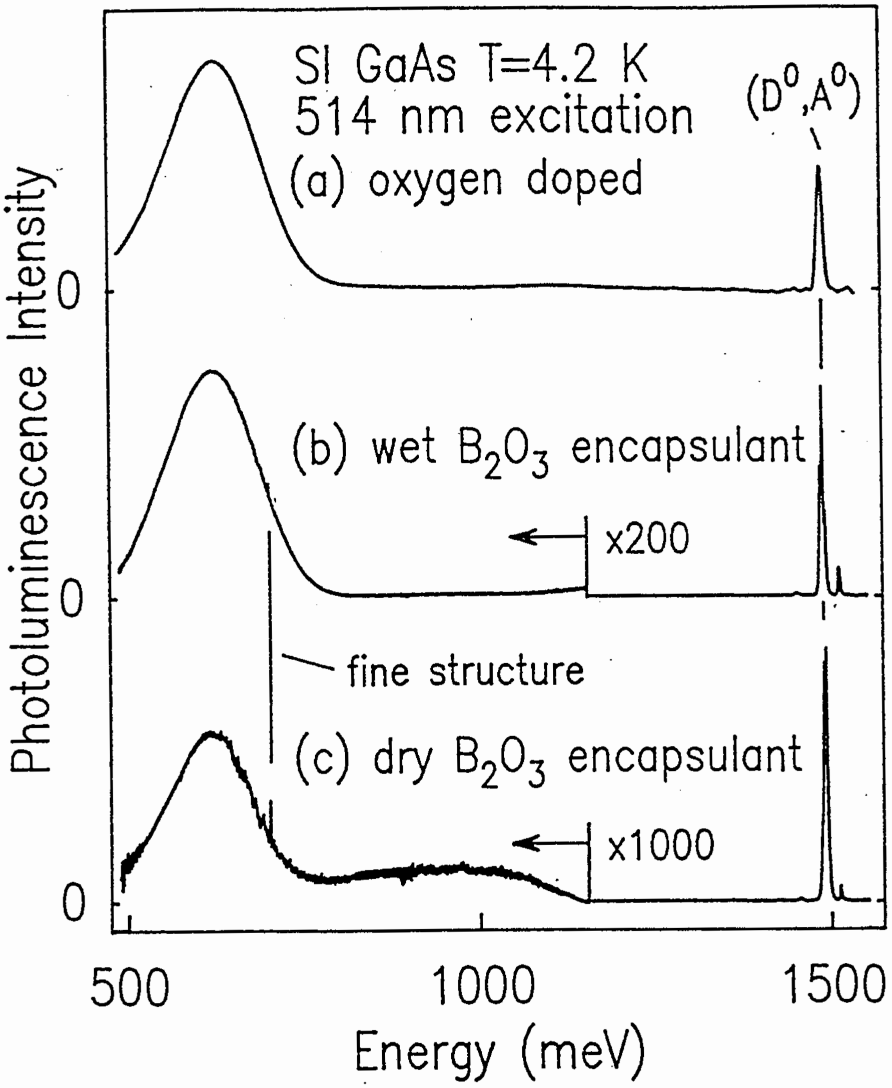

Figure 4.1

These spectra show the effect on the PL of progessively lower concentrations of oxygen under above-gap excitation. The Ga-O-Ga concentration in (a), the O-doped sample is 2 x 10^{15} cm^{-3}. The water content of the B_2O_3 encapsulant is (b) 2000 ppm and (c) 500 ppm. The indicated structure is present in (b) but is difficult to discern on this scale. Also shown is the near-gap (D_0,A_0) luminescence as a reference for the relative intensities. The resolution is 0.5 meV and the spectra have been corrected for instrumental response.

from the deeper band can still be discerned in the B-type samples as for example in Figure 4.1(b), it is usually obscured by the 0.63 eV band.

Before going on to a more detailed discussion of the 0.61 eV EL2 related band a few more remarks concerning oxygen in GaAs should be made. The absence of oxygen in the samples grown under dry encapsulant has been confirmed by LVM analysis [90A1] and it is interesting to note that even the addition of Ga_2O_3 to the melt when using C-type encapsulant does not appear to introduce detectable levels of oxygen. Contrary to a previous report, there is no evidence here of structure on the 0.63 eV O-related band [86K1].

4.3 The 0.61 eV PL Band and EL2

As grown SI GaAs can now be reliably produced because the conditions under which EL2 is present in concentrations around 10^{16} cm^{-3} are now well understood [88H1]. Hence EL2 should be present whether or not there is also oxygen present. The presence of the 0.61 eV band in the oxygen-doped and B-type SI GaAs samples is clearly demonstrated in Figure 4.2. These results are from the same samples used in Figure 4.1, but the PL spectra are quite different because they were obtained with 1.3 μm excitation which is found to not efficiently pump the oxygen-related band at 0.63 eV. The spectrum from the O-doped sample, Figure 4.2(a), still shows a background contribution from the 0.63 eV band but the distinctive structure of the 0.61 eV band is now unmistakably present. The effect is even more dramatic for the B-type samples, Figure 4.2(b). The spectrum is virtually indistinguishable

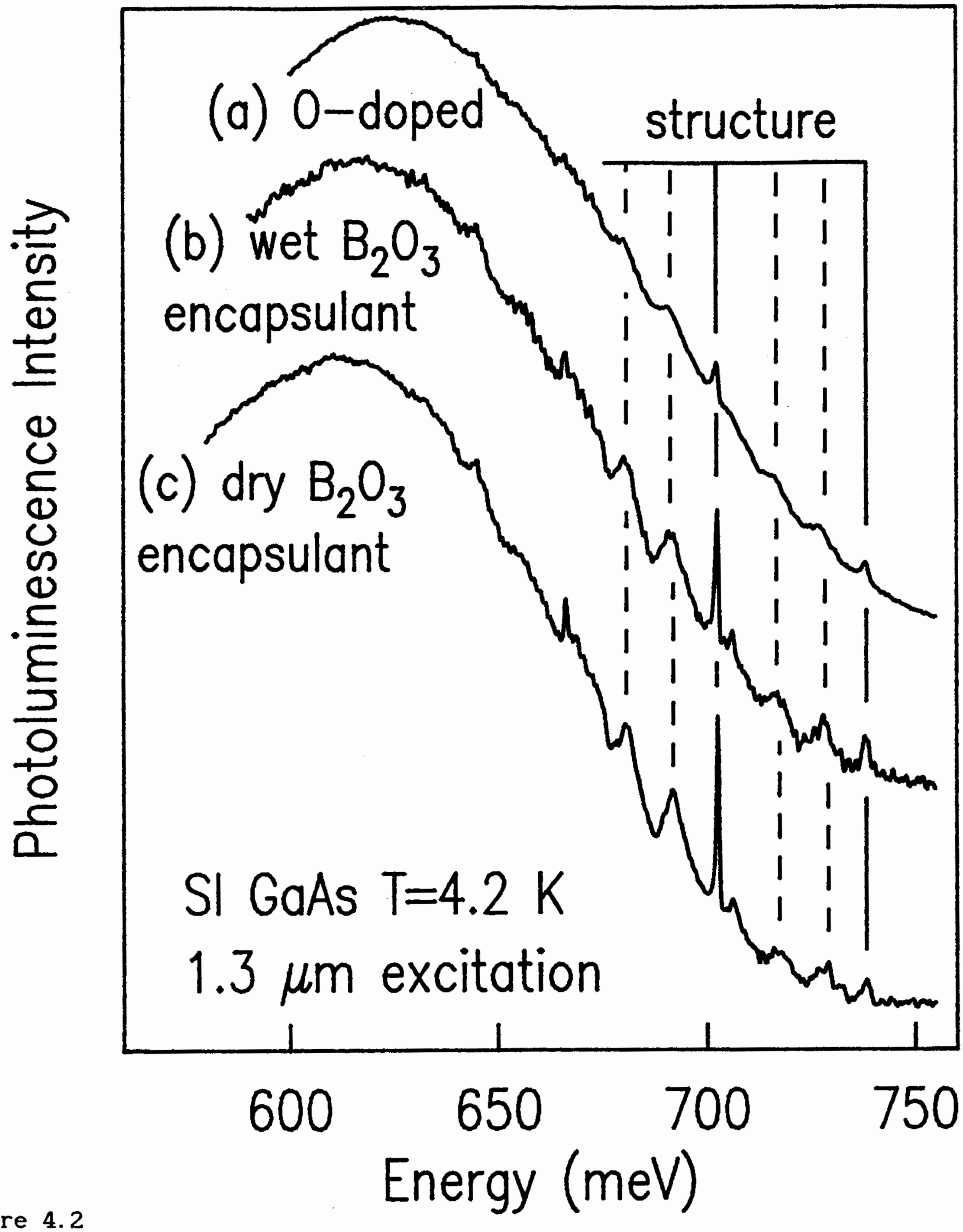

Figure 4.2
PL spectra from the same samples as in Figure 4.1. The O-related band is evidently suppressed under the 1.3 μm excitation and the same distinctive structure can be seen all three samples. The resolution is 0.5 meV and the spectra have been corrected for instrumental response.

from that of the typical dry encapsulant samples, Figure 4.2(c).

All of the B-type and C-type samples investigated showed the 0.61 eV band under these conditions. Some of the D-type samples, however, have higher residual acceptor concentrations which, as will be shown in a following section, gives rise under these conditions to a different but related PL band. The details of the indicated structure in Figure 4.2 will be discussed later, the important result is that, under the appropriate excitation conditions, the 0.61 eV band was observed in all SI GaAs samples.

The most widely recognized signature of EL2 is its unusual bleaching or photo-quenching behavior. Although earlier studies showed that the 0.63 eV band could be quenched under 1 μm excitation [82L1], it was subsequently shown that it was the excitation path that was quenched and that even after bleaching with the 1 μm excitation, the 0.63 eV band was still present when using above-gap excitation [84S1]. This is similar to the interconversion of the oxygen related LVMs discussed earlier. To avoid these pitfalls, the quenching behaviour was studied using only above-gap excitation for the PL and the samples were bleached for several minutes with white light of wavelength longer than 850 nm. The results are shown in Figure 4.3.

The spectra of Figures 4.3(a) and 4.3(b) show the 0.61 eV band from a dry encapsulant sample at 4.2 K before and after bleaching, respectively. The quenching of the distinctive 0.61 eV band is obvious, only a weak band at ≅ 0.67 eV remains in Figure 4.3(b). Full recovery of 0.61 eV band is achieved after annealing at T = 140 K and cooling in the dark back to liquid helium temperature. The presence of the weak

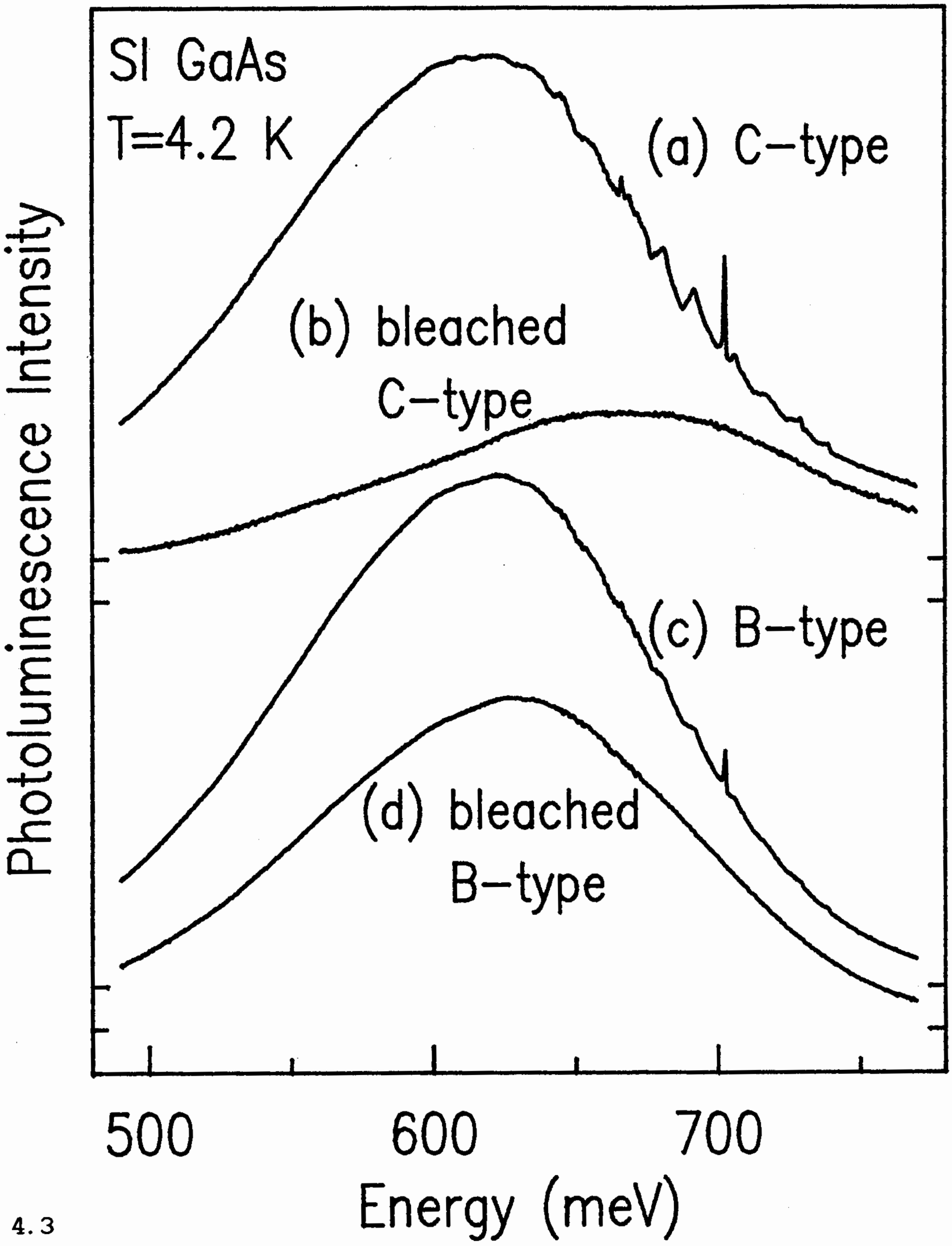

Figure 4.3
The photo-quenching behaviour of the deep PL is shown under 514 nm excitation. Fig. 4.3(a) and (c) show spectra before bleaching with white light for C and B-type samples respectively. The corresponding after bleaching spectra are shown in Fig. 4.3(b) and (d). The resolution is 0.5 meV and the spectra have been corrected for instrumental response.

0.67 eV band that remains after bleaching is an interesting effect that is not yet understood. It is slowly induced by above gap excitation and eventually leads to a background band with intensity comparable to that of the 0.61 eV band. While it remains unaffected after annealing at 140 K, it can be eliminated by annealing at 300 K.

To further contrast the 0.61 eV and O-related 0.63 eV bands, the bleaching of a B-type sample is shown in Figure 4.3 as well. The before bleaching spectrum, Figure 4.3(c), shows that the 0.63 eV band is dominant and the structure of the 0.61 eV band is weak in comparison. After bleaching, Figure 4.3(d), most of the original intensity remains but the distinctive structure of the 0.61 eV band is quenched. In fact subtraction of the bleached spectrum from the unbleached spectrum gives a spectrum of the 0.61 eV band alone. Again, full recovery of the original spectrum is achieved after annealing at 140 K. No quenching at all was observed in the 0.63 eV band from the oxygen doped sample shown in Figure 4.1(a). In this case the contribution of the 0.61 eV band is negligible in comparison to the O-band.

It should be noted that the above-gap excitation used for these results causes a slow regeneration of the 0.61 eV band after bleaching. This is not surprising since it is known that the presence of free electrons in the conduction band induces a slow recovery of EL2 from its metastable to normal state as discussed in Chapter 2. For this reason the quenched spectra shown in Figure 4.3 were acquired quickly without a lot of signal averaging so as to avoid optical regeneration.

The onset of the transition to the metastable state is generally believed to occur at the 1.039 eV NP intracentre absorption line. This corresponds to a wavelength of 1.193 µm. The 0.61 eV band was found, however, to be slowly quenched by excitation from diode lasers operating at wavelengths of 1.2 µm and 1.3 µm. This unexpected result cast some doubt on the assignment of this band to transitions involving EL2. To overcome this question a series of measurements were made which showed that the 0.61 eV PL and the 1.039 eV absorption line quenched at the same rate under 1.2 µm excitation.

The bleaching at these longer wavelengths likely occurs as a two step process having as its intermediate state where the electron is excited first to the initial state of the PL transition and from there to the metastable state. This is made possible by the long lifetime of this state as evidenced by the luminescence lifetime measurements which will be further discussed later in this chapter. It is not surprising that this behaviour has not been previously observed because, typically, measurements of the photo-quenching cross section are performed with a white light source through a monochromator. The resulting intensities are much lower than that from the diode lasers and have likely been too low to observe this slow process.

An unfortunate consequence is evident in the relative poor quality of the spectra shown in Figure 4.2. Due to the bleaching of the luminescence, high signal to noise spectra could not be collected using these long wavelength excitation sources which have the advantage of being very simple and relatively noise free, and selectively excite only the EL2 related PL. This leads to the question of what the best excitation energies are. The use of an argon-ion laser has already been shown to be impractical because of the photo-induced background at

0.67 eV as well as the efficient pumping of the overlapping O-band.

The EL2 photo-ionization cross section, σ_n^o, [81C1] and the PLE results of Tajima [87T1] suggest, however, that the conduction band to EL2 PL should be most efficiently pumped by excitation just below the gap. This was indeed found to be the case for the 0.61 eV band. This excitation did not pump the O-band nor did any photo-induced background interfere with the spectra. Also, the bleaching effects were negligble for pumping just below the bandgap. This allowed for the collection of spectra with much higher signal to noise ratios than those that have already been presented.

This is evident in the spectrum of Figure 4.4 which shows the 0.61 eV band under 835 nm excitation from the Ti:Al_2O_3 laser. The full width at the half maximum of the band is approximately 140 meV and the onset is distinctly marked with a weak no phonon (NP) transition at 739.33 meV. The more obvious sharp transition is at 702.82 meV. The separation between these two is equal to the low temperature longitudinal optical zone center phonon (LO_Γ) energy and hence the stronger line can be identified as a LO_Γ phonon assisted transition. In such a transition, the emission of the luminescence photon is accompanied by the creation of one or more phonons. Both the LO_Γ and $2LO_\Gamma$ assisted transitions are indicated in Figure 4.4. Also shown is a transverse acoustic phonon from the X point of the Brillouin zone (TA_X). In addition to these lattice phonons, there is also strong coupling to local vibrational modes (LVM) of energy 10.8 ± 0.2 meV. These are strikingly similar to the 11 ± 1 meV LVMs which couple to the 1.039 meV NP transition of the EL2 intracentre absorption [83K1].

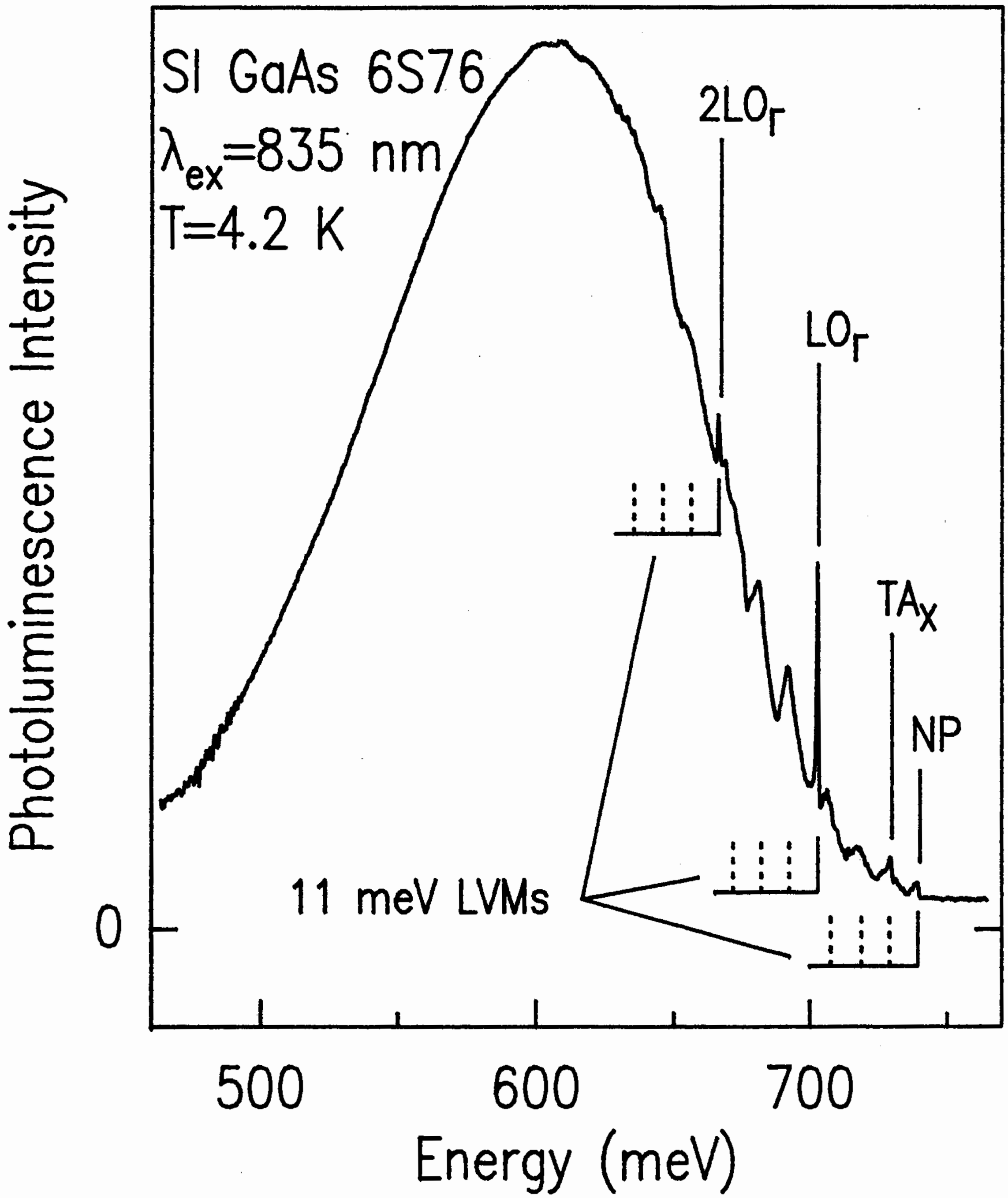

Figure 4.4
The 0.61 eV PL band with phonon-assisted transitions indicated. Note that there is very little background below the band, the onset of the band is on a flat region just above zero. The resolution is 0.5 meV and the spectra have been corrected for instrumental response.

These results strongly support the identification of the 0.61 eV band with EL2. The next section will examine the fine structure of the band in greater detail. The presence of the fine structure will allow many conclusions to be drawn, the first of which concerns the nature of the transition responsible for the band.

4.4 The Fine Structure of the 0.61 eV Band

Greater sensitivity is achieved with the cold 2 μm short pass filter in front of the InSb detector and although this does not allow the entire band to be observed, the enhanced sensitivity is very useful for detailed studies of the fine structure on the high energy side of the band. This region is shown in the spectrum of Figure 4.5 which features both an improved signal to noise ratio and higher resolution than those previously presented and is the result of long signal averaging.

The spectrum is rich with structure that indicates coupling to a surprisingly large variety of lattice phonons. In addition to the LO_Γ and TA_X phonons, three transitions involving transverse optical (TO) phonons from the Γ, L, and X points of the Brillouin zone are clearly apparent and are labelled TO_Γ, TO_L and TO_X. There is also a weak shoulder that corresponds to the LO_L and LO_X phonons and distinct peaks that can be identified with the L point longitudinal acoustic (LA) phonon, labelled LA_L, and the TA_L phonon. These are summarized in Table 4.1 which lists the phonons involved, the energy of the transition, the separation from the NP transition and finally, for

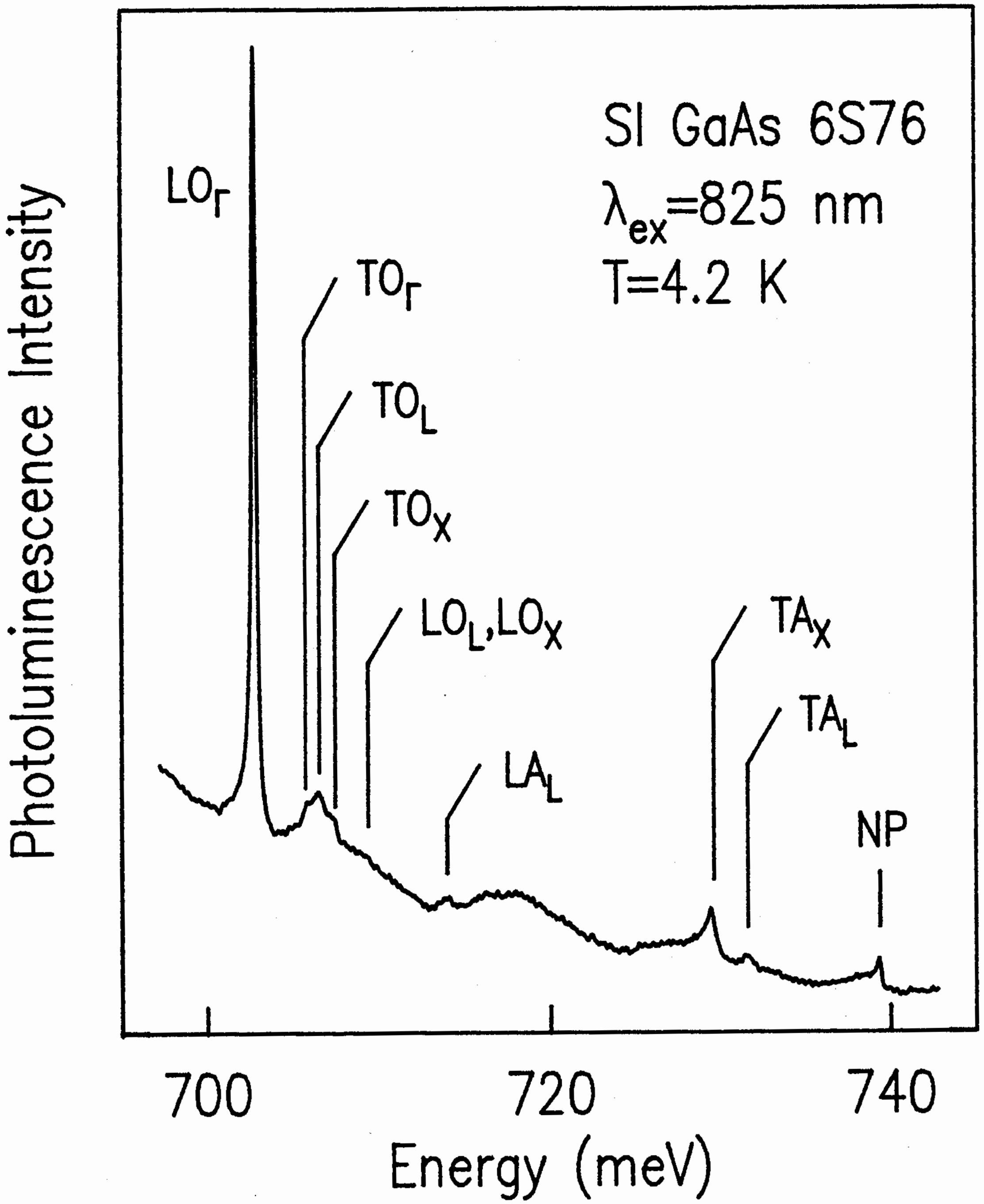

Figure 4.5
High resolution, low noise spectrum showing the detailed fine structure of the EL2 0.61 eV band due to coupling to a wide variety of lattice phonons. The resolution is 0.12 meV and the spectrum is uncorrected.

Table 4.1

The lattice phonons that are observed as replicas in the 0.61 eV band are listed in the first column. This is followed by the energy of the observed transition and then the separation from the NP line at 739.33 meV which can be compared to the phonon energy determined from 12 K inelastic neutron-scattering experiments [90S2].

Phonon	Transition Energy (meV)	Energy from NP (meV)	Phonon Energy (meV)
TA_L	731.4	7.8	7.86
TA_X	729.41	9.92	10.1
LA_L	714.1	25.2	25.6
LO_X	709.4	29.9	29.8
LO_L			30.0
TO_X	707.3	32.0	31.8
TO_L	706.5	32.8	32.7
TO_Γ	705.9	33.4	33.6
LO_Γ	702.82	36.51	36.4

comparison, the corresponding phonon energy from the recent phonon dispersion measurements in GaAs at T = 12 K [90S2].

There are several aspects of this phonon coupling that are unusual but before discussing it in greater detail, it is useful to first make some comments on the initial and final states of the transition. The sharpness of the NP transition and the phonon replicas, particularly the LO_Γ and the TA_X, implies that the initial and final states are both localized on the same center. Since EL2 is a double donor, it should have shallow Coulombic excited states below the conduction band edge that are analogous to the excited states of the helium atom. On varying the sample temperature, it was noted that the PL was very strongly temperature dependent. The PL intensity decreased rapidly as the temperature increased, indicating that the initial state was depopulating into another state at slightly higher energy.

This was confirmed by acquiring spectra as a function of temperature. These results are presented in Figures 4.6(a), 4.6(b) and 4.6(c) which show the high energy edge of the band starting from the LO_Γ phonon replica and extending well beyond the NP transition. The spectrum in Figure 4.6(a) is the familiar result from a sample at 4.2 K and serves as a reference for the spectra from a sample at 20 K, Figure 4.6(b), and at 30 K, Figure 4.6(c). At 20 K, a new transition from a thermally populated level has appeared at an energy just above the NP transition. In the 30 K spectrum, this new transition is somewhat stronger and, although the spectrum is far from noise free, it can be seen to have a Boltzmann-like line shape that is indicative of a free to bound transition. This is consistent with a shallow hydrogenic

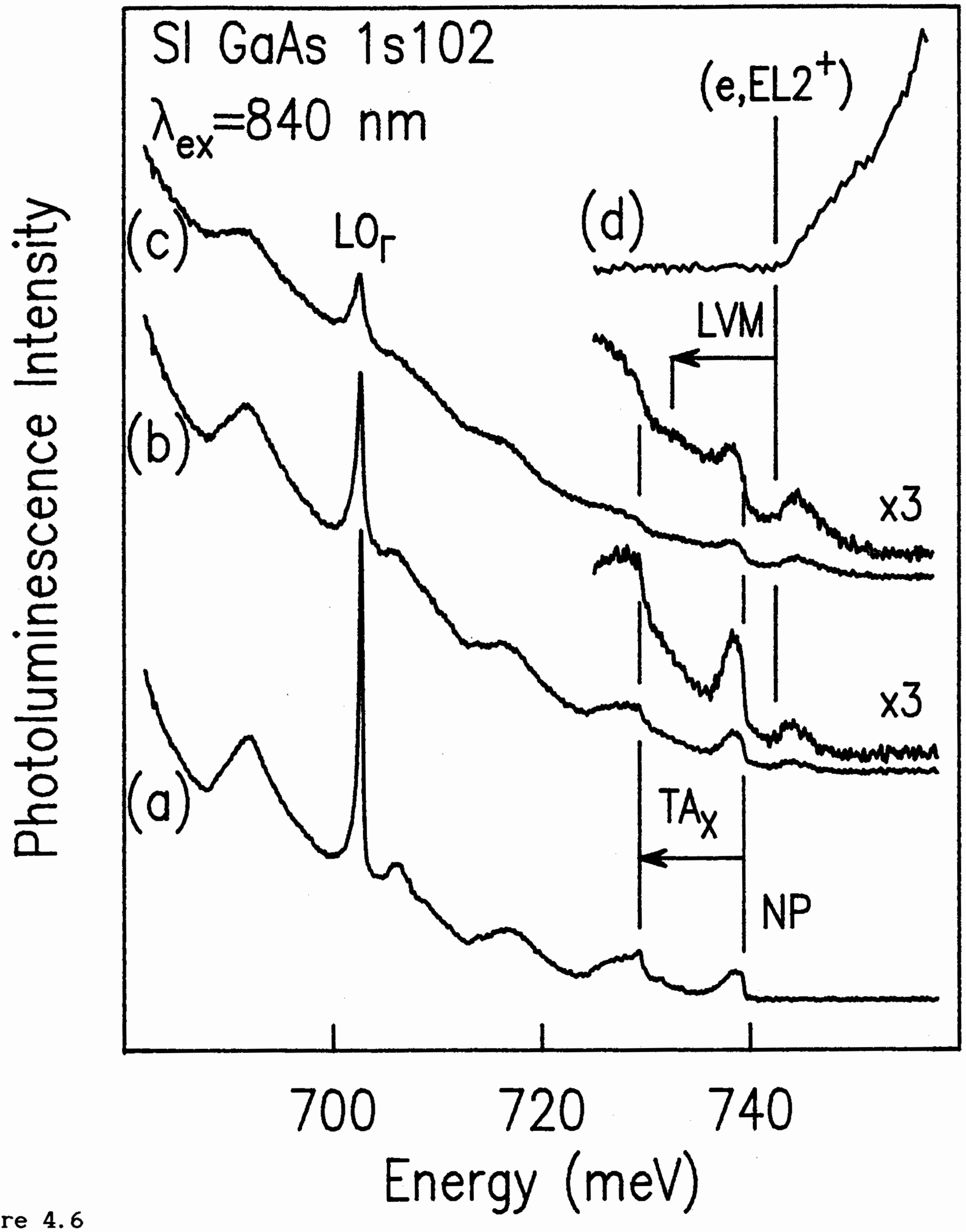

Figure 4.6

Spectra showing (a) the structured region of the 0.61 eV PL band at 4.2 K, and the free to bound transition at (b) 20 K and (c) 30 K. The resolution is 0.12 meV and the spectrum is uncorrected. (d) The PLE of the 0.61 eV band at 1.6 K with approximately 1 meV resolution.

excited state depopulating into the conduction band and hence this new PL line is the $(e, EL2^+)$ free to bound transition.

This argument is further supported by the PLE spectrum shown in Figure 4.6(d) where the onset of the absorption into a continuum agrees well with the edge of the free to bound transitions in Figures 4.6(b) and 4.6(c). The spectroscopic binding energy of the shallow state is measured from these spectra to be 3.2 ± 0.5 meV, which puts the EL2 ground state at 742.5 ± 0.5 meV below the conduction band at 4.2 K. This is the first direct measurement of the EL2 binding energy at 4.2 K and is by far the most accurate measurement yet of this important level. It is in good agreement with the extrapolated low temperature results of Omling [86O1].

These results establish that the low temperature transition responsible for the 0.61 eV PL band is an electron in a shallow excited state of EL2 relaxing back down to the EL2 ground state. This will be denoted as a $EL2^0_{n=2} \longrightarrow EL2^0_{n=1}$ transition. One can exploit the fact that this double donor system is the solid state analogue of the helium atom. The 1s2s excited states of the helium atom in which one electron remains in the 1s orbital and the other in the 2s orbital are extremely long lived. For the spin singlet state, the lifetime is 20 ms and for the triplet, it is over an hour [87S2]. This is because the transitions from these even parity excited states back down to the $1s^2$ ground state are dipole forbidden. This behaviour is similar to the observed lifetime of the 0.61 eV luminescence which was measured to be approximately 5 ms. It is interesting to consider the strength of the lattice phonon coupling in terms of this picture.

One mechanism that might explain the strength and diverse number of lattice phonons is the need to conserve **k**-vector between the initial and final states of the transition. Recalling that since the EL2 ground state is very deep, it is therefore comprised of states from all of the bands in the Brillouin zone and hence the total **k**-vector of the wavefunction is likely to be displaced from the conduction band minimum at the centre of the Brillouin zone. On the other hand, the initial state is shallow and therefore largely effective mass like and the total **k**-vector will be dominated by contributions from the conduction band minimum. It is plausible then that the participation of a lattice phonon might be needed to conserve the change in momentum between these two states.

There is, however, a severe problem with this interpretation. The strongest lattice phonon coupling is to the LO_Γ phonon, but this phonon, and the TO_Γ, carry no crystal momentum, so **k**-vector conservation cannot be a factor for these phonons. Secondly, the net displacement in **k**-vector between the initial and final state should be a single fixed quantity. The **k**-vector conserving phonons should then all carry the same crystal momentum and be from the same point in the Brillouin zone, which would not necessarily correspond to the high symmetry points. The observed lattice phonons, however, are from the Γ,X and L points. This corresponds to three distinct values of crystal momentum, all of which are at high symmetry points.

It is also possible that the participation of the lattice phonons might be due to vibrational coupling. Some observations can be made, however, that cast doubt upon this as well. For instance, the PL spectra as a function of temperature in Figure 4.6 show that while the low temperature $EL2^{0}_{n=2} \rightarrow EL2^{0}_{n=1}$ transition couples strongly to the LO_{Γ} and TA_{X} phonons, the $(e, EL2^{+})$ transition clearly does not. If the coupling of these phonons was purely vibrational, this would not be the case because the vibrational coupling will be the same for these transitions. This argument also supports the refutation of **k**-vector conservation as the change in **k**-vector should also be the same for these two transitions.

It should also be noted that this results in a seemingly anomalous increase in the energy of the center of the band as the temperature increases. Although this effect is not apparent in Figure 4.6 because the spectra were taken with the 2.0 μm short pass filter and hence the entire band was not observed, other spectra showed that the band centre shifted from 0.61 eV at liquid helium temperature to 0.63 eV at 30 K.

Further evidence that the participation of these phonons is not mediated by vibrational coupling can be found by comparing the relative intensities of the NP transition and the first and second LO_{Γ} phonon replicas. To obtain a rough estimate of what the relative intensities of these transitions should be if the coupling was vibrational, the simplified theory of Huang and Rhys that assumes coupling to only one mode can be used and the relative intensities are given by equation 1.4 in Chapter 1. From Figure 4.5, the Huang-Rhys factor ,S, for the LO_{Γ} phonon can be obtained by taking the ratio of the first LO_{Γ} assisted transition intensity to that of the NP transition and a value of approximately 23 is obtained. This indicates very strong coupling. The intensity of the second LO_{Γ} transition is then predicted to be $\frac{S}{2}$ times that of the first LO_Γ replica. The second LO_Γ transition is indicated in Figure 4.4 and rather than being ten to twelve time stronger, it is weaker than the preceding LO_Γ transition.

With these two conventional phonon coupling mechanisms ruled out, the idea that this double donor system is the solid state analogue to the helium atom can be returned to. The fact that the $(e,EL2^+)$ free to bound transition does not show the strong coupling to the lattice phonons suggests that the mechanism arises from a unique property of the transition from the shallow excited state and it is plausible that the participation of these particular high symmetry phonons somehow relax the forbidden nature of the transition, which is analogous to the dipole forbidden transitions of the helium atom. This is consistent with some other observations.

If the spectra of Figures 4.5 and 4.6(a) are carefully compared, clear differences are apparent in both the shape of the NP line and its relative intensity compared to the phonon replicas. The NP line in Figure 4.6(a) does not show the distinct peak seen in Figure 4.5 but rather it consists of a sharp high energy edge and a broad low energy tail. These differences are primarily sample dependent but are also influenced by the excitation wavelength and can shed some light on the nature of the coupling to the lattice phonons.

A more extreme example of the sample to sample variation is shown in Figure 4.7. The spectrum of Figure 4.7(a) is from sample 6S76. This is the same sample as in Figure 4.5 and again the NP line is seen to have a distinct sharp component but when the vertical scale is expanded there is also very clearly a low energy tail which extends to about

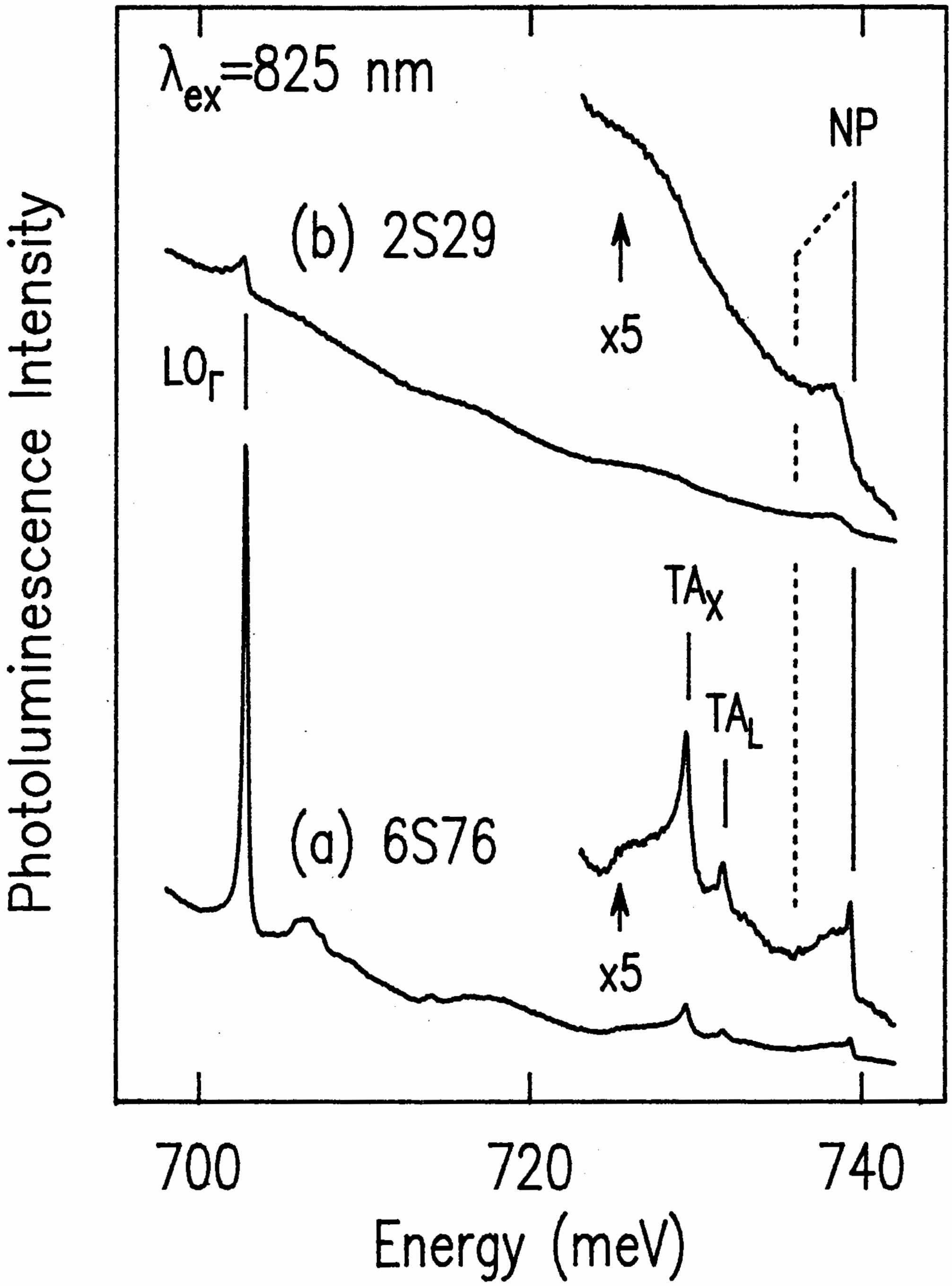

Figure 4.7
Spectra showing an extreme case of the sample to sample variations in the structure of the 0.61 eV EL2 PL band. The broad, low energy portion of the NP transition is indicated by the dashed line. The temperature is 1.6 K and The resolution is 0.12 meV and the spectra are uncorrected.

3 meV below the peak. The spectrum from sample 2S29, shown above in Figure 4.7(b), is dramatically different. Here the NP line has no sharp peak or edge and is shifted somewhat down in energy. This can be explained by considering interactions with the shallow donors, all of which are ionized at equilibrium.

The lifetime of $\tau = 5$ ms for this luminescence has already been mentioned. This value was obtained from sample 6S76, and was acquired simply by placing a chopper in the excitation path and measuring the onset or decay of the luminescence on an oscilloscope. This long lifetime is significant in that it allows electrons in the EL2 shallow excited state to lower their energy by tunneling to neighbouring ionized donors. The reduction in energy is given by the difference in the binding energies of the EL2 excited state and the neutral donor, which gives 2.5 ± 0.5 meV. This compares well with the edge of the low energy tail at 3 meV below the NP line.

The exact line shape of such a transition from the shallow donors to the EL2 ground state will depend on the concentrations and distribution of the shallow donors and EL2 throughout the crystal but a simple argument can show that the observed line shape is consistent with this process. The initial state consists simply of an electron at a neutral shallow donor with energy

$$E_i = E_{gap} - E_D \qquad 4.1$$

where E_D is the shallow donor binding energy. The energy of the final state relative to the initial state must, however, include the residual

Coulomb interaction between the electron and the now ionized shallow donor which for a large separation, R, can be written

$$E_f = E_{gap} - E_{EL2} - \frac{e^2}{\varepsilon R} \qquad 4.2$$

where E_{EL2} is the EL2 binding energy. The transition will then occur with photon energy

$$h\nu = E_i - E_f = E_{EL2} - E_D + \frac{e^2}{\varepsilon R} \qquad 4.3$$

and hence is very similar to donor acceptor pair luminescence. This additional energy is consistent with the observed lineshape between the low energy edge and the distinct EL2-only NP line.

The transitions associated with the broad band lying below the sharp NP line, can be considered as being perturbed by the presence of shallow donors and take place under reduced symmetry and for convenience will be denoted as $(D^0,EL2^+)$. As can be seen in Figure 4.7(b), these reduced symmetry transitions do not require the participation of lattice phonons. The small LO_Γ phonon replica in this spectrum is likely from a small portion of unperturbed centres that is too weak to be observed in the NP region. In this way, the LO_Γ phonon assisted transition can be considered to select the unperturbed centres and the ratio of this transition to the $(D^0,EL2^+)$ transition is like a quality factor which provides a measure of the degree of interaction with the shallow donors. A large value (greater than say 10) signifies a relatively small degree of interaction.

To support the conclusion that it is interactions with the shallow donors that causes the variations in the spectra, it is of course necessary to compare the samples. To this end, the concentrations of the shallow donors, N_D, the shallow acceptors, N_A, and neutral EL2, N_{EL2}, are listed in Table 4.2 in decreasing order of the ratio of the LO_Γ assisted transition to the $(D^0,EL2^+)$ transition. The concentrations were obtained by the all-optical technique of Steiner *et al.* [90S3]. Before referring more explicitly to this information, it is best to first establish what the important parameters are.

The shallow donor concentrations are certainly relevant for the obvious reason that the higher the concentration is, the more likely they are to interact with the EL2. Also, the EL2 concentration is expected to be important, but this usually does not show great sample to sample variation. Less obvious is the importance of the shallow acceptor concentration, which largely determines the equilibrium concentration of $EL2^+$, since $N_{EL2^+} = N_A - N_D$. The effect of the acceptor concentration is indirect, the important quantity is the $EL2^+$ concentration.

The importance of the $EL2^+$ can be understood by considering the spatial extent and long lifetime of the $EL2^0_{n=2}$ state. If it is assumed that this shallow excited state is hydrogenic, the binding energy of 3.2 meV gives an effective Bohr radius of 180 Å. This is comparable to the average separation of the $EL2^+$, which at a concentration of 3×10^{15} cm^{-3} is 690 Å. This large wavefunction, combined with the long lifetime, likely allows the excited electrons to readily tunnel between adjacent $EL2^+$ sites. Some will become trapped at an ionized donor and

Table 4.2

The concentrations of the shallow donors, N_D; the shallow acceptors, N_A; neutral EL2, N_{EL2}; ionized EL2$^+$, N_{EL2^+}; and the ratio of the peak heights of the LO_Γ assisted transition to the $(D^0,EL2^+)$ transition for a variety of samples including those used for the spectra of Figures 4.4 through 4.7.

Sample	N_D (10^{14} cm^{-3})	N_A (10^{15} cm^{-3})	N_{EL2} (10^{16} cm^{-3})	N_{EL2^+} (10^{15} cm^{-3})	$\frac{LO}{(D^0,EL2^+)}$
6S76	6.7	1.7	1.5	1.0	40
C1S2	3.3	1.2	1.3	0.9	33
1S102	8.4	3.2	1.4	2.4	14
8T6	1.4	6.1	1.6	4.7	7.8
2S29	1.4	12	1.2	11	3.0

the $(D^0,EL2^+)$ transition can then occur. The likelihood of such an event will be greater for higher concentrations of $EL2^+$ because the mobility of the tunneling electrons will be enhanced by the reduced distance between the centres.

This is fully supported by the results presented in Table 4.2. The LO_Γ to $(D^0,EL2^+)$ ratio can be seen to decrease as the ionized EL2 concentration increases. In fact, the effective Bohr radius of approximately 180 Å corresponds to a metal-insulator transition [88R1] at a concentration of 3.2×10^{15} cm^{-3}. The metal-insulator transition occurs when the impurity concentration reaches a critical point where there is sufficient wavefunction overlap that metallic behaviour is achieved. This is certainly consistent with the data in Table 4.2 where for concentrations below the metal-insulator transition, the $EL2^0_{n=2} \rightarrow EL2^0_{n=1}$ transition dominates, and above the critical concentration, the $(D^0,EL2^+)$ is dominant.

This explanation is also consistent with the excitation energy dependence. The most distinct NP lines were obtained with 825 nm excitation. This corresponds to an energy of 1503 meV and is high enough that the predominant process will be the excitation of electrons from the shallow acceptors to the conduction band. The recombination then takes place at the ionized EL2, the concentration of which will still be close to its equilibrium value. If, however, the PL is pumped with excitation of wavelength longer than approximately 833 nm, this process is no longer possible. In this case it becomes more likely that the excitation process takes electrons from the neutral EL2 level, creating higher concentrations of ionized EL2. Although this longer wavelength excitation did have the advantage of exciting only the 0.61 eV EL2 PL as evident in Figure 4.4, it did, however, also increase the low energy tail on the NP line. This supports the hypothesis that it is the ionized EL2 concentration that is most important in determining whether the interactions with the shallow donors are likely to be important.

It is also significant that the PL lifetime from samples such as 2S29 is considerably lower than it is from samples with sharper structure. In fact, sample 6S76 showed the sharpest structure and the longest lifetime, and also the largest LO_{Γ} to $(D^0, EL2^+)$ ratio. This not only supports the argument that the lattice phonon coupling is related to relaxing the dipole forbidden nature of the unperturbed transition, but is also consistent with the proposal that the electron tunneling from $EL2^0_{n=2}$ to D^+ sites is dependent on the $EL2^+$ concentration. For high concentrations, this process happens quickly and the transition, no longer forbidden, occurs readily.

The results presented in this section show that 0.61 eV PL band in SI GaAs is due primarily to transitions involving an electron in a shallow excited state of EL2 relaxing down into the EL2 ground state. The exact nature of the resulting PL spectrum was shown to depend on the concentrations of shallow impurities. The other deep PL band that is often mentioned in the context of EL2 is the 0.68 eV band reported by Tajima [86T1]. The next section will confirm that it is EL2 related, but its presence is governed also by the concentrations of shallow impurities.

4.5 The 0.68 eV PL Band

The 0.68 eV PL band was shown by Tajima [86T1] to have a broad NP line followed by 11 meV phonon replicas and was attributed to the free to bound transition $(h^+,EL2^0)$ involving free holes from the valence band to neutral EL2 or equivalently electrons relaxing from neutral EL2 to the valence band. As noted in a later paper by Tajima [87T1], this band is best excited at 1.3 μm, near where the optical cross section for promoting an electron from the valence band to neutralize $EL2^+$, $\sigma_p^{\,o}$, reaches its maximum [81C1]. In contrast to this previous work, however, most of the samples studied here did not show this band.

Instead, it was found only in samples where the shallow acceptor concentration exceeded the shallow donor concentration by approximately 10^{15} cm^{-3}, which again results in a significant concentration of ionized EL2. In these samples, electrons from the valence band can be excited to neutralize the EL2 and the luminescence occurs when the electrons subsequently relax back down to the lower energy configuration. In p-type samples, in which $N_A > N_D + 2\ N_{EL2}$, this band was observed under both above-gap and below-gap excitations wavelengths whereas in samples with some neutral EL2, it was observed only under 1.3 μm excitation.

A typical spectrum obtained at 6.0 K is shown in Figure 4.8(a). It is very similar to that reported by Tajima [86T1] although the quality here is somewhat higher. The NP line peaks at 756 meV and is followed by the characteristic EL2 11 meV LVMs. The improved quality allows the observation of additional structure at approximately 720 meV which is too strong to be the third LVM replica but rather is due primarily to an

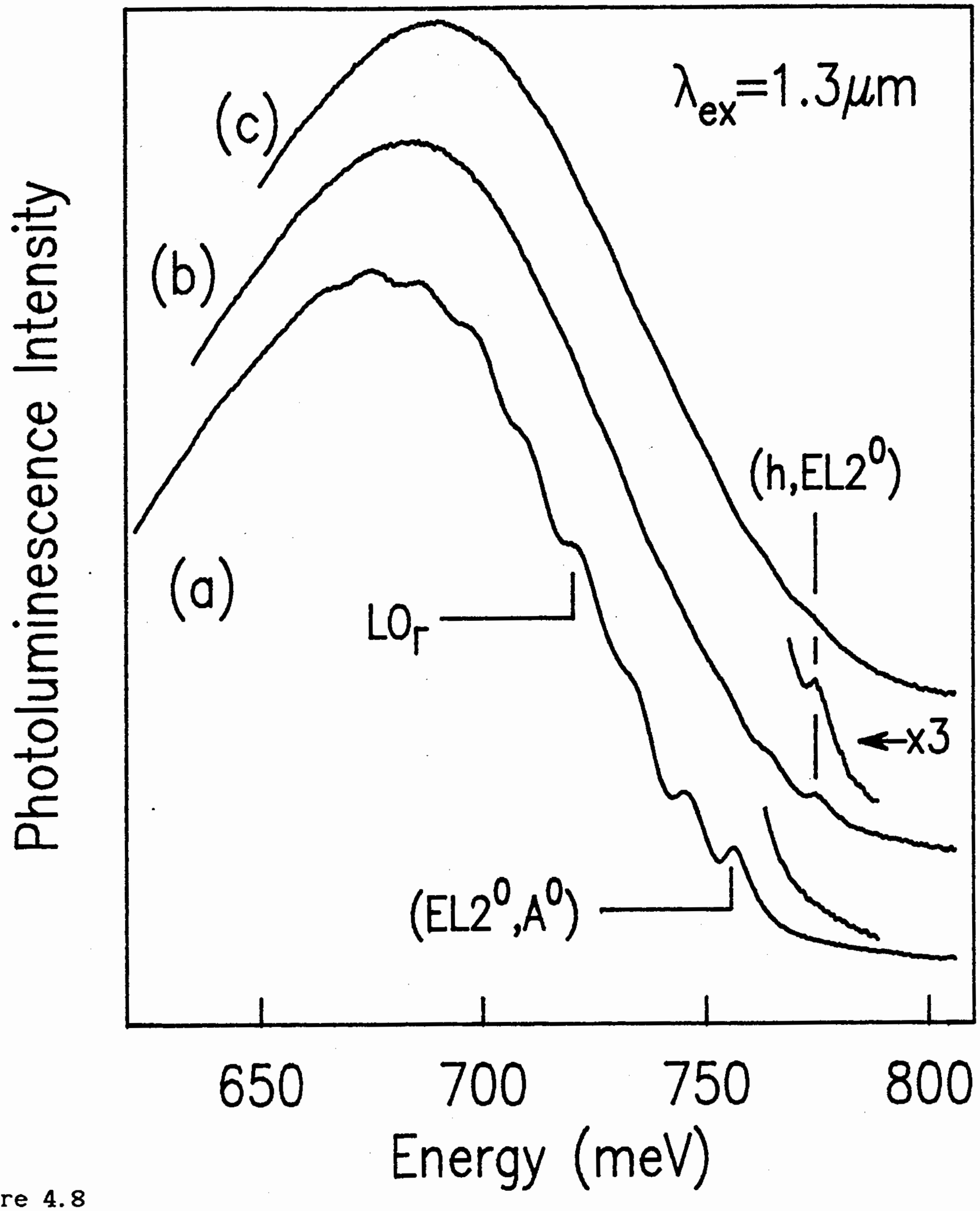

Figure 4.8

Spectra of the 0.68 eV EL2 PL band as a function of temperature from a sample with carbon concentration of 5.5 x 10^{15} cm^{-3}. The sample temperature is (a) 6.0 K, (b) 40 K, and (c) 70 K. The resolution is 0.5 meV and the spectra have been corrected for the instrumental response.

LO_Γ phonon replica. Thus this EL2 transition shows significant LO_Γ coupling as well.

The determination of the exact nature of the transition responsible for the 0.68 eV PL is again aided by valuable information obtained by the temperature dependence of the PL. In the spectrum collected at 40 K, shown in Figure 4.8(b), a free to bound transition with an edge at 773.0 ± 0.6 meV has become evident, and at 70 K, Figure 4.8(c), this transition has become dominant and the band has shifted to higher energy by approximately 15 meV.

The appearance of this free to bound transition and the approximately 23 meV shift from its lower edge to the lower edge of the NP transition indicates that the 756 meV transition is the NP transition of the EL2 to neutral acceptor $(EL2^0,A^0)$ DAP luminescence and the 773.0 meV transition is $(h,EL2^0)$. This is also supported by the broad lineshape of the 756 meV NP transition which is consistent with the residual Coulomb interactions found in DAP recombination. The acceptor involved in the $(EL2^0,A^0)$ DAP transition is likely carbon with $E_A = 26.0$ meV [83K2]. When the energy of the $(h,EL2^0)$ transition edge is added to the energy of the $(e,EL2^+)$ edge, a value of 1515.5 ± 1.1 meV is obtained, which compares well to the 40 K band gap, 1516.6 meV [82B1].

The primary importance of this result is that it is complementary to the previous conclusion that the 0.61 eV band is due to $EL2^0_{n=2} \rightarrow EL2^0_{n=1}$ transitions at low temperature and $(e,EL2^+)$ transitions at higher temperatures. Some other comments are, however, also useful. It was argued in the previous section that the strong LO_Γ phonon replica of the 0.61 eV band is characteristic of the initial state of the $EL2^{0}_{n=2} \rightarrow EL2^{0}_{n=1}$ transition and not the final state. Hence the strength of the first LO_{Γ} phonon replica of this transition is not dominated by vibrational coupling to this lattice phonon but rather that its participation is dictated by the symmetry of the initial and final states. The previous results do not, however, rule out a significant contribution from vibrational coupling. It is reasonable to assume that the ratio of the $1LO_{\Gamma}$ to the $2LO_{\Gamma}$ shown in Figure 4.4 is indicative of the strength of the vibrational coupling and this is roughly in agreement with the ratio of the NP to LO_{Γ} phonon replica in the 0.68 eV PL band.

It is interesting to note that similar structure has been reported in the phonon replicas of the 1.039 eV EL2 intracentre absorption [86S1], but it was attributed instead to an LA + TA assisted transition. In light of the results presented here, it is more likely that the structure observed in the absorption spectrum is in fact due to the LO_{Γ} lattice phonon. The similar contribution of this phonon in both the absorption and 0.68 eV PL spectra indicates that in addition to the strong coupling mechanism found in the 0.61 eV PL band, there is also vibrational coupling to the LO_{Γ} phonon that is not insignificant.

The separation between the NP line and the centre of the 0.68 eV band is 80 ± 5 meV, whereas the corresponding value of this value for the 0.61 eV band less the LO_{Γ} phonon energy is 85 ± 5 meV. Assuming that the value from the 0.68 eV band is more accurate because there is less influence from the non-vibrational coupling of the LO_{Γ} and other lattice phonons to the 0.61 eV band, this suggests that the lattice relaxation energy of neutral EL2 is in fact 80 ± 5 meV.

This is a quantity that has not previously been reported and is not taken into account in the lattice relaxation involved in the 1.039 eV intracentre absorption. This and the obvious participation of phonons of energy higher than the 11 meV LVMs may help future attempts to explain the discrepancies between the strength of the NP line and the apparent phonon coupling and lattice relaxation involved in the absorption transition.

4.6 Summary

The primary goal of this chapter was to identify the EL2-related PL bands in SI GaAs and to determine the nature of the underlying electronic transitions. To summarize and give a concise picture of these results, the transitions are depicted in Figure 4.9. The most significant of these results is the presence of the sharp fine structure in the 0.61 eV band which arises from an intracentre $EL2^{0}_{n=2} \longrightarrow EL2^{0}_{n=1}$ transition. The narrow line width of these transitions has allowed perturbation studies of EL2 to be carried out with much greater precision than was previously achievable. These results will be presented in Chapter 5.

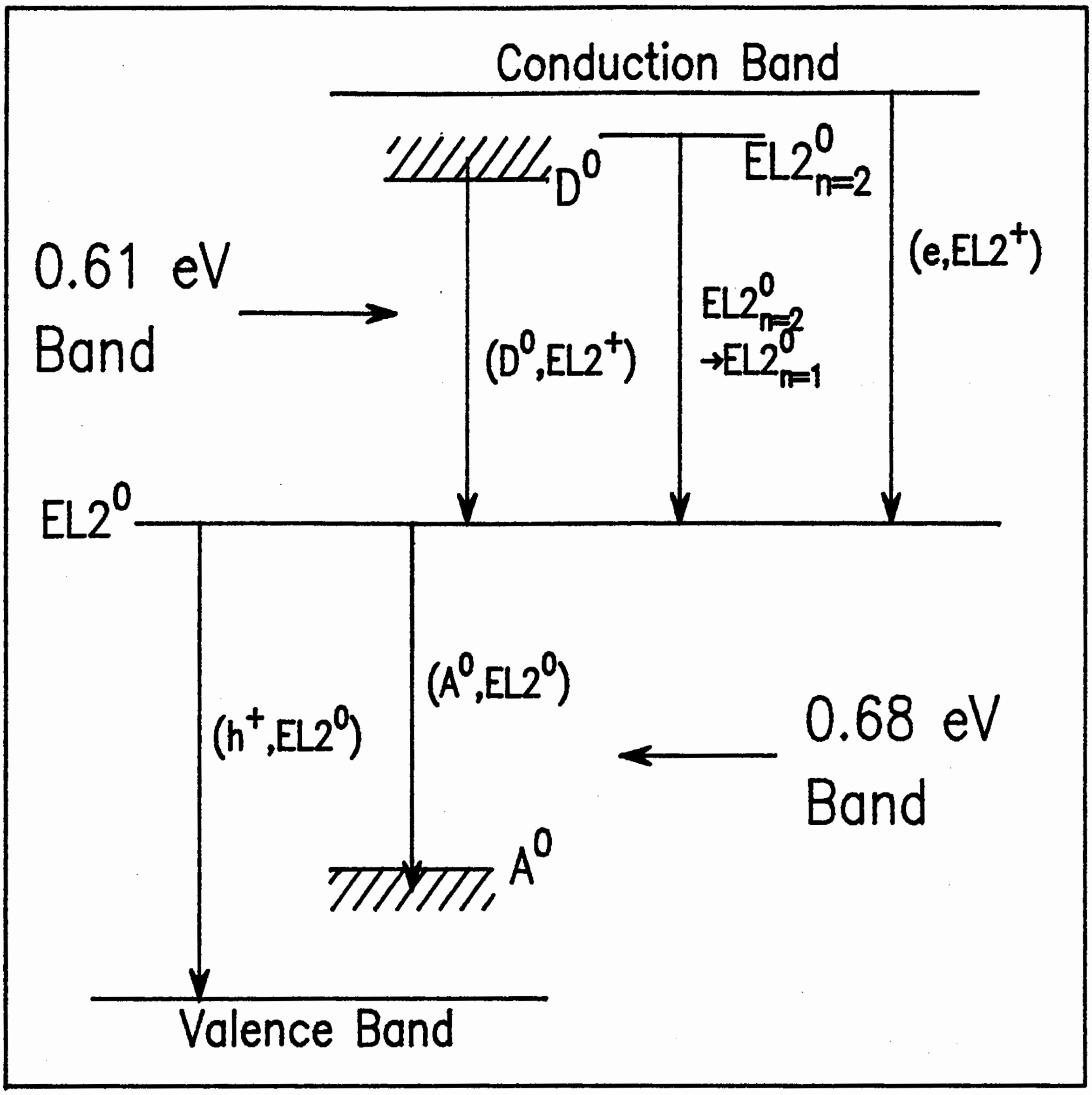

Figure 4.9

A summary of the results of this Chapter. The 0.61 eV EL2 band is from transitions across the upper half of the gap and the 0.68 eV EL2 band is from transitions across the lower half of the gap.

CHAPTER 5. THE SITE SYMMETRY OF EL2

5.1 Introduction

It is well established that the EL2 defect involves the arsenic antisite, As_{Ga}. This was discussed in section 4.3 of Chapter 2. Sections 4.4 through 4.6 then went on to elaborate on the two predominant models of the structure of EL2. It was shown that one school of thought has the EL2 defect comprised solely of an isolated As_{Ga} [85K1, 88C1, 88D1] and the other has it as an arsenic antisite-arsenic interstitial pair, As_{Ga}-As_i, with C_{3v} symmetry [87M1]. In addition, there are still those who persist in including oxygen as a sometimes present constituent [91B2].

The fine structure on the 0.61 eV band [90N1], introduced in Chapter 4, is the sharpest spectroscopic signature of EL2 and as such can provide a sensitive probe of the defect structure under external perturbations. This chapter will report the results of experiments on the behaviour of this fine structure under the external perturbations of uniaxial stress and magnetic field. The interpretation of the results is very clear. They indicate full T_d symmetry and hence strongly support the isolated As_{Ga} model of EL2 [91N1].

5.2 Uniaxial Stress Perturbation

Before proceeding with the presentation of the uniaxial stress results, it is useful to briefly review the strengths and weaknesses of the previous piezospectroscopy of EL2 [85K1] in the context of the subsequent conflicting results [87M1] that have fueled the present day controversy. A clear and reasonably up to date treatment on the current state of affairs with a pro-isolated As_{Ga} slant can be found in the review by Kaufmann [89K1]. The opposing view is presented in another review by Bourgoin *et al* [88B1].

The strongest evidence that EL2 is not a point defect is the ODENDOR results which show C_{3v} symmetry [87M1]. They have been interpreted as being from an As_{Ga}-As_i pair, with the As_i displaced from the antisite by 1.5 bond lengths along the [111] direction. These results are at odds with the uniaxial stress splittings of the 1.039 eV intracentre absorption line reported by Kaminska [85K1]. The results were interpreted in terms of a $A_1 \rightarrow T_2$ transition in full T_d symmetry. The A_1 state is nondegenerate and does not split, but the T_2 state is three-fold orbitally degenerate and the splittings were attributed to the removal of this electronic degeneracy. There was no indication of orientational degeneracy.

It is possible that the electronic wavefunctions of the states involved in this transition are relatively insensitive to the presence of the As_i and hence may not be strongly affected by the perturbation introduced by the uniaxial stress. Recent electronic structure calculations on the defect structure reported in the ODENDOR studies show, however, that this is not the case [89B1]. It was shown that the effects of the Coulomb potential of the As_i are in fact large and, in particular, that stress-induced splittings for such a defect structure should have been resolved in the intracentre absorption studies of Kaminska. This analysis does, however, remain complicated because of the large Jahn-Teller relaxation of the final state of the transition that is implied by the non-linear shift of the lines as a function of the stress [85K1, 89B1].

The results presented here will be shown to not suffer from this complication. The electronic nature of the states involved in the transition will first be discussed in terms of the observed behaviour under uniaxial stress. The results will be shown to be fully consistent with the identification of the transition made in Chapter 4 as the simple relaxation of an electron in an EL2 shallow hydrogenic excited state to the EL2 ground state. After this, the possibility of an orientational degeneracy will be investigated.

The essential result from the uniaxial stress experiments can be stated very succinctly. There was no evidence of any splitting whatsoever in any of the three directions. This is illustrated in the series of spectra shown in Figure 5.1. These spectra show the effect of uniaxial stress along the [111] direction starting with the zero stress spectrum of Figure 5.1(a) followed by spectra obtained under uniaxial stress increasing in increments of 130 MPa up to a final value of 520 MPa. The only effect is a shift to higher transition energies that is linear with the stress. At high stress a broadening of the lines is observed. Such broadening is an avoidable consequence of applying stress, and places an upper limit on resolving any real induced splittings.

Before discussing these results and their significance in greater

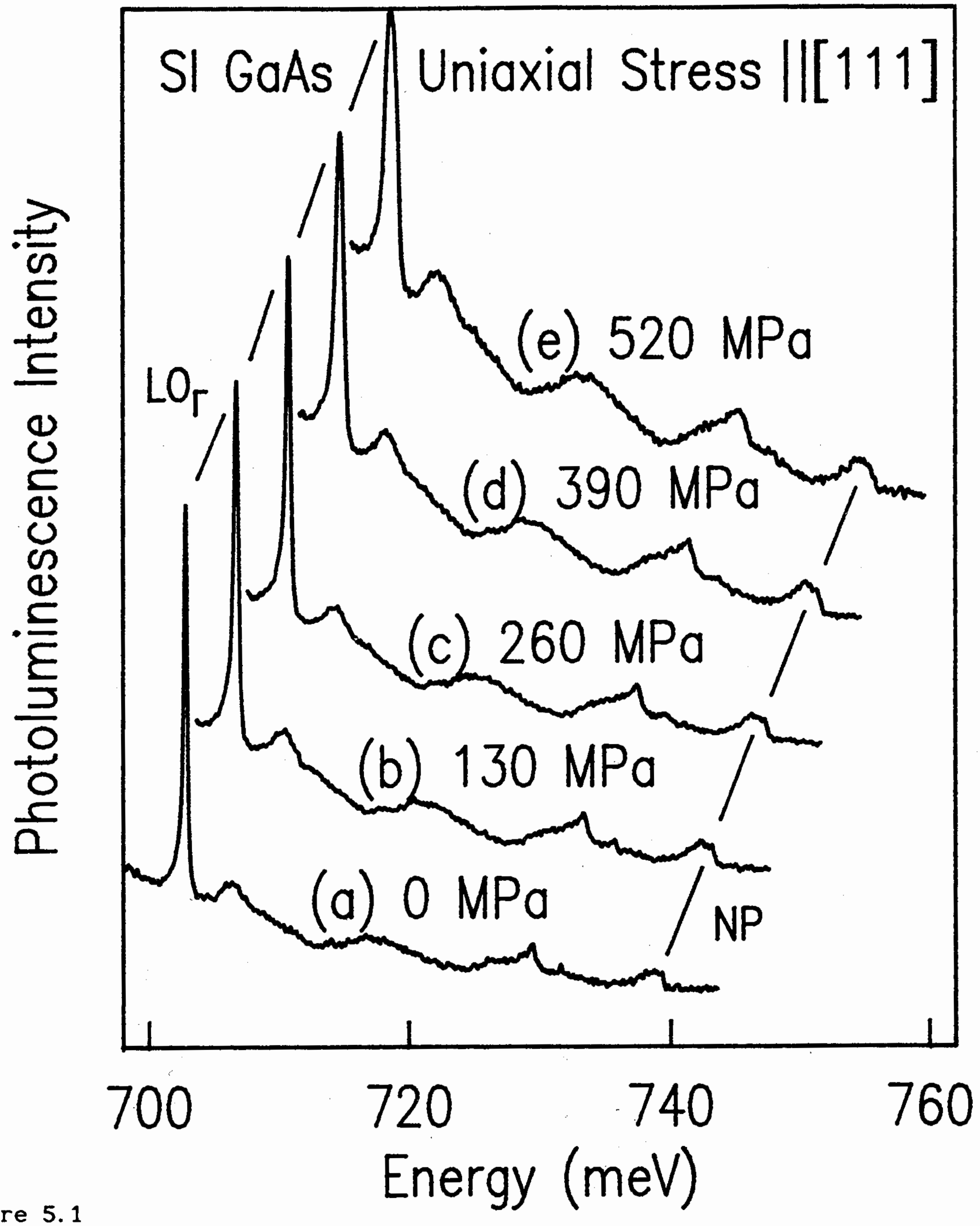

Figure 5.1
PL spectra showing the fine structure of the 0.61 eV EL2 band as a function of stress along the [111] direction. The temperature is approximately 2.0 K, the resolution is 0.12 meV and the spectra are uncorrected.

detail it is useful to make some comments on the spectra presented in Figure 5.1. As can be seen in these spectra, the available material that was suitable for preparing stress samples did not show a NP line as clearly as some other samples. Fortunately, the LO_{Γ} phonon replica is, as usual, sharp and well defined and it was this transition that was monitored as a function of stress. This is somewhat less desirable than being able to cleanly observe the behaviour of the NP line, but the stresses achieved were quite high, particularly in the [111] direction, and if splittings were present in the NP line they would have been observed. No deviation in behaviour between the NP and LO_{Γ} transitions was observed in any of the results.

These spectra also illustrate the homogeneity of the uniaxial stress in that there is very little line broadening. This is especially apparent in the spectrum of Figure 5.1(c) at 260 MPa which shows very little broadening over the zero stress spectrum of Figure 5.1(a). At 390 MPa, Figure 5.1(d), the line has begun to show some appreciable broadening and Figure 5.1(e) at 520 MPa shows the worst case of broadening just before sample failure. This spectrum represents the highest stress achieved in any direction which is fortuitous since the [111] direction is the most important one to investigate for C_{3v} symmetry.

The high stresses achieved with minimal broadening in conjunction with the narrow line width of the transition allowed for much greater sensitivity in the detection of any splitting than has previously been achieved. It should be emphasized that 260 MPa is already a very high stress. The studies of the 1.039 eV absorption line report stresses only up to 250 MPa and already at 130 MPa in the [111] direction, the observed splitting was approximately 12 meV. This is in contrast to the upper limit for splitting in the present study which from the measured line widths is 0.67 meV at 295 MPa along [100], 0.48 meV at 288 MPa along [110] and 0.55 meV at 328 MPa along [111].

The spectra in Figure 5.1 show the effect of stress along the [111] direction and not only was no splitting observed in the [110] and [100] directions but the shift of the lines as a function of the applied stress was also found to be the same. The complete stress results are presented in Figure 5.2 where the LO_Γ transition energy is plotted as a function of the stress for the three crystallographic directions. As can be seen, all the points lie on the same straight line.

These results indicate a high degree of symmetry and it is useful to proceed on the assumption of a point defect with full T_d symmetry and examine first the electronic orbital degeneracies of the initial and final states. The effect of the applied stress is customarily treated by expanding the resulting perturbation potential, V, to first order in the stress [81L1]

$$V = \sum_{i,k} V_{ik}\sigma_{ik} \qquad 5.1$$

where V_{ik} is the piezospectroscopic tensor, σ_{ik} is the stress tensor and $i,k = x,y,z$. It is convenient to express this in terms of the irreducible representations of the group that describes the symmetry of the crystal. This can be written

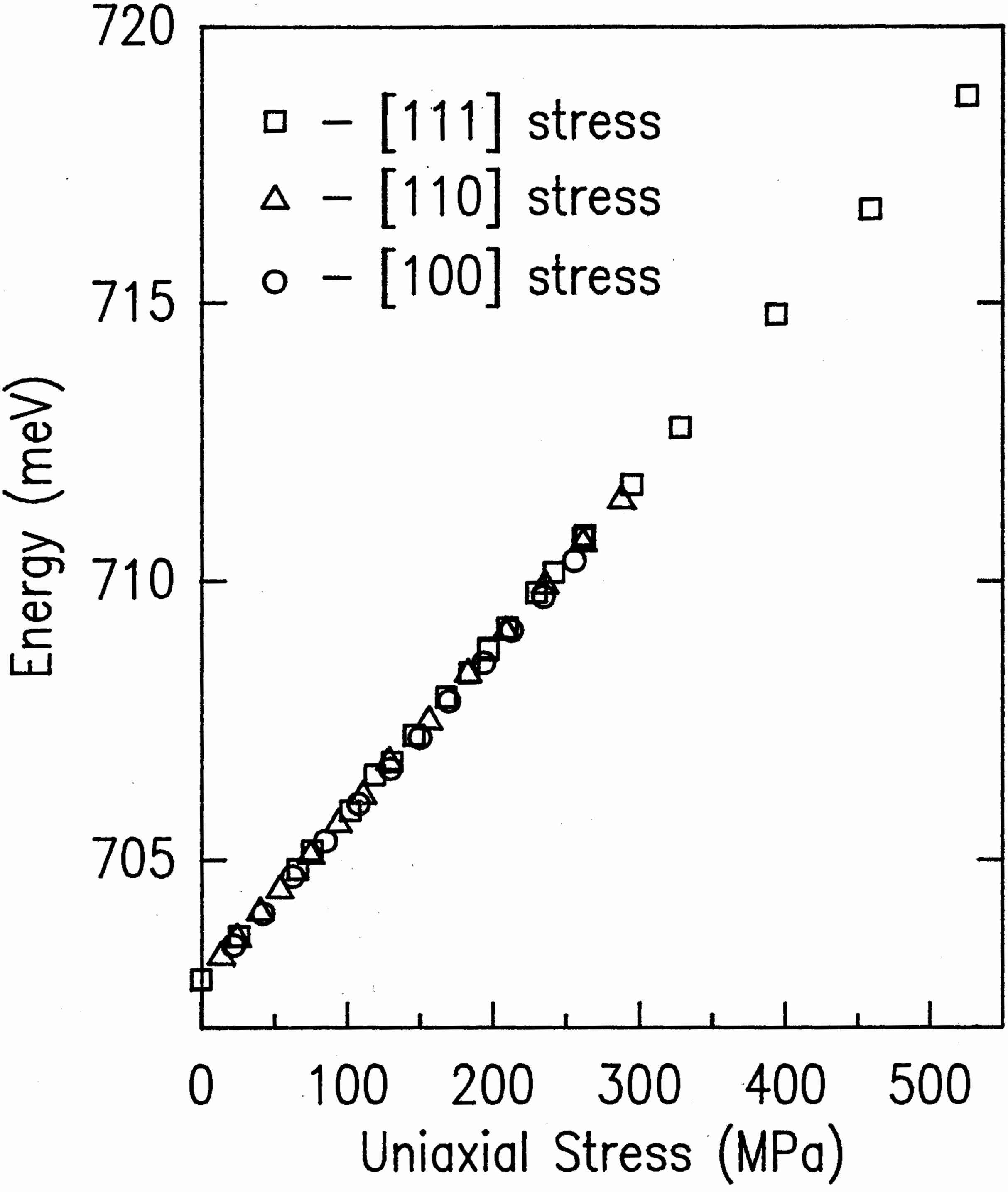

Figure 5.2

The energy of the LO_Γ phonon replica as a function of uniaxial stress for the [111], [110], and [100] directions.

$$V = \sum_{\Gamma} \sum_{\mu} V_{\mu}^{\Gamma} \sigma_{\mu}^{\Gamma} \qquad 5.2$$

where Γ stands for the irreducible representations and μ is the basis functions of that representation. For T_d symmetry, the only non-zero contributions are from the A_1, E and T_2 representations . Only wavefunctions that have the symmetry of these representations have non-zero matrix elements in the perturbation V.

It is shown in Lannoo and Bourgoin [81L1] that states with wavefunctions that transform as E are two-fold degenerate and will split under [100] and [110] stresses and those that transform as T_2 are three-fold degenerate and will split under all three stresses. In contrast, states that transform as A_1 have full T_d symmetry and are non-degenerate. For such states, there is only one matrix element of the perturbation V and it is of of the form $<\phi_{A1}| V |\phi_{A1}>$ and the only non-zero term for all stresses will be for $V = V_{A1} \sigma_{A1}$. The decomposition of the V_{ij} and σ_{ij} into classes that transform as the irreducible representations can be done very simply with the aid of the transformation matrices listed in a paper by Baraff [89B1] which for the A_1 representation results in

$$\begin{aligned} V_{A_1} \sigma_{A_1} &= \frac{1}{3} (V_{xx} + V_{yy} + V_{zz})(\sigma_{xx} + \sigma_{yy} + \sigma_{zz}) \qquad 5.3 \\ &= V_0 \ (\sigma_{xx} + \sigma_{yy} + \sigma_{zz}) \end{aligned}$$

where for T_d symmetry, $V_0 = V_{xx} = V_{yy} = V_{zz}$. For [100] stress, $\sigma_{xx} = \sigma_0$

and $\sigma_{yy} = \sigma_{zz} = 0$, and for [110] stress, $\sigma_{xx} = \sigma_{yy} = \frac{\sigma_o}{2}$ and $\sigma_{zz} = 0$, and for [111] stress $\sigma_{xx} = \sigma_{yy} = \sigma_{zz} = \frac{\sigma_o}{3}$, and finally for hydrostatic pressure, $\sigma_{xx} = \sigma_{yy} = \sigma_{zz} = \sigma_o$. Thus the sole result of uniaxial stress on an A_1 state in T_d symmetry is a shift in energy linear with the stress that is equal in all three directions and is one third of the hydrostatic shift.

The measured shifts from the results shown in Figure 5.2 are 29.5 ± 0.8 meV/GPa for [100] stress, 29.9 ± 0.8 meV/GPa for [110] stress and 30.2 ± 0.8 meV/GPa for [111] stress which add up to 89.6 ± 2.4 meV/GPa. Due to the shallow nature of the initial state, it will largely track the hydrostatic shift of the conduction band and hence the shift of the initial state relative to the conduction band is negligble. The observed hydostatic shift of the transition is thus entirely due to the ground state which is in excellent agreement with the hydrostatic pressure results of Dreszer and Baj where a value of 87 meV/GPa was reported for the shift of the EL2 ground state with respect to the conduction band [88D2]. The shift and lack of splitting of the PL transition under uniaxial stress is completely consistent with an A_1 to A_1 EL2 transition in T_d symmetry. This is also in agreement with the analogy to the 1s2s to $1s^2$ transition of the helium atom made in Chapter 4.

The preceding argument was based on the assumption of a point defect with full T_d symmetry. In general, the lack of splitting under uniaxial stress shows that there is no evidence that either of the states involved in the PL transition are orbitally degenerate. The possibility that these states are nondegenerate states of a complex defect with the reduced symmetry of a sub-group of T_d must also be addressed. It will now be argued that this too can be ruled out.

If the defect involved is not a point defect but is instead a complex defect with the reduced symmetry of one of the subgroups of T_d several effects would be apparent. For the sake of concreteness, consider the case of a defect with C_{3v} symmetry. This choice is obviously predicated by the As_{Ga}-As_i models of EL2 with this symmetry. The specific alignment of such a defect would be randomly distributed among the [111], [$1\bar{1}\bar{1}$], [$\bar{1}1\bar{1}$] and [$\bar{1}\bar{1}1$] directions. Uniaxial stress along one of these directions would perturb the one quarter of the defects aligned parallel to the stress differently than the other three quarters aligned along the remaining three equivalent directions and a doublet splitting with a three to one intensity ratio should result. Similarly, a [110] stress would equally perturb the [111] and [$\bar{1}\bar{1}1$] aligned defects and would cause no relative displacement of those aligned along [$\bar{1}1\bar{1}$] and [$1\bar{1}\bar{1}$] and should lead to two equally intense lines. A [100] stress would perturb all four orientations equally, and thus produce no splitting.

This can be treated more formally using the results of Kaplyanskii [63K1]. Explicitly making the summation in Equation 5.1 gives

$$V = V_{xx}\sigma_{xx} + V_{yy}\sigma_{yy} + V_{zz}\sigma_{zz} + 2V_{xy}\sigma_{xy} + 2V_{yz}\sigma_{yz} + 2V_{zx}\sigma_{zx} \qquad 5.4$$

and by considering the stress tensor in relation to the different orientations of the defect, the possible splittings introduced by the orientational degeneracy can be obtained. Keeping to the concrete example of C_{3v} symmetry, Equation 5.4 can be written

$$V = V_0(\sigma_{xx} + \sigma_{yy} + \sigma_{zz}) + 2V_1(\sigma_{xy} + \sigma_{yz} + \sigma_{zx}) \qquad 5.5$$

where $V_0 = V_{xx} = V_{yy} = V_{zz}$ and $V_1 = V_{xy} = V_{yz} = V_{zx}$ by symmetry.

For stress along [111], the stress tensor for the defects parallel to [111] is given by $\sigma_{ij}^{[111]} = \frac{\sigma_0}{3}$ and the shift in energy per unit stress is $V = V_0 + 2V_1$. For the other three orientations of the defect,

$$\sigma_{ij}^{[1\bar{1}\bar{1}]} = \sigma_{ij}^{[\bar{1}\bar{1}1]} = \sigma_{ij}^{[\bar{1}1\bar{1}]} = \sigma_0 \begin{bmatrix} \frac{1}{3} & \frac{-1}{3} & \frac{1}{3} \\ \frac{-1}{3} & \frac{1}{3} & \frac{-1}{3} \\ \frac{1}{3} & \frac{-1}{3} & \frac{1}{3} \end{bmatrix} \qquad 5.6$$

and the shift is $V = V_0 - \frac{2}{3}V_1$.

Similarly for stress along [110] the stress tensors for the $[\bar{1}1\bar{1}]$ and $[1\bar{1}\bar{1}]$ orientations that are perpendicular to the stress are

$$\sigma_{ij}^{[1\bar{1}\bar{1}]} = \sigma_{ij}^{[\bar{1}1\bar{1}]} = \sigma_0 \begin{bmatrix} \frac{1}{2} & \frac{-1}{2} & 0 \\ \frac{-1}{2} & \frac{1}{2} & 0 \\ 0 & 0 & 0 \end{bmatrix} \qquad 5.7$$

and the shift is $V = V_0 - V_1$. For the other two orientations the stress tensor is of the same form but the elements are all positive and the shift is $V = V_0 + V_1$. For [100] stress, the stress tensor for all four orientations is $\sigma_{xx} = \sigma_0$ and the shift is $V = V_0$.

The observed lack of splitting under [110] and [111] stresses is clearly inconsistent with an orientational degeneracy particularly when account is taken of the calculations by Baraff which show that the As_i would have a large effect on the electronic states [89B1]. The lack of splitting alone, however, is not sufficient to rule out a defect with reduced symmetry. One more possibility must be addressed.

It is possible that the energy barriers between the equivalent (at zero stress) orientations of the centre are low enough that the constituent atoms of the defect can tunnel from one orientation to another even at T = 2 K, and hence the defects may align themselves under uniaxial stress in such a way that the orientational degeneracy is removed to the extent that no observable splittings occur. This question can be quickly settled by noting that the shift in energy with stress has been experimentally observed to be equal to the hydrostatic term for all three stress directions, whereas the above analysis shows that even if the defects were realigning under stress the shift of the levels would be anisotropic. This can be readily seen by noting that the shift for any orientation under [110] or [111] stress would be either greater than or less than the purely hydrostatic component induced by the [100] stress.

These stress results are in complete agreement with the conclusions of Kaminska *et al* [85K1] and are much more direct. The criticisms recently applied to the interpretations of the uniaxial stress behaviour of the 1.039 eV absorption transition [90S1], can not be applied here. The lack of splitting provides evidence that no orientational degeneracy has been lifted and that both the initial and final state have full T_d symmetry.

5.3 Magnetic Field Perturbations

Another way to probe the defect structure and its electronic states is to place the sample in a magnetic field and observe the Zeeman splitting of the transitions. The results of the previous section showed that the states involved in the 0.61 eV EL2 PL are orbitally nondegenerate. One would then expect that the application of a magnetic field would then serve only to remove the remaining degeneracy due to the electron spin. For a state described by a quantum number n = i, the change in the corresponding energy level for an applied magnetic field, B, is

$$E_{n=i} = m_s \mu_B g_{n=i} B \qquad 5.8$$

where $m_s = \pm \frac{1}{2}$ is the magnetic spin quantum number, μ_B is the electron Bohr magneton and $g_{n=i}$ is the g-factor for the i^{th} state. Each level will thus be split by

$$\Delta E_{n=i} = \mu_B g_{n=i} B \qquad 5.9$$

The g-factor of an electron bound to a defect in a semiconductor deviates from that of an electron bound to a free atom in two ways. Since the Bohr magneton of a free electron is used in Equations 5.8 and 5.9, the effective mass of the bound electron will clearly have to be included in the g-factor. More important though, is the effect of the magnetic field induced dipolar moments of the atoms in the vicinity of the defect. These induced moments serve to reduce the effect of the applied field in a way that reflects the local environment of the defect [83B1]. Hence, information on the structure of the defect can be obtained by studying the orientational dependence of the g-factor which is, in general, a tensor.

To introduce the effect of the applied magnetic field on the transition responsible for the 0.61 eV PL band, spectra of the structured portion of the band are shown in Figure 5.3 as a function of increasing applied magnetic field in a direction parallel to the [110] crystallographic axis. The most important result here is that the transition is indeed seen to be split under the influence of an applied magnetic field. This is most clearly seen in Figures 5.3(a) and 5.3(b) where the strong LO_{Γ} transition has split into two transitions labelled LO_{Γ}^{1} and LO_{Γ}^{2}. The same splitting is present in the NP region where the two transitions are now labelled $NP^{1}$and NP^{2}. The NP^{2} transition is only weakly apparent in these spectra but stronger evidence of its presence will be presented later.

Once again, before discussing this result in greater detail, it is useful to mention some other noteworthy aspects of these spectra. The zero field spectrum is actually the zero-stress reference spectrum shown in Figure 5.1(a) and was obtained, not from the magnet cryostat, but from the conventional vari-temp optical cryostat. This was done because a significant amount of signal is lost due to the longer path traversed by the luminescence from the magnet dewar to the interferometer and the extra optical elements in the path. Since the same material was used for these studies as was used for the uniaxial stress work, it still

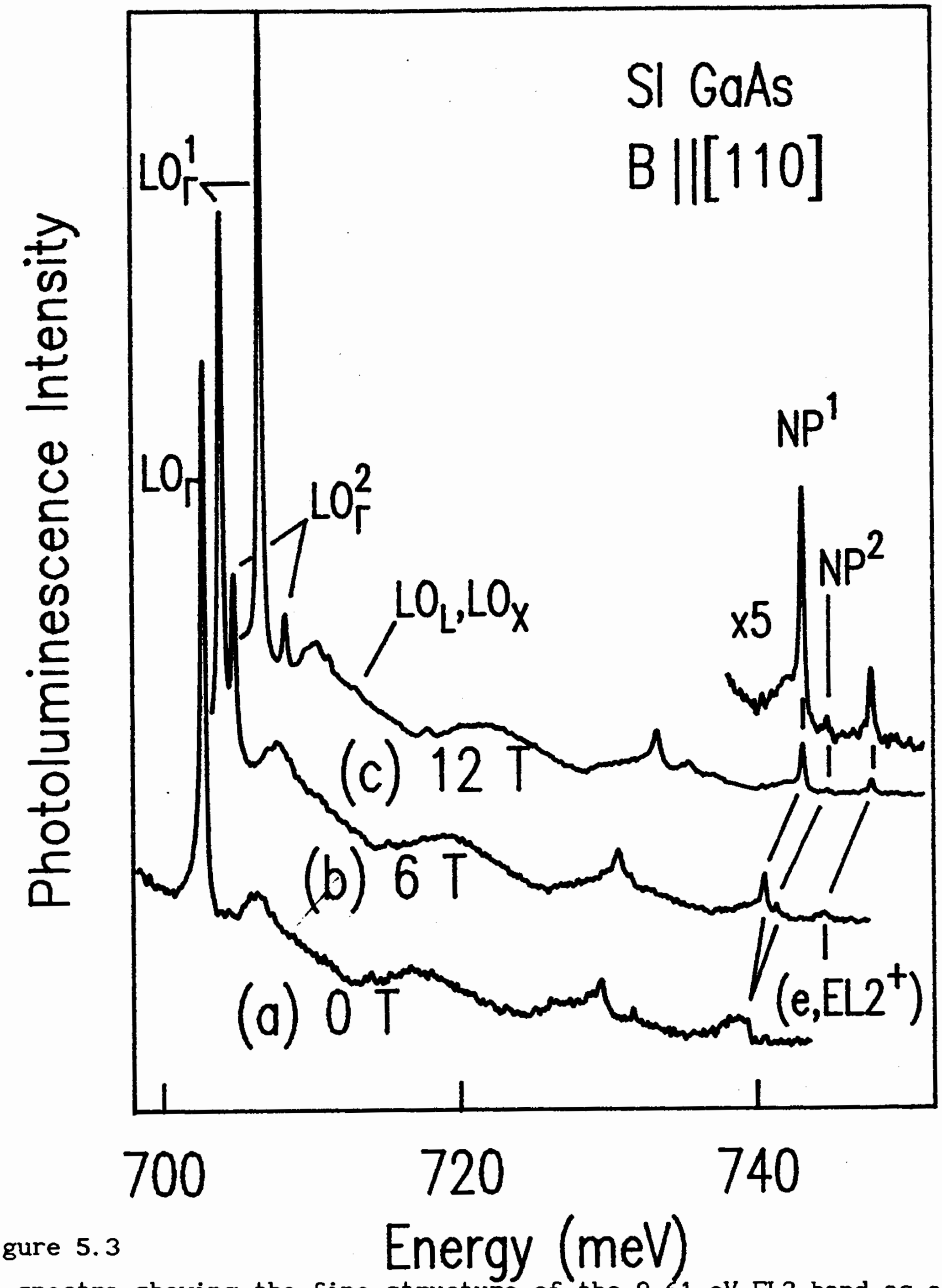

Figure 5.3

PL spectra showing the fine structure of the 0.61 eV EL2 band as a function of magnetic field along the [110] direction. The 4.2 K spectrum at zero field, (a), is a reference for the 8 K spectra at (b) B = 6 T and (c) B = 12 T. The resolution is 0.12 meV and the spectra are uncorrected.

provides a suitable reference for Figures 5.3(b) and 5.3(c).

Fortunately, the application of the magnetic field results in an increase in the PL signal strength and the collection of high quality spectra from samples in the magnetic field such as those shown in Figures 5.3(b) and 5.3(c) was possible. The increase in the signal strength is most apparent in the expanded NP region of Figure 5.3(c) where the sharp portion of the NP transitions are especially enhanced in comparison to the low energy tail. This behaviour has some relevance to the discussion in Chapter 4 on the nature of the transition.

Calculations show that the s-orbital electron wavefunctions of hydrogenic systems are elongated and compressed by the application of a magnetic field [84R1]. Both of these effects are consistent with the observed behaviour in terms of the model proposed in Chapter 4. The compression of the wavefunctions leads to less mobility of the excited electron tunneling to adjacent $EL2^+$ sites. This reduces the interaction with the ionized shallow donors and hence the increase in intensity of the $EL2^0_{n=2} \rightarrow EL2^0_{n=1}$ transition relative to the low energy tail of the NP line due to $(D^0, EL2^+)$ transitions. The intensity of the NP $EL2^0_{n=2} \rightarrow EL2^0_{n=1}$ transition also increases relative to the LO_Γ replica. This is consistent with the reduced symmetry of the wavefunctions which is likely to relax the forbidden nature of the transition and increases the probability of the transition proceeding without the participation of a lattice phonon.

Also enhanced and sharpened is the free to bound $(e, EL2^+)$ transition which now appears at a much lower temperature than is the case at B = 0 T even though the binding energy of the $EL2^0_{n=2}$ state increases to 4.65 meV at B = 12 T compared to 3.2 ± 0.5 meV at zero field. The sharpness of this transition reflects the formation of discrete Landau levels in the conduction band [89S1].

The increase in the PL signal strength with magnetic field allowed for the collection of spectra at B = 12 T with very high signal to noise ratios and the structure due to the phonon coupling introduced in Figure 4.5 is more evident in the spectrum of Figure 5.3(c). The LO_L and LO_X phonon assisted transition is indicated here since this transition is only weakly apparent in Figure 4.5 where the details of the lattice phonon coupling was previously introduced.

When the behaviour of this PL band was first investigated under the perturbation of magnetic fields, the splitting was almost missed because the sample was held at very low temperatures. The only obvious effect was a strong shift of the lines to higher energy. At this time, the magnet cryostat allowed the sample to be cooled only by direct immersion in the liquid helium bath. Furthermore, to obtain maximum signal to noise ratios, these initial experiments were performed with the helium in the superfluid state at temperatures of approximately T = 2 K or lower. It was only when the liquid helium in the sample chamber ran out and the sample began to warm that evidence of a splitting at B = 3 T was fortuitously observed.

This suggested that the initial state of the transition was splitting under the magnetic field and the experiment would have to be performed at higher sample temperatures where the upper split-off initial state would be thermally populated. The experiments were then repeated in boiling liquid helium at 4.2 K and the presence of the splitting at B = 3 T was confirmed but the intensity of the upper split-off transition diminished quickly with increasing magnetic field and the noise introduced by the boiling helium was prohibitive. This prevented sufficient data to track to the behaviour from being obtained.

Subsequently, the vari-temp insert to the sample chamber of the magnet dewar was built and the experiments were again repeated with the ability to vary the temperature from approximately T = 6 K and up. It was only then that the field-split doublet could be clearly resolved at the higher magnetic fields as shown in the spectra of Figures 5.3(b) and 5.3(c) which were collected with the sample at T = 8 K. This allowed the splitting to be followed as a function of the field and these results will be presented in more detail later, but it also allowed the thermalizing behaviour of the doublet to be investigated at a fixed field. This is shown in Figures 5.4(a), 5.4(b) and 5.4(c) where spectra are presented from a sample oriented with the [111] crystallographic axis parallel to B = 12 T at temperatures of T = 7.3 K, T = 11 K and T = 19 K, respectively.

The low temperature spectrum is virtually identical to that of Figure 5.3(c). The LO_Γ^2 transition is much weaker than LO_Γ^1, the NP^2 transition is just barely observable above the signal to noise limit and again the free to bound $(e,EL2^+)$ transition is present at roughly one third the intensity of the NP^1 line. At T = 12 K, the intensity of the upper split-off transition has increased relative to the lower energy transition in both the NP and LO_Γ regions, with the NP^2 transition now more clearly present above the noise. In addition, the free to bound transition is now stronger than the NP transitions and it too is split

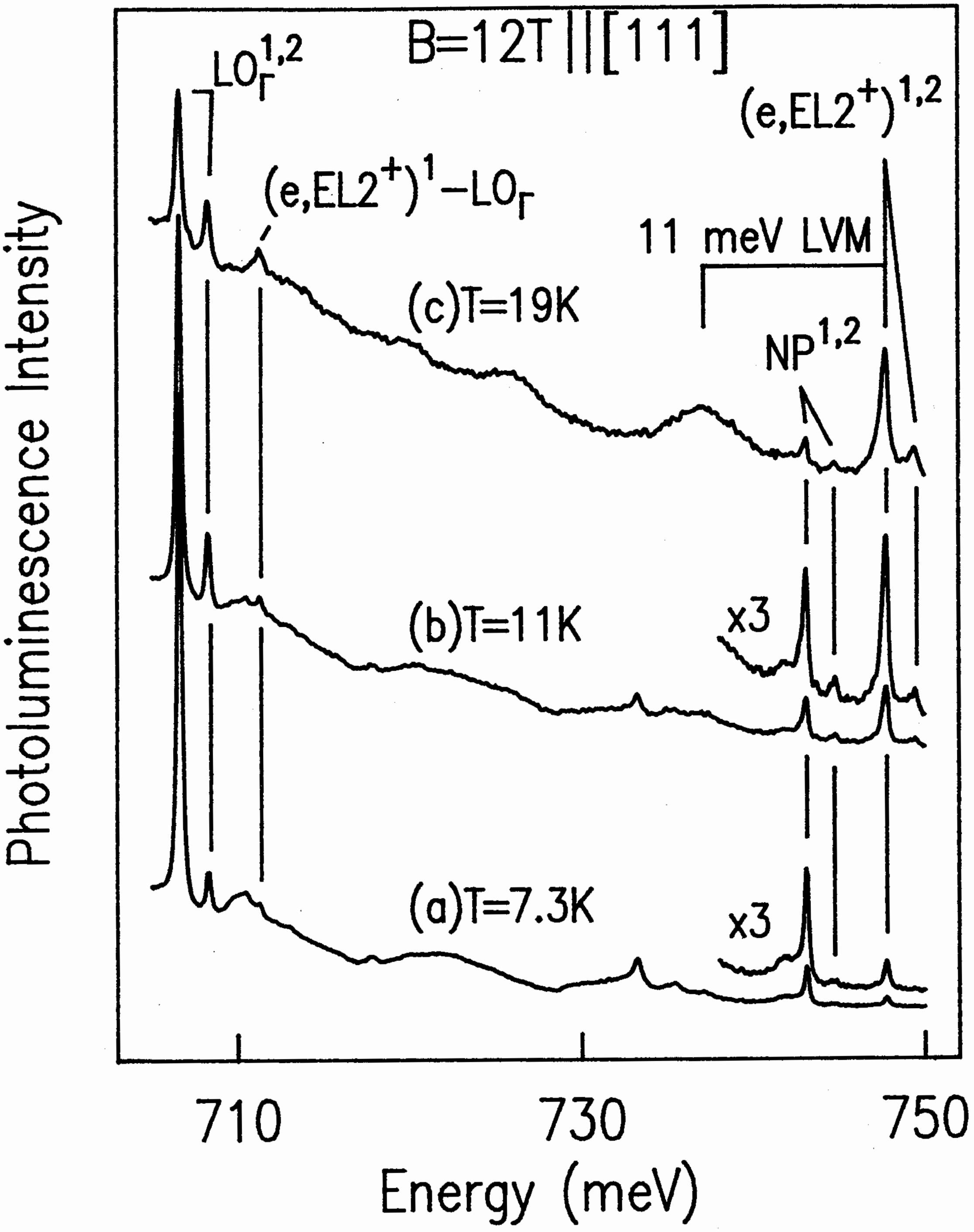

Figure 5.4

PL spectra showing the temperature dependence of the fine structure on the 0.61 eV EL2 band at B = 12 T along the [111] direction. The resolution is again 0.12 meV and the spectra are not corrected.

by the same amount into transitions labelled as $(e,EL2^+)^1$ and $(e,EL2^+)^2$. This trend is seen to continue in the T = 18 K spectrum, Figure 5.4(c), where the upper field-split transitions have again increased in intensity relative to the lower ones and the free to bound transitions are now much stronger than the NP transitions.

The relative population of two energy levels in thermal equilibrium is governed by the Boltzmann distribution

$$\frac{n_2}{n_1} = e^{-\Delta E/k_B T} , \qquad 5.10$$

where n_2 and n_1 are the populations of the two levels, ΔE is their separation in energy and k_B is the Boltzmann constant. If electrons in these two levels decay with equal probability to a lower state, the relative intensity of the resulting lines will also follow the Boltzmann distribution. On the other hand, if the splitting is in the final state of the transition, the relative intensities will be a fixed quantity and will not vary as a function of temperature. To confirm that the observed splitting is only from the initial state, the ratio of the LO_Γ^2 to LO_Γ^1 intensities is plotted versus the Boltzmann factor in Figure 5.5 for the measured splitting of $\Delta E = 13.65\ cm^{-1} = 1.692$ meV at B = 12 T. As can be seen, the resulting line has a slope of one and passes through the origin, as expected.

Figures 5.3 and 5.4 have presented spectra that were obtained with the magnetic field parallel to the [110] and [111] directions and the similarity of these spectra was commented on. In fact, the spectra for the [100], [110] and [111] oriented samples were identical in all respects. This is shown in Figures 5.6(a), (b) and (c) where spectra

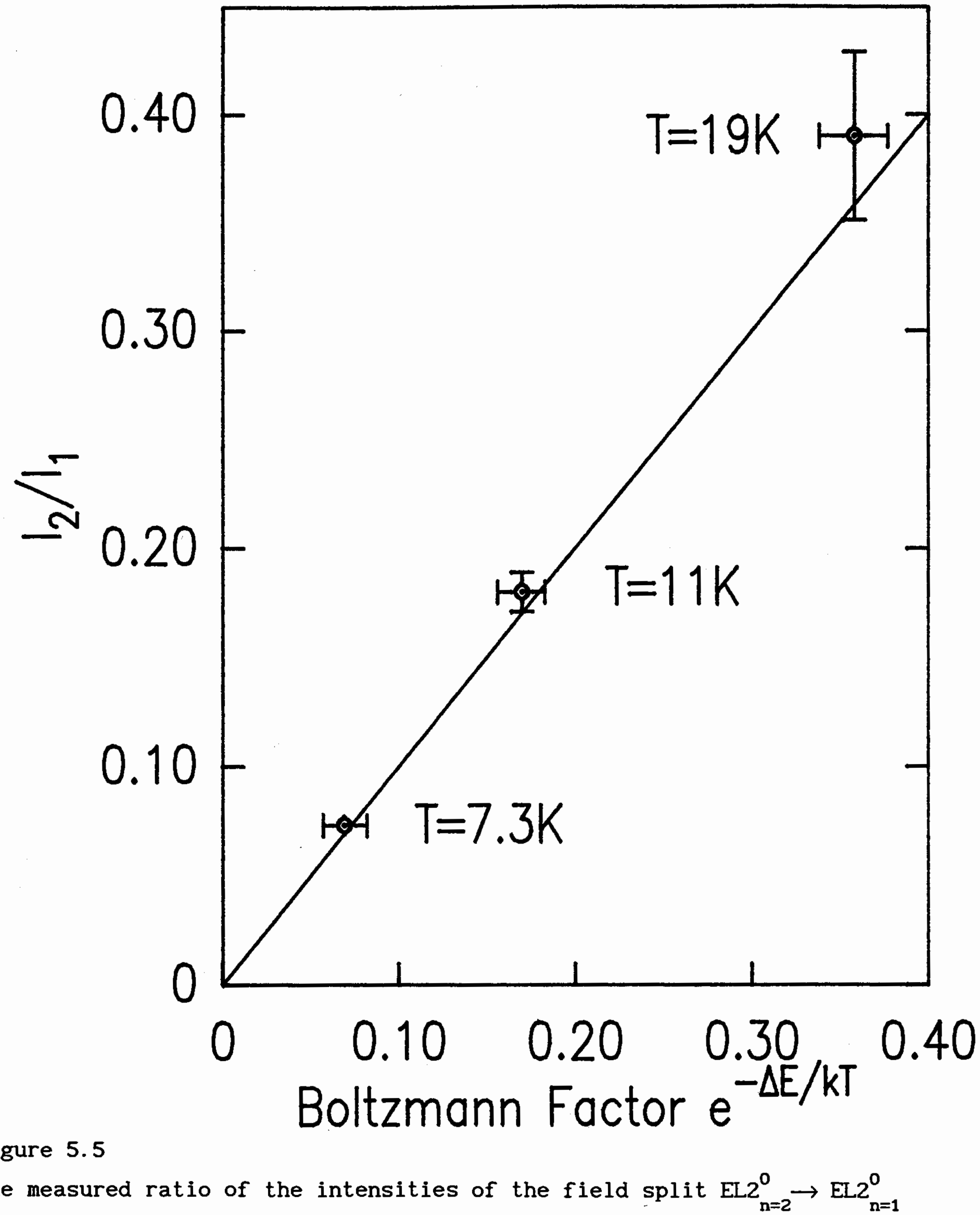

Figure 5.5

The measured ratio of the intensities of the field split $EL2^0_{n=2} \rightarrow EL2^0_{n=1}$ transition compared to the Boltzmann factor for the measured splitting of 1.692 meV at B = 12 T. The large error bars on the T = 19 K data point arise from the weak signal and broad lines at this temperature.

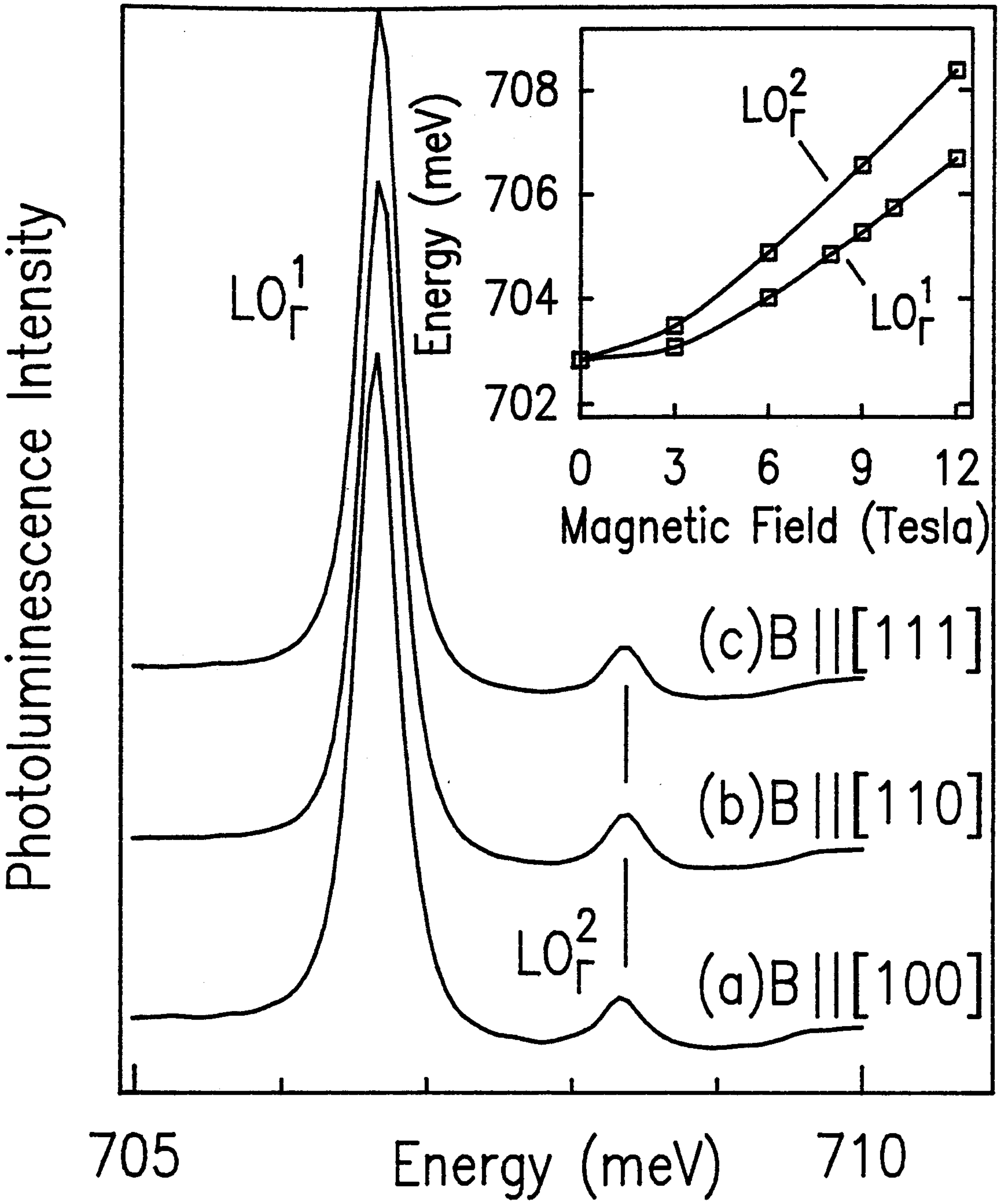

Figure 5.6

PL spectra showing the T = 8 K splitting of the LO_Γ transition at a resolution of 0.12 meV for B = 12 T along the three indicated directions. The inset shows the energy of these transitions as a function of magnetic field.

are presented of the LO_{Γ}^{1} and LO_{Γ}^{2} transitions obtained with the magnetic field parallel to the [100], [110] and [111] directions. The most significant aspect of this result is that there is no detectable anisotropy in the splitting. In agreement with the uniaxial stress results, there is no evidence to suggest that EL2 is anything but a point defect.

For completeness, the energies of the LO_{Γ} transitions are plotted as a function of the magnetic field in the inset of Figure 5.6. This summarizes both the shift and the splitting of the transition. A more informative picture of the observed behaviour can be obtained by considering the free to bound transitions as well as the $EL2^{0}_{n=2} \rightarrow EL2^{0}_{n=1}$ transitions. This allows the ground and excited states to be tracked relative to the conduction band as shown in Figure 5.7. This diagram provides a clear illustration of the nature of the splitting and the shift of the ground and excited states.

The linear nature of the splitting is shown in the upper central portion of the diagram which depicts the two-fold splitting of the free to bound transition with increasing field. The same splitting is found in the shallow excited state and is accompanied by a non-linear shift in energy with respect to the conduction band. The ground state does not split, but shows a considerable increase in binding energy with increasing field. Although these shifts are not central to the conclusions of this thesis, they do merit some discussion.

In addition to the splitting of states from the removal of spin degeneracy, the interactions of an electron in a hydrogenic system with a magnetic field can be included in the Hamiltonian by making the

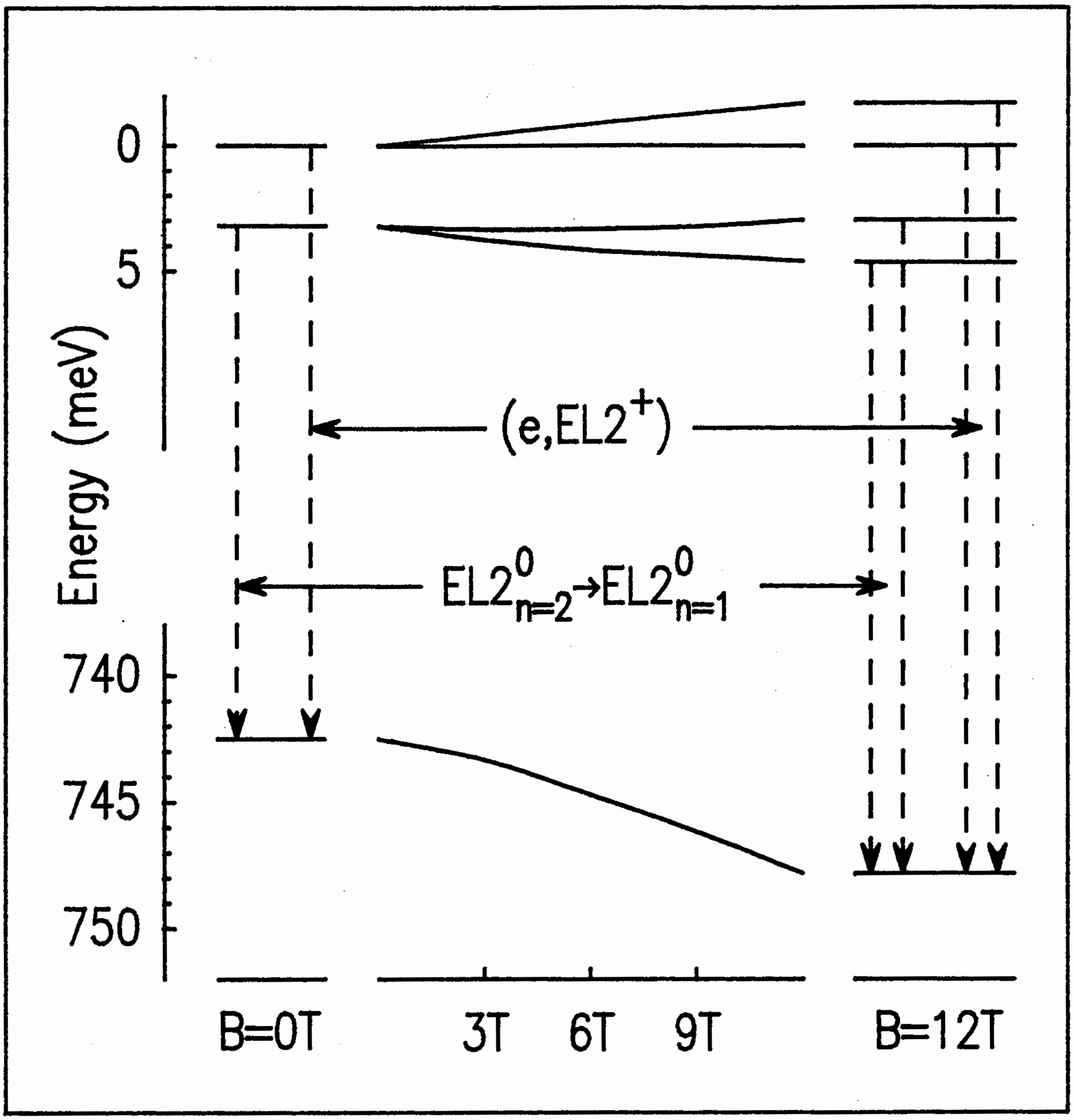

Figure 5.7

Diagram showing the energies of the initial and final states of the $EL2^0_{n=2} \longrightarrow EL2^0_{n=1}$ and free to bound transitions as a function of magnetic field. The zero field transitions are shown on the left and the high field transitions on the right.

substitution [85S1]

$$\mathbf{p} \longrightarrow \mathbf{p} - \frac{e}{c}\mathbf{A} \qquad 5.11$$

where **p** is the momentum operator, **A** is the vector potential of the magnetic field, e is the electron charge and c is the speed of light. In addition to a term linear in B which acts on the z-component of the orbital angular momentum, this gives rise to a term which is quadratic in B,

$$H_D = \frac{e^2}{8mc^2} B^2 \left(x^2 + y^2 \right) \qquad 5.12$$

where B is the magnitude of the applied magnetic field in the z direction, m is the mass of the electron and x and y are electron coordinates. This term represents the diamagnetic shift of the bound states which is typically a small effect and can be estimated using first order perturbation theory. If hydrogenic wavefunctions are used, the diamagnetic shift for an atom with nuclear charge Z is

$$E_D = \frac{4a_0^2}{Z^2} \frac{e^2}{8mc^2} B^2 \qquad 5.13$$

where a_0 is the Bohr radius.

The key result here is that the diamagnetic shift amounts to a reduction in the electron binding energy that is proportional to B^2.

This is not what is observed for the EL2 ground state. The shift is very nearly quadratic in B but is in the opposite direction from the diamagnetic shift. The origin of this shift is likely due to the compression of the ground state wavefunction by the applied field which enhances the effect of the strong short range central cell potential. A similar, but less dramatic, effect is observed for the shallow donors in GaAs. They too are observed to undergo an increase in binding energy under applied magnetic fields [90B2 and 89S3].

Of greater importance than the shift is the splitting. To understand the nature of this splitting, one must bear in mind that the initial state of the $EL2^0_{n=2} \rightarrow EL2^0_{n=1}$ transition consists of one electron in the deep n = 1 level and one electron in the shallow n = 2 level. As shown in the level diagram of Figure 5.8, each of these levels is split by the application of the field into two states, one with spin up, $m_s = \pm \frac{1}{2}$, and the other with spin down, $m_s = - \frac{1}{2}$. The deep n = 1 level is split by an amount $\Delta E_{n=1} = \mu_B\ B\ g_{n=1}$ and the shallow n = 2 level is split by $\Delta E_{n=2} = \mu_B\ B\ g_{n=2}$. The initial state thus consists of four levels. The final state is nondegenerate with respect to spin, it consists of both electrons in the 1s level, one with spin up and the other with spin down and therefore does not split. Also depicted in the level diagram are the two possible transitions from the four levels of the initial state to the final state that are consistent with the selection rule, $\Delta m_s = 0$, which is well known from the helium atom [73W1]. The energy separation of the resulting two lines is then the difference in the splitting of the n = 1 and n = 2 states, $\Delta E_{1,2} = \mu_B\ B\ (\ g_{n=1} - g_{n=2})$.

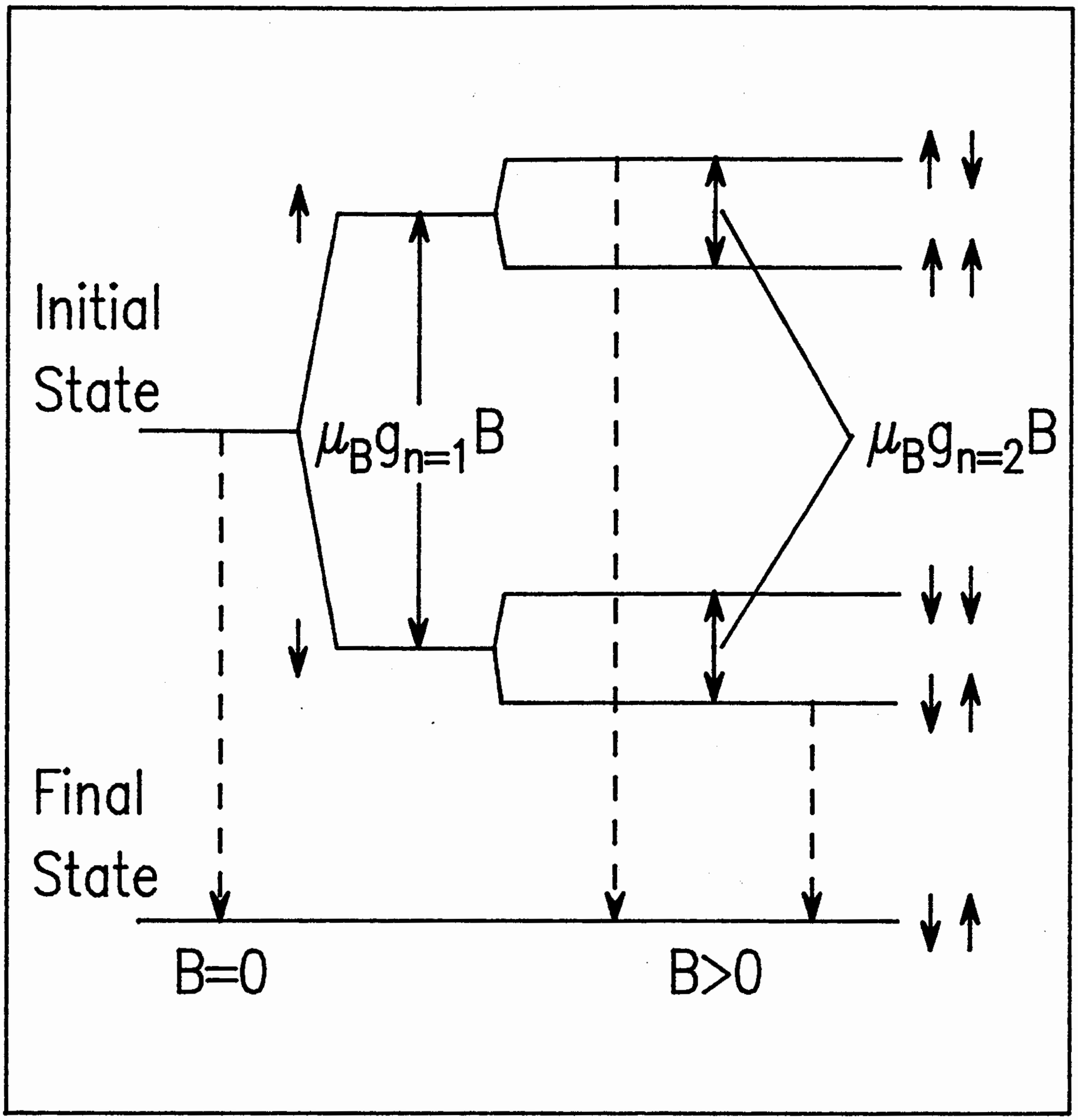

Figure 5.8
Level diagram showing the origin of the magnetic field induced splitting. The ordering of the field split n = 2 level reflects the negative g-value for the electron in this level.

The splitting at B = 12 T was measured to be $\Delta E = 13.65 \pm 0.03$ cm^{-1} = 1.692 ± 0.004 meV. Using $\mu_B = 0.0578838$ meV/T, this gives $(g_{n=1} - g_{n=2}) = 2.44 \pm 0.04$. The increase in the relative uncertainty in this value compared to the measured splitting is from the estimated uncertainty in the precise value of the magnetic field as a function of position within the magnet.

The n = 2 state is shallow, so the g-factor for an electron in this state will be close to that for a conduction band electron. In a recent study of the PL associated with the shallow donors in GaAs, the g-factor for shallow bound electrons was found to be $g = -0.402 \pm 0.008$ [90B2]. Using this value for $g_{n=2}$, a value of $g_{n=1} = 2.04 \pm 0.05$ is obtained, in excellent agreement with value of $g = 2.04 \pm 0.01$ from EPR studies of $\mathrm{As_{Ga}}^{+}$ [80W1]. This is yet further evidence that the 0.61 eV PL band is from the EL2 defect and the transition is from a shallow hydrogenic excited state to the deep ground state.

5.4 Summary

The results presented here provide strong evidence that EL2 is the point defect $\mathrm{As_{Ga}}$. The $\mathrm{EL2}^0_{n=2} \rightarrow \mathrm{EL2}^0_{n=1}$ transition does not split under uniaxial stress and both the hydrostatic shift and the EL2 g-factor are isotropic.

The identification originally made in Chapter 4 that the luminescence process is a transition from a shallow hydrogenic state to the deep EL2 ground state, $\mathrm{EL2}^0_{n=2} \rightarrow \mathrm{EL2}^0_{n=1}$ has also been strengthened. It was shown that the hydrostatic component of the shift from the uniaxial stress is in agreement with the totol hydrostatic shift of the EL2 ground state as measured by DLTS and optical absorption. The g-factor electrons in the EL2 ground state was also observed to agree with the As_{Ga}^{+} g-factor. Both the lack of splitting under uniaxial stress and the detailed behaviour of the splitting under magnetic field are completely consistent with the initial state of the transition being the solid state analogue of the 1s2s excited state of helium. These results and those from the previous Chapter will be further summarized in Chapter 6.

CHAPTER 6

SUMMARY AND CONCLUSIONS

6.1 Fourier Transform Photoluminescence

Before summarizing the experimental results, the importance of using a Fourier transform interferometer for the study of deep level photoluminescence should be again stressed. The Fellget and Jacquinot advantages that were introduced in Chapter 3 are both significant for this work.

The Fellget advantage describes the multiplex advantage of Fourier transform spectroscopy which allows all spectral information to be gathered simultaneously. This is a very convenient ability for deep level photoluminescence because, as has been seen, the strong electron-phonon coupling of these levels results in the photoluminescence lying in a broad band rather than in single discrete transitions as is typically the case for shallow levels. The Fellget advantage is said to be negated if photon counting detectors are available, but this is not the case for most deep levels and certainly not for the work presented here.

The Jacquinot advantage arises from the higher optical throughput of interferometers. It is harder to quantify because it depends on the details of the optical components of the instruments being compared but a measure of this advantage was experienced in research done prior to the work reported here.

The system under study was the triple acceptor copper in germanium

[90N2]. The photoluminescence spectrum is in virtually the same energy region as the structured portion of the 0.61 eV EL2 band and is similarly weak. Initially, this work was attempted on a grating spectrometer but the project was soon abandoned when no significant features were apparent above the noise level. Subsequently, the project was revived and high quality spectra were obtained on a Fourier transform interferometer which featured a very sharp no-phonon transition. Out of curiousity, the old grating spectrometer spectra were compared with the new results. With the aid of the new results, the no-phonon transition could be located but otherwise it could not be realistically discerned above the noise. The old experiments were performed over a fairly small energy interval and the Fellget advantage was therefore quite small and the vast improvement obtained with the interferometer was due primarily to the Jacquinot advantage.

This improvement is not out of line with the throughput advantage of 200 given by Griffiths and de Haseth [86G1]. Combined with the Fellget advantage of approximately 55 that was estimated in Chapter 3, this gives a net advantage on the order of one thousand. Although this is an upper limit on the real advantage, it leaves little doubt that this work would not have been feasible on a traditional grating spectrometer.

6.2 The Photoluminescence Transitions of EL2

The EL2-related photoluminescence in semi-insulating GaAs has been shown to consist of two bands that are centred at 0.61 eV and 0.68 eV.

The oxygen-related deep photoluminescence, which previously has often been confused with EL2, is a distinctly different band at 0.63 eV.

At low temperatures, the 0.68 eV band arises from donor-acceptor pair recombination, $(EL2^0, A^0)$, where the donor is EL2 and the acceptor is the dominant residual acceptor impurity, typically carbon. At temperatures of approximately T = 35 K, free hole to neutral EL2, $(h^+, EL2^0)$ transitions begin to emerge and at higher temperatures these free to bound transitions dominate the spectrum.

The 0.61 eV band had not been previously distinguished from the much stronger oxygen-related band at 0.63 eV and is richly structured on the high energy side. This spectrally sharp structure arises from electrons relaxing from a never before observed shallow hydrogenic excited state of EL2 down to the EL2 ground state. This shallow excited state is 3.2 ± 0.5 meV below the conduction band and is identified as the solid state analogue to the 1s2s excited state of helium and the transition is hence labelled $EL2^0_{n=2} \longrightarrow EL2^0_{n=1}$.

The no-phonon transition of this process is weak but is followed by 11 meV LVMs and a large number of lattice phonon replicas. Of these the one phonon LO_Γ replica is exceptionally strong and remains spectrally narrow. Also observed is a broad low energy tail below the NP line which is attributed to transitions of electrons from shallow donors to the EL2 ground state and these perturbed transitions are labelled $(D^0, EL2^+)$.

At temperatures above T = 30 K, the $(e, EL2^+)$ free to bound transition emerges and this allows the first direct measurement of the energy level of neutral EL2 in the bandgap. The value obtained is

742.5 ± 0.5 meV and is unprecedented in its precision. This value and the energy of the complementary $(h,EL2^0)$ transition add up precisely to the bandgap energy as they should.

The identification of this band with EL2 is solid. In addition to the agreement of the sum of the free to bound energies with the bandgap, it is supported by the presence of the band in all SI samples, the observation of the characteristic 11 meV local vibrational modes, the photo-quenching behaviour, the hydrostatic shift and the electron g-factor.

The 11 meV LVMs were found to couple to all the EL2-related PL transitions but the strong lattice phonon coupling, particularly the LO_Γ, was unique to the $EL2^0_{n=2} \rightarrow EL2^0_{n=1}$ transition. The strong presence of these lattice phonon replicas was shown to be consistent with neither momentum conservation nor vibrational coupling but it was argued instead that their participation relaxes the dipole forbidden nature of the unperturbed $EL2^0_{n=2} \rightarrow EL2^0_{n=1}$ transition.

6.3 The Site Symmetry of EL2

These results can be stated quite succinctly. Under the perturbation of uniaxial stress, there was no evidence in the LO_Γ assisted transition of any splitting. There was only an isotropic shift with stress that agreed with the hydrostatic pressure results. These results are consistent with an $A_1 \rightarrow A_1$ transition in T_d symmetry and are inconsistent with any detectable orientational degeneracy. The Zeeman splittings were also isotropic and the electron g-factor of the EL2 ground state agrees with that of As_{Ga}^{+} as measured by EPR. These results strongly support the isolated arsenic antisite model of EL2.

6.4 Future Work

The results on the site symmetry of the EL2 are a clear indication of full T_d symmetry and support the conclusions of Kaminska [85K1] but are difficult to reconcile with the ODENDOR results which indicate C_{3v} symmetry [8M71]. It is clearly important that ODMR and ODENDOR now be performed using the 0.61 eV photoluminescence as the optical signal. This work is undoubtedly in progress somewhere at the present time.

Two recent reports also deserve attention. An exciting development is the evidence under hydrostatic pressure of an acceptor-like level associated with the metastable state of EL2 [91B1]. Work is currently under way to examine if there is any manifestation of this level on the photoluminescence. Although it would be non-trivial to combine uniaxial stress with hydrostatic pressure, the symmetry of this state might be revealed with Zeeman spectroscopy. This would provide important information on the site symmetry of the metastable state of EL2.

Less exciting is a suggestion that the deep EL2 PL at 0.59 eV and 0.65 eV is polarized [89B3]. This is taken as evidence that the defect has axial symmetry. Performing this experiment on samples with and without oxygen will likely show that it is the oxygen related deep PL that is polarized. Oxygen is already thought to form a defect with axial symmetry [89A1].

REFERENCES

BM Bomem, Hartmann & Braun, 450 St-Jean-Baptiste, Québec, Québec G2E 5S5, Canada.

HO Hoya Optics, Inc., 3400 Edison Way, Fremont, CA 94538-6190, USA.

JA Janis Research Company, Inc., 2 Jewel Drive, P.O. Box 696, Wilmington, MA 01887-0896, USA.

LS Lake Shore Cryotronics, Inc., 64 E. Walnut St., Westerville, Ohio 43081, USA.

LT Lasertechnics, 5500 Wiltshire Ave. NE, Albuquerque, NM 87113, USA.

OI Oxford Instruments Ltd., Eynsham, Oxford OX8 1TL, England.

SC Schott Glass Tecnologies Inc., 400 York Ave., Duryea, PA 18642, USA.

SP Spectra-Physics, 1250 W. Middlefield Road, P.O. Box 7013, Mountain View, CA 94039-7013, USA.

50H1 K. Huang and A. Rhys, Proc. R. Soc. A **204**, 406 (1950).

55K1 W. Kohn and J.M. Luttinger, Phys. Rev. **98**, 915 (1955).

55L1 J.M. Luttinger and W. Kohn, Phys. Rev. **97**, 869 (1955).

62A1 N.G. Ainslie, S.E. Blum, and J.F. Woods, J. Appl. Phys. **33**, 2391 (1962).

63K1 A.A. Kaplyanskii, Optics Spectrosc. **16**, 329 (1963)

65M1 J.B. Mullin, B.W. Straughan, and W.S. Brickell, J. Phys. Chem. Solids **26**, 782 (1965).

72B1 H.B. Bebb and E.W. Williams, in *Semiconductors and Semimetals*, Vol. 3, edited by R.K. Willardson and A.C. Beer (1972), Academic Press, New York.

73W1 S. Wieder, *The Foundations of Quantum Theory*, (1973), Academic Press, New York.

77B1 D. Bois and G. Vincent, J. Phys. Lett. **38**, 351 (1977).

77M1 G.M. Martin, A. Mitonneau, and A. Mircea, Electron. Lett. **13**, 191 (1977).

77S1 E.M. Swiggard, S.H. Lee, and F.W. von Batchelder, Inst. Phys. Conf. Series, 33**b**, 23 (1977).

79H1 A.M. Huber, N.T. Linh, M. Valladon, J.L. Debrun, G.M. Martin, A. Mitonneau, and A. Mircea, J. Appl. Phys. **50**, 4022 (1979).

79Y1 P. W. Yu, Solid St. Commun. **32**, 1111 (1979).

80M1 G.M. Martin, J.P. Farges, G. Jacob, J.P. Hallais, and G. Poibland, J. Appl.Phys. **51**, 2840 (1980).

80W1 R.J. Wagner, J.J. Krebs, G.H. Strauss, and A.M. White, Solid State Commun. **36**, 15 (1980).

81C1 A. Chantre, G. Vincent, and D. Bois, Phys. Rev. B**23**, 5335 (1981).

81K1 C. Kittel, *Introduction to Solid State Physics*, 6th ed., (1981), Wiley, New York.

81L1 M. Lannoo and J. Bourgoin, *Point Defects in Semiconductors I*, (1981), Springer-Verlag, Berlin.

81M1 A. Mircea-Roussel and S. Makram-Ebeid, Appl. Phys. Lett. **38**, 1007, (1981).

81R1 A.K. Ramdas and S. Rodriguez, Rep. Prog. Phys. **44**, 1297 (1981).

81S1 S.M. Sze, *Physics of Semiconductor Devices*, 2nd ed., (1981), Wiley, New York.

82B1 J.S. Blakemore, J. Appl. Phys. **53**, R123, (1982).

82D1 W. Demtröder, *Laser Spectroscopy*, (1982), Springer-Verlag, Berlin.

82J1 M. Jaros, *Deep Levels in Semiconductors*, (1982), Hilger, Bristol.

82K1 A.S. Kaminskii, V.A. Karasyuk, and Ya.E. Pokrovskii, Sov. Phys. JETP **56**, 1295 (1982).

82L1 P. Leyral, G. Vincent, A. Nouailhat and G. Guillot, Solid State Commun. **42**, 67, (1982).

82M1 S. Makram-Ebeid and M. Lannoo, Phys. Rev. B**25**, 6406 (1982).

82M2 G.M. Martin, G. Jacob, J.P. Hallais, F.Grainger, J.A. Roberts, B.Clegg, P. Blood, and G. Poiblaud, J. Phys. C: Solid State Phys. **15**, 1841 (1982).

82W1 R. Wörner, U. Kaufmann, and J. Schneider, Appl. Phys. Lett. **40**, 141 (1982).

82W2 E.R. Weber, H. Ennen, U. Kaufmann, J. Windscheif, J. Schneider, and T. Wosinski, J. Appl. Phys. **53**, 6140 (1982).

82Y1 P. W. Yu and D.C. Walters, Appl. Phys. Lett. **41**, 863 (1982).

82Y2 P. W. Yu, Solid St. Commun. **43**, 953 (1982).

83B1 J. Bourgoin and M. Lannoo, *Point Defects in Semiconductors II*, (1983), Springer-Verlag, Berlin.

83B2 G. B. Bachelet, M. Schlüter, and G. A. Baraff, Phys. Rev. B**27**, 2545 (1983).

83K1 M. Kaminska, M. Skowronski, J. Lagowski, J.M. Parsey, and H.C. Gatos, Appl. Phys. Lett. **43**, 303 (1983).

83K2 D.W. Kisker, H. Tews, and W. Rehm, J. Appl. Phys. **54**, 1332 (1983).

83S1 B. V. Shanabrook, P. B. Klein, E. M. Swiggard, and S. G. Bishop, J. Appl. Phys. **54**, 336 (1983).

83T1 M. Taniguchi and T. Ikoma, J. Appl. Phys. **54**, 6448 (1983).

83W1 W. Walukiewicz, J. Lagowski, and H.C. Gatos, Appl. Phys. Lett. **43**, 112 (1983).

84H1 D. M. Hofmann, B. K. Meyer, F. Lohse, and J.-M. Spaeth, Phys. Rev. Lett. 53, 1187 (1984).

84K1 U. Kaufmann, Phys. Rev. Lett. **54**, 1332 (1985).

84L1 J. Lagowski, D.G. Lin, T.Aoyoma, and H.C. Gatos, Appl. Phys. Lett. **44**, 336 (1984).

84M1 B. K. Meyer, J.-M. Spaeth, and M. Scheffler, Phys. Rev. Lett. **52**, 851 (1984).

84M2 M.B. Morris, T.J. McIlrath, and J.J. Snyder, Applied Optics **23**, 3862 (1984).

84R1 W. Rösner, G. Wunner, H. Herold, and H. Ruder, J. Phys. B: At. Mol. Phys. **17**, 29 (1984).

84S1 L. Samuelson, P. Omling and H. G. Grimmeiss, Appl. Phys. Lett **45**, 521 (1984).

85B1 M. Baeumler, U. Kaufmann, and J. Windscheif, Appl. Phys. Lett.**46**, 781 (1985).

85E1 H. Emori, T. Kikuta, T. Inada, T. Obokata, and T. Fukuda, Jap. J. Appl. Phys. **24**, L29 (1985).

85K1 M. Kaminska, M. Skowronski, and W. Kuszko, Phys. Rev. Lett. **55**, 2204 (1985).

85S1 J.J. Sakurai, *Modern Quantum Mechanics*, (1985), Benjamin/Cummings, Menlo Park.

85T1 N. Tsukada, T. Kikuda, and K. Ishida, Jpn. J. Appl. Phys. **24**, L689 (1985).

86B1 H. J. von Bardeleben, D. Stiévenard, D. Deresmes, A. Huber, and J. C. Bourgoin, Phys. Rev. B**34**, 7192, (1986).

86G1 P.R. Griffiths and J.A. de Haseth, *Fourier Transform Infrared Spectrometry*, (1986), John Wiley and Sons, New York.

86K1 T. Kazuno, Y. Sawada, and T. Yokoyame, Jap. J. Appl. Phys. **25**, L878 (1986).

86L1 D.V. Lang, in *Deep Centers in Semiconductors*, edited by S.T. Pantelides, p. 489, (1986), Gordon and Breach, New York.

86M1 G. M. Martin and S. Makram-Ebeid, in *Deep Centers in Semiconductors*, ed. by S. T. Pantelides, (Gordon and Breach, New York, 1986), p.399.

86O1 P. Omling, P. Silverberg, and L. Samuelson, Material Science Forum Volumes 10-12, Defects in Semiconductors, 1986, pp. 329-324.

86P1 S.T. Pantelides, in preface to *Deep Centers in Semiconductors*, edited by S.T. Pantelides, (1986), Gordon and Breach, New York.

86P2 S.T. Pantelides, in *Deep Centers in Semiconductors*, edited by S.T. Pantelides, p. 1, (1986), Gordon and Breach, New York.

86S1 M. Skowronski, J. Lagowski, and H.C. Gatos, J. Appl. Phys. **59**, 2451 (1986).

86T1 M. Tajima, in *Defects in Semiconductors*, ed. H. J. von Bardeleben, Material Science Forum, Volumes **8-12**, (1986), p.493.

87B1 G. A. Baraff and M. Schluter, Phys. Rev. B35, 6154 (1987).

87D1 C. Delerue, M. Lannoo, D. Stiévenard, H. J. von Bardeleben, and J. C. Bourgoin, Phys. Rev. Lett. 59, 2875 (1987).

87F1 T. Figielski and T. Wosinski, Phys. Rev. B36, 1269 (1987).

87G1 H. C. Gatos and J. Lagowski, Phys. Rev. B36, 7668, (1987).

87L1 M. Levinson and J.A. Kafalas, Phys. Rev. B35, 9383 (1987).

87M1 B. K. Meyer, D. M. Hofmann, J. R. Niklas, and J.-M. Spaeth, Phys.

Rev. **B36**, 1332 (1987).

87N1 D. D. Nolte, W. Walukiewicz, and E. E. Haller, Phys. Rev. **B36**, 9374 (1987).

87S1 C. Song, W. Ge, D. Jiang, and C. Hsu, Appl. Phys. Lett. **50**, 1666 (1987).

87S2 W. Sesselman, B. Woratschek, J. Küppers, G. Ertl, and H. Haberland, Phys. Rev. **B35**, 1547 (1987).

87T1 M. Tajima, Jap. J. Appl. Phys. **26**, L885 (1987).

87T2 M. Tajima, T. Iino, and K. Ishida, Jap. J. Appl. Phys. **26**, L1060 (1987).

87W1 J.F. Wager and J.A. van Wechten, Phys. Rev. **B35**, 2330 (1987).

88B1 J.C. Bourgoin, H.J. von Bardeleben, and D. Stiévenard, J. Appl. Phys. **64**, R65 (1988).

88B2 K. Bergman, P. Omling, L. Samuelson, and H. G. Grimmeiss, in *Semi-insulating III-V Materials, Malmö 1988,* edited by G. Grossman and L. Ledebo, p. 397 (1988) Adam Hilger, Bristol.

88B3 M. Baj and P. Dreszer, in *Proceedings of the 15th International Conference on Defects in Semiconductors*, Vols 38-41 of Materials Science Forum, ed. G. Ferenczi, (Trans Tech., Aedermannsdorf, Switzerland, 1988) p. 101.

88B4 G. A. Baraff, M. Lannoo, and M. Schlüter, Phys. Rev. **B38**, 6003 (1988).

88C1 D. J. Chadi and K. J. Chang, Phys. Rev. Lett. **60**, 2187 (1988).

88D1 J. Dabrowski and M. Scheffler, Phys. Rev. Lett. **60**, 2183 (1988).

88D2 P. Dreszer and M. Baj, Acta Phys. Pol. **A73**, 219 (1988).

88H1 D.T.J. Hurle, in *GaAs Integrated Circuits*, edited by J. Mun, p. 1, (1988), BSP Professional Books, Oxford.

88K1 U. Kaufmann and J. Windsheif, Phys. Rev. **B38**, 10060 (1988).

88K2 M. Kaminska, Revue Phys. Appl. **23**, 793 (1988).

88M1 Y. Mochizuki and T. Ikoma, Revue Phys. Appl. **23**, 747, (1988).

88R1 B.K. Ridley, *Quantum Processes in Semiconductors*, (1988), Clarendon Press, Oxford.

88T1 M.L.W. Thewalt and D.J.S. Beckett, Can. J. Phys. **66**, 868 (1988).

88Y1 K. Yamasaki, N. Kato, and Y. Matsuoka, in *GaAs Integrated Circuits*, edited by J. Mun, p. 149, (1988), BSP Professional Books, Oxford.

88Z1 X. Zhong, D. Jiang, W. Ge, and C. Song, Appl. Phys. Lett. **52**, 628 (1988).

89A1 H.Ch. Alt, Appl. Phys. Lett. **54**, 1445 (1989).

89B1 G.A. Baraff, Phys. Rev. **B40**, 1030 (1989).

89B2 G.A. Baraff, Phys. Rev. Lett. **62**, 2156 (1989).

89B3 I.A. Buyanova, E.I. Oborina, and S.S. Ostapenko, Semicond. Sci. Tecnol. **4**, 797 (1989).

89D1 J. Dabrowski and M. Scheffler, Phys. Rev. **B40**, 10391 (1989).

89D2 J. Dabrowski and M. Scheffler, Mater. Sci. Forum, Vols. 38-41, 51 (1989).

89K1 U. Kaufmann, in Festkörperprobleme/Advances in *Solid State Physics*, Vol. 29, ed. by U. Rössler (Vieweg, Braunschweig, 1989), p. 183.

89L1 Landolt-Börnstein, *Numerical Data and Functional Relationships in Science and Technology, New Series*, O. Madelung (Editor in Chief). Group III, Vol. 22 Semiconductors, Subvolume b (1989), Springer-Verlag, Berlin.

89P1 G. Parry, M. Whitehead, and J.E. Midwinter, in *GaAs technology and its impact on circuits and systems*, edited by D. Haigh and J. Everard, p. 4070 (1989), Peter Peregrinus, London.

89S1 K. Seeger, *Semiconductor Physics*, 4th ed., (1989), Springer-Verlag, Berlin.

89S2 P.H. Saul, in *GaAs technology and its impact on circuits and systems*, edited by D. Haigh and J. Everard, p. 165 (1989) , Peter Peregrinus, London.

89S3 B.J. Skromme, R. Bhat, H.M. Cox, and E. Colas, IEEE J. Quantum Electron. 25, 1035 (1989).

90A1 H. Ch. Alt, private communication.

90B1 G.A. Baraff, Phys. Rev. B**41**, 3074 (1990).

90B2 D.J.S. Beckett, PhD. thesis, (1990), Simon Fraser University, unpublished.

90D1 G. Davies, Phys. Rev. B**41**, 9850 (1990).

90N1 M.K. Nissen, T. Steiner, D.J.S. Beckett, and M.L.W. Thewalt, Phys. Rev. Lett. 65, 2282 (1990).

90N2 M.K. Nissen, A.G. Steele and M.L.W. Thewalt, Phys. Rev. B**41**, 7926 (1990).

90O1 P. Ohmling and L. Samuelson, in *Proceedings of the 6th Conf. on Semi-Insulating III-V Materials, Toronto, 1990,* ed. A.G. Milnes and C.J. Miner, (Adam Hilger, Bristol, 1990), p. 17.

90S1 J.-M. Spaeth, K. Krambrock, and D.M. Hofman, in *Proceedings of the 20th International Conference on the Physics of Semiconductors, Thessaloniki, 1990*, ed. E.M. Anastassakis and J.D. Joannopoulos

(World Scientific, Singapore, 1990), p. 441.

90S2 D. Strauch and B. Dorner, J. Phys. Condens. Matter, **2**, 1457 (1990).

90S3 T.W. Steiner, Yu Zhang, M.L.W. Thewalt, M. Maciaszek, and R.P. Bult, Appl. Phys. Lett. **56**, 467 (1990).

90T1 M.L.W. Thewalt, M.K. Nissen, D.J.S. Beckett, and K.R. Lundgren, Mat. Res. Soc. Symp. Proc. Vol. 163, 221 (1990).

90T2 P. Trautman, J.P. Walczak, and J.M. Baranowski, Phys. Rev. B**41**, 3074 (1990).

91B1 M. Baj, P. Dreszer, and A. Babinski, Phys. Rev. B**43**, 2070 (1991).

91B2 J.C. Bourgoin, D. Stievenard, D. Deresmes, and J.M. Arroyo, J. Appl. Phys. **69**, 284 (1991).

91B3 N.T. Bagraev, JETP Lett. **53**, 573 (1991).

91D1 U.V. Desnica, D.I. Desnica, and B. Santic, Appl. Phys. Lett. **58**, 278 (1991).

91N1 M.K. Nissen, A. Villemaire, and M.L.W. Thewalt, Phys. Rev. Lett. **67**, 112 (1991).